NAVAL POSTGRADUATE SCHOOL

MONTEREY, CALIFORNIA

THESIS

EVALUATION OF THE AFWA WRF 4-KM MOVING NEST MODEL PREDICTIONS FOR WESTERN NORTH PACIFIC TROPICAL CYCLONES

by

William R. Ryerson

March 2006

Thesis Advisor:	Russell L. Elsberry
Second Reader:	Karl D. Pfeiffer

Approved for public release; distribution is unlimited

THIS PAGE INTENTIONALLY LEFT BLANK

REPORT DOCUMENTATION PAGE		Form Approved OMB No. 0704-0188
Public reporting burden for this collection of information is estimated to average 1 hour per response, including the time for reviewing instruction, searching existing data sources, gathering and maintaining the data needed, and completing and reviewing the collection of information. Send comments regarding this burden estimate or any other aspect of this collection of information, including suggestions for reducing this burden, to Washington headquarters Services, Directorate for Information Operations and Reports, 1215 Jefferson Davis Highway, Suite 1204, Arlington, VA 22202-4302, and to the Office of Management and Budget, Paperwork Reduction Project (0704-0188) Washington DC 20503.		
1. AGENCY USE ONLY *(Leave blank)*	**2. REPORT DATE** March 2006	**3. REPORT TYPE AND DATES COVERED** Master's Thesis
4. TITLE AND SUBTITLE: Evaluation of the AFWA WRF 4-km Moving Nest Model Predictions for Western North Pacific Tropical Cyclones		**5. FUNDING NUMBERS**
6. AUTHOR(S) Ryerson, William R.		
7. PERFORMING ORGANIZATION NAME(S) AND ADDRESS(ES) Naval Postgraduate School Monterey, CA 93943-5000		**8. PERFORMING ORGANIZATION REPORT NUMBER**
9. SPONSORING /MONITORING AGENCY NAME(S) AND ADDRESS(ES) N/A		**10. SPONSORING/MONITORING AGENCY REPORT NUMBER**
11. SUPPLEMENTARY NOTES The views expressed in this thesis are those of the author and do not reflect the official policy or position of the Department of Defense or the U.S. Government.		
12a. DISTRIBUTION / AVAILABILITY STATEMENT Approved for public release; distribution is unlimited		**12b. DISTRIBUTION CODE** A

13. ABSTRACT (maximum 200 words)

The Air Force Weather Agency (AFWA) version of the Advanced Research Weather Research and Forecasting (ARW) model with a moving 4-km nested grid is examined for 10 track and intensity predictions of six western North Pacific tropical cyclones during 2005. In three of the 10 integrations, the ARW vortex tracker algorithm based on the 500-mb height minimum failed to appropriately move the nest and thus lost track of the storm vortex. For the other seven cases, the ARW track forecasts are more skillful than the AFWA MM5 forecasts and (except at 12 h) the CLIPER-type forecasts. The ARW intensity forecasts were less skillful than the MM5 and CLIPER-type forecasts at all forecast intervals, and were severely degraded by a large negative bias at the initial time. The deficiency in these intensity forecasts is shown to be related to model spin-up (lasting 12-54 h) problems caused by the lack of a bogus vortex and a cold start initialization from the interpolation of the NCEP Global Forecast System (GFS) analysis to the 12-km and 4-km grids. Thus, a more appropriate initial vortex representation will be required to improve intensity forecasts.

14. SUBJECT TERMS Numerical Weather Prediction; Tropical Meteorology; Weather Research and Forecasting Model; Tropical Cyclone Track; Tropical Cyclone Intensity; Tropical Cyclone Prediction	**15. NUMBER OF PAGES** 134
	16. PRICE CODE

17. SECURITY CLASSIFICATION OF REPORT	**18. SECURITY CLASSIFICATION OF THIS PAGE**	**19. SECURITY CLASSIFICATION OF ABSTRACT**	**20. LIMITATION OF ABSTRACT**
Unclassified	Unclassified	Unclassified	UL

NSN 7540-01-280-5500

Standard Form 298 (Rev. 2-89)
Prescribed by ANSI Std. 239-18

THIS PAGE INTENTIONALLY LEFT BLANK

Approved for public release; distribution is unlimited.

EVALUATION OF THE AFWA WRF 4-KM MOVING NEST MODEL PREDICTIONS FOR WESTERN NORTH PACIFIC TROPICAL CYCLONES

William R. Ryerson
Captain, United States Air Force
B.S., The Pennsylvania State University, 2001

Submitted in partial fulfillment of the
requirements for the degree of

MASTER OF SCIENCE IN METEOROLOGY

from the

NAVAL POSTGRADUATE SCHOOL
March 2006

Author: William R. Ryerson

Approved by: Professor Russell L. Elsberry
Thesis Advisor

Lieutenant Colonel Karl D. Pfeiffer
Second Reader

Professor Philip A. Durkee
Chairman, Department of Meteorology

THIS PAGE INTENTIONALLY LEFT BLANK

ABSTRACT

The Air Force Weather Agency (AFWA) version of the Advanced Research Weather Research and Forecasting (ARW) model with a moving 4-km nested grid is examined for 10 track and intensity predictions of six western North Pacific tropical cyclones during 2005. In three of the 10 integrations, the ARW vortex tracker algorithm based on the 500-mb height minimum failed to appropriately move the nest and thus lost track of the storm vortex. For the other seven cases, the ARW track forecasts are more skillful than the AFWA MM5 forecasts and (except at 12 h) the CLIPER-type forecasts. The ARW intensity forecasts were less skillful than the MM5 and CLIPER-type forecasts at all forecast intervals, and were severely degraded by a large negative bias at the initial time. The deficiency in these intensity forecasts is shown to be related to model spin-up (lasting 12-54 h) problems caused by the lack of a bogus vortex and a cold start initialization from the interpolation of the NCEP Global Forecast System (GFS) analysis to the 12-km and 4-km grids. Thus, a more appropriate initial vortex representation will be required to improve intensity forecasts.

THIS PAGE INTENTIONALLY LEFT BLANK

TABLE OF CONTENTS

LIST OF FIGURES

THIS PAGE INTENTIONALLY LEFT BLANK

LIST OF TABLES

THIS PAGE INTENTIONALLY LEFT BLANK

ACKNOWLEDGMENTS

I offer my sincerest gratitude to Professor Russell Elsberry for his unwavering patience and support in addition to his invaluable advice. It was truly a pleasure conducting this research under his skillful guidance. Lieutenant Colonel Karl Pfeiffer committed numerous hours reviewing the manuscript and providing extremely beneficial suggestions. Dr. Jerry Wegiel, Mr. Steve Rugg, and Major Tony Eckel of the AFWA Meteorological Models Branch not only provided most of the model output for the research, but also helped mold the framework for the study from the early stages. Their willingness to champion the project and provide technical support is tremendously appreciated. Mr. Bob Creasey of the Naval Postgraduate School spent countless hours converting and configuring the model output and figures, and never lost patience with my sometimes excessive requests. Mr. Mark Boothe also contributed greatly by providing a wide variety of data as well as tropical meteorology expertise.

Lastly, I owe the utmost appreciation to my beautiful wife Teresa, whose enduring love and support kept me in high spirits throughout, just as they have always done.

THIS PAGE INTENTIONALLY LEFT BLANK

I. INTRODUCTION

A. BACKGROUND

Tropical cyclone (TC) track and intensity prediction in the western North Pacific is a matter of extremely high interest to the United States Pacific Command of the Department of Defense (DOD). Several large military installations in the command are affected by TCs on a nearly annual basis, including Andersen Air Force Base, Guam; Kadena Air Base, Okinawa; and Camp Butler Marine Corp Base, Okinawa. Several other very large installations containing billions of dollars of assets across Korea and Japan are affected less frequently.

The importance of TC prediction was brought to the forefront following the poor forecasts of Typhoon Pongsona in December 2002, which passed directly over Andersen Air Force Base and produced wind gusts of nearly 140 kt and 20 in of rain. Less than the three days before landfall, the official DOD forecast provided by the Joint Typhoon Warning Center (JTWC) was for the TC to miss Andersen by 120 n mi. This track forecast was revised as the TC moved toward Guam, but the intensity of the storm was continually under-forecast right until Pongsona reached the island (National Weather Service Assessment [available online at http://www.nws.noaa.gov/om/assessments/pdfs/Pongsona.pdf]).

The primary dynamical models used for prediction in the western North Pacific have limited horizontal resolution that is generally not sufficient to fully resolve eyewall structure and the large gradients of temperature, moisture, and wind that exist in a TC vortex and are crucial to the overall intensity of a TC. Whereas observed TC eye diameters in the western North Pacific average around 40 km (Weatherford and Gray 1988), the Navy version of the Geophysical Fluid Dynamics Lab hurricane model (GFDN) and the Air Force Mesoscale Model-Version 5 (MM5) have horizontal resolutions of only 18 km and 15 km, respectively.

In the 1990s, development began on the next-generation mesoscale model intended to eventually replace the MM5. This model, which is a collaborative effort among multiple universities and government agencies (including the DOD), has been named the Weather Research and Forecasting (WRF) model. The version used in this research is the Advanced Research WRF (ARW). The ARW can be used with a user-selected resolution depending on the application, but present limitations in computational resources preclude the model from being routinely integrated for the entire western North Pacific at a resolution high enough to adequately resolve a TC vortex. Most of the centers doing ARW integrations are using a 12 km horizontal resolution for regional applications, which is only a modest improvement over the MM5 model resolution.

Goerss et al. (2004) concluded that numerical weather prediction of TC track has gradually improved over the last decade due mostly to steadily-improving model dynamics as opposed to improvements in model resolution. However, an improvement in horizontal resolution will be required for intensity prediction. A recent upgrade to the ARW model (version 2.1) includes a moving inner-nest option with 4 km resolution. The domain of the inner nest is kept small so as not to unreasonably prolong the calculation time. This inner nest is designed to move with a TC so that it is always over the vortex, which is where the highest resolution grid is desired. Since the resolution of the inner nest is nearly a four-fold increase over the MM5 grid, the ARW inner nest has much greater potential for resolving mesoscale changes in eyewall structure and associated TC intensity. Consequently, the dynamical differences between the MM5 and ARW models may affect TC prediction performance for both intensity and track.

B. MOTIVATION

Statistical, statistical-dynamical, and dynamical models have little to no skill in predicting TC intensity in the western North Pacific (Blackerby 2005).

Specifically, the Air Force Weather Agency (AFWA) MM5 model was found to have no intensity prediction skill relative to a climatology and persistence technique. If a skillful consensus intensity technique is to be developed similar to the consensus track technique called the Systematic Approach to Tropical Cyclone Forecasting Aid (SAFA) (Carr et al. 2001), then each of the intensity techniques must have skill. If the ARW is to garner acceptance as a TC forecasting aid, it must be demonstrated to add value relative to the current MM5 model.

This study will examine the feasibility of using the ARW model to forecast western North Pacific tropical cyclone track and intensity. The study will also examine whether the updated dynamics and superior resolution of the ARW compared to the MM5 will produce more accurate track forecasts. In addition, a preliminary evaluation of the strengths, weaknesses, and biases of the ARW will be made to indicate where it may be useful to the forecaster as a TC prediction tool (for both track and intensity) and suggest issues that may be considered by the ARW development team to make future upgrades to the model.

C. CHAPTER OVERVIEW

Before assessing the performance of the AFWA version of the ARW model, a full description of the model is provided in Chapter II, including details about the moving inner nest. The methodology used for the evaluation and a description of the ten cases used in the study are given in Chapter III. An explanation of the initialization procedures and boundary conditions used for the ARW and MM5 in this work are also provided in this chapter. Chapter IV presents the results of the evaluations of the track prediction performance and then the intensity prediction performance. Lastly, Chapter V offers a summary of the findings and recommendations for improvements to the model and future work.

THIS PAGE INTENTIONALLY LEFT BLANK

II. MODEL DESCRIPTION

A. WEATHER RESEARCH AND FORECASTING MODEL

1. Overview

The Advanced Research WRF (ARW) and the Non-hydrostatic Mesoscale Model WRF (NMM WRF) are the two main subsets of the WRF modeling system. While there are important differences regarding certain aspects of each subset (for example, the vertical coordinate and time integration scheme), both share a similar framework for their physics and software packages. The ARW, whose development was led by the Mesoscale and Microscale Meteorology (MMM) division of the National Center for Atmospheric Research (NCAR), is the subset used in this research.

The first version of ARW (version 1.0) was released in December 2000 after being developed in close partnership from the Air Force Weather Agency (AFWA), and both the MMM and AFWA have the capability to assimilate, run, and post-process newer versions of the model at their respective facilities. The ARW integrations used in this study were provided by the Meteorological Models Branch of AFWA at Offutt Air Force Base, Nebraska.

The ARW uses an Eulerian mass dynamical core, and is a non-hydrostatic, fully-compressible model developed for modeling on a wide range of physical scales. Numerous physics and dynamics options in the model can be selected to provide the most appropriate settings for a given scenario and horizontal scale. For example, the cumulus parameterization technique can be toggled off for the high resolution simulation of individual convective cells. If planetary waves are the feature of interest, an appropriate cumulus parameterization scheme can be selected from several options.

Except where otherwise annotated, the information for this chapter was obtained from the WRF website [available online at http://wrf-model.org/index.php], the NCAR technical notes on WRF Version 2 [available

online at http://www.mmm.ucar.edu/wrf/users/docs/arw_v2.pdf], and the ARW User's Guide [available online at http://www.mmm.ucar.edu/wrf/users/docs/user_guide/contents.html] (all current as of 2 Feb 2006). In addition, information was provided via personal correspondence with Steve Rugg of AFWA/DNXM between August 2005 and February 2006.

2. Physics and Dynamics

For this study of TCs, the ARW was integrated with a horizontal resolution of 12 km in the parent grid (hereafter outer nest). As this is too large to resolve individual convective cells, the "New Kain-Fritsch" cumulus parameterization scheme (Kain 1998) was used on the 12 km outer nest grid. This parameterization scheme, which is also used in the AFWA operational regional MM5 model, uses a mass flux approach (with downdrafts) and distinguishes between deep and shallow convection. The scheme also incorporates cloud detrainment into the algorithm. Due to its high computational cost, this parameterization scheme was called every six time steps as opposed to every time step.

With a horizontal resolution of 4 km on the inner nest, cumulus parameterization was turned off, which means any convective elements were simulated explicitly. Although no firm rule exists as to the upper limit of horizontal resolution for the effective use of explicit cumulus simulation, no parameterization schemes are specifically designed for resolutions in the range of 3 km to 10 km (Dudhia 2005).

The microphysics scheme used was the WRF single-moment (WSM) 3-class scheme from Hong et al. (2004), which replaced the similar National Centers for Environmental Prediction-3 (NCEP3) scheme. The WSM scheme accounts for snow, graupel, and ice sedimentation, since all of these water species can occur in the upper portions of tropical convective cells. While WSM was used in both the outer and inner nests, it was especially important in the outer nest to resolve individual deep updrafts with associated liquid to ice phase changes.

As is done in the MM5, sea-surface temperature (SST) data were retrieved from the 1/4° lat./long. resolution daily global SST analysis product from the Fleet Numerical Meteorology and Oceanography Center (FNMOC). The ARW currently is not capable of coupling air and ocean processes as is done in research versions of the Navy Coupled Ocean-Atmosphere Mesoscale Prediction System (COAMPS). Instead, the SST field obtained during initialization did not change during the ARW model integration.

While not the main thrust of this study, several of the cases involved a TC that made landfall, which can be expected to drastically affect storm structure. Over land surfaces, the NOAH Land Surface Model (LSM) was used to determine characteristics of heat, moisture, and roughness of the ground surface. NOAH is a four-layer model of soil temperature and moisture routinely used by NCEP, NCAR, and AFWA in atmospheric modeling. Each grid point is also assigned one of 24 land-use categories that characterize the vegetative cover, albedo, emissivity, and roughness length.

The energy fluxes from the sea and the ground surface to the atmosphere were modeled using a Monin-Obukhov scheme that employs similarity theory relationships to describe vertical flux and turbulence based on a few key parameters. These relationships were identical to those typically used in the MM5 and the Medium Range Forecast (MRF) models.

Despite the relatively high horizontal resolution of the inner nest and high vertical resolution (which averages $\Delta z < 300$ m below 700 mb), several important processes in the planetary boundary layer (PBL) occur at scales well below 1 km and need to be parameterized in both the outer and inner nests. One of these is vertical mixing of eddies in an unstable PBL, which was done using the Yonsei University (YSU) scheme. This scheme models vertical eddy diffusion by assuming a parabolic profile of momentum transfer through the PBL, with explicit modeling of entrainment at the top of the mixed layer.

Horizontal turbulence diffusion at sub-grid scales was modeled using the Smagorinsky first-order closure scheme. In this two-dimensional scheme (vertical eddy diffusion is parameterized by the YSU scheme), horizontal eddy diffusion is calculated directly from horizontal deformation.

Longwave (LW) radiation was modeled using the Rapid Radiative Transfer Model (RRTM), which uses the k-distribution concept and climatological concentrations of ozone, CO_2, and trace gases to account for LW interaction with these gases and with clouds. The scheme also accounts for multiple bands in the LW spectrum.

As is done in the MM5 model, the Dudhia scheme was used for shortwave (SW) radiation. This scheme entails a simple downward integration of SW radiation, and accounts for varying cloud albedo and absorption properties as well as scattering and absorption due to water vapor. As with the cumulus parameterization, both the LW and SW radiation schemes were not called every time step due to the high computational cost. The radiation schemes were called every 19 time steps (about every 15 min).

The ARW model utilizes the flux-form of the equations for mass, momentum, and entropy so that all of these parameters are conserved. Horizontal advection is computed using a 5^{th} order scheme.

3. Domain, Time Control, and the Moving Nest

The variables in both the outer- and inner-nest grids are represented with an Arakawa C staggering, i.e., the velocity grid points for calculating horizontal and vertical motion are directly above, below, and to the sides of the mass grid points. For this study, the top boundary was a constant pressure surface. Due to the strong updraft cores associated with the TCs studied in this research, vertical motions were damped near the top boundary to prevent the model from becoming unstable. Otherwise, no damping was included. The bottom boundary was affected by the frictional and flux interactions with the sea or ground as described in Chapter II.A.2. In the vertical, AFWA has configured the ARW with 35 terrain-following hydrostatic pressure levels, which are commonly called

sigma-p levels. These range from 0.9965 near the surface to 0.0065 near the model top, and each represents the fractional pressure value between the surface and the theoretical top of the atmosphere (0 mb). For example, a sigma-p level of 0.4940 signifies a level where the pressure is 49.40% of the surface pressure value in the column (it also indicates a level above which 49.40% of the atmospheric mass exists). When multiplied by 1000, a sigma-p level roughly corresponds to a conventional pressure level in millibars (i.e., sigma-p level 0.4940 is approximately equivalent to 500 mb).

The ARW uses 3rd order Runge-Kutta time integration. The model uses complete Coriolis, curvature, and mapping terms. The output in this study was displayed on a Mercator projection, which is most suitable for low latitudes.

The ARW version 2.1 was released for non-operational use in August 2005, and is the first version with the automatic vortex-following nest option. Once the initial location of the inner nest within the outer nest is defined by the user, the inner nest is automatically recentered every 15 min to be near the lowest 500 mb geopotential height within the inner nest. This center position for the recentering is computed by considering the average of several grid points near the lowest height value as opposed to relying on a single grid point (see Appendix). The inner nest can be shifted by one or more of the inner nest grid points, but does not need to be centered on a grid point of the outer nest. The movement of the inner nest may not exceed 40 m/s, which is equivalent to nine inner nest grid points for every 15 min interval.

For this study, a two-way nest interaction was used so that the solutions computed in the inner nest were passed to the outer nest in real-time. As opposed to a one-way influence approach, two-way interaction requires the outer nest and inner nest to be integrated concurrently. The lateral boundary conditions along the outer edge of the inner nest were interpolated from the outer nest at every time step.

B. DIFFERENCES BETWEEN MM5 AND ARW

The prognostic equations of the MM5 model are formulated as a set of advective equations as opposed to conservation concepts. While mass, momentum, and entropy are all conserved in the ARW model, there is no requirement to conserve these parameters in the MM5. In addition, the MM5 uses 2nd order advection differencing as opposed to the 5th order differencing in the ARW. Time integration in the MM5 model is with a 1st order time-filtered leapfrog scheme, whereas the split-explicit scheme is used in the ARW.

Although the vertical coordinate system of the MM5 model is also terrain-following, it is in sigma-h coordinates, which means the values represent fractional heights between the surface and model top as opposed to fractional hydrostatic pressure values. Thirty-one sigma-h levels are used in the tropical MM5 version designed for TC prediction, which is the comparison model used in this research. The MM5 model uses an Arakawa B staggered grid arrangement in which the velocity grid points are offset diagonally from the mass points instead of directly up, down, and to the sides as in the AWR.

The MM5 predictions of TCs in the western North Pacific region are on an inner nest of 15 km resolution inside an outer nest of 45 km resolution. The inner nest is manually positioned in the domain during the model initialization, and is then stationary throughout the model run. Unlike the moving inner nest of the ARW, the MM5 inner nest is usually large enough to predict the 72-h track of a moving TC, although fast-moving storms may occasionally exit the boundaries of the inner nest (Blackerby 2005).

A distinction must be made between the “real-time” MM5 used for this study, and the “interpolated” MM5 predictions used by the JTWC as a prediction aid. When the JTWC issues a TC warning at six-hour intervals, the “real-time” MM5 integration is not yet available. For this reason, it will use the forecast from the previous MM5 integration, but translate the track forecast so that the six-hour position forecast agrees with the current observed position. Therefore, the “interpolated” MM5 is always listed as having a 00-h forecast error near zero,

even though it is a product that is six hours old. Using the “real-time” MM5 for this study provides the most relevant comparison with ARW since both models were initialized at the same time.

THIS PAGE INTENTIONALLY LEFT BLANK

III. METHODOLOGY

A. FRAMEWORK FOR PREDICTION ANALYSIS

To compare overall prediction performance between the ARW and MM5 models, six TCs were selected from the 2005 western North Pacific typhoon season. A total of 10 ARW model integrations to 72 h were completed by AFWA and supplied to the Naval Postgraduate School for analysis. The ARW position and intensity forecasts in the ATCF format (Sampson et al. 2000) were compared to the verification values from the JTWC Working Best Track statistics. The final Best Tracks will be generated later from a comprehensive post-storm analysis, and thus were not available for this study. The output from the ARW was also compared to the MM5 forecasts and a climatology and persistence technique to provide an overview of the relative performance of each model.

It should be noted that while TC positions are normally easily derived from satellite or microwave imagery, intensity estimates are subject to a certain degree of error due to the absence of aircraft reconnaissance observations in the western North Pacific. Analysts thus rely primarily on satellite data for intensity determination, but this should only be considered a skillful estimate and is probably not precise in all cases (Elsberry et al. 1992). In addition, “sustained wind” is defined by the JTWC to be a one-minute average, and will be higher than the 10-minute average winds used by many other TC prediction agencies. Unless otherwise noted, for this study sustained wind will refer to the JTWC definition.

B. CASE SELECTION

Although the track predictions are also important, the cases were selected primarily to represent intensity change scenarios that are difficult to forecast (Blackerby 2005; Lambert 2005): (i) Formation (defined as beginning at 25 kt and increasing through 35 kt); (ii) Rapid intensification (defined as at least 30 kt in 24 h); (iii) Decay and re-intensification cycles in which a typhoon of greater than

100 kt may (or may not) decrease in intensity more than 10 kt and then re-intensify; and (iv) rapid decay over land that is primarily a problem of timing and location of landfall.

Because of computer code and resource availability, the sample had to be limited to 10 cases after 1 July 2005. Each case had to begin on 00 UTC or 12 UTC when archived data sets were available. Each of the six TCs will be briefly described in the following sections. Because of the small sample and specific intensity forecast scenarios were targeted, these results are not representative of the performance of the ARW in a sample over the entire season.

Except where otherwise noted, the storm descriptions for this section were extracted from the Tropical Cyclone Summaries written by Gary Padgett that are available online at http://australiasevereweather.com/cyclones/index.html, the JTWC website http://www.npmoc.navy.mil/jtwc.html, and the Digital Typhoon Website http://agora.ex.nii.ac.jp/digital-typhoon/index.html.en (all current as of 27 January 2006).

1. Typhoon Matsa

Typhoon Matsa began as an area of convection approximately 600 n mi southwest of Guam on 29 July. The JTWC issued the first TC warning at 00 UTC 31 July, and the storm reached tropical storm strength (35 kt sustained wind) six hours later. The track and intensity of Typhoon Matsa are shown in Figure 3.1. The storm would eventually make landfall in China as a weak typhoon before turning northward and rapidly weakening. The last warning was issued by JTWC at 18 UTC 6 August.

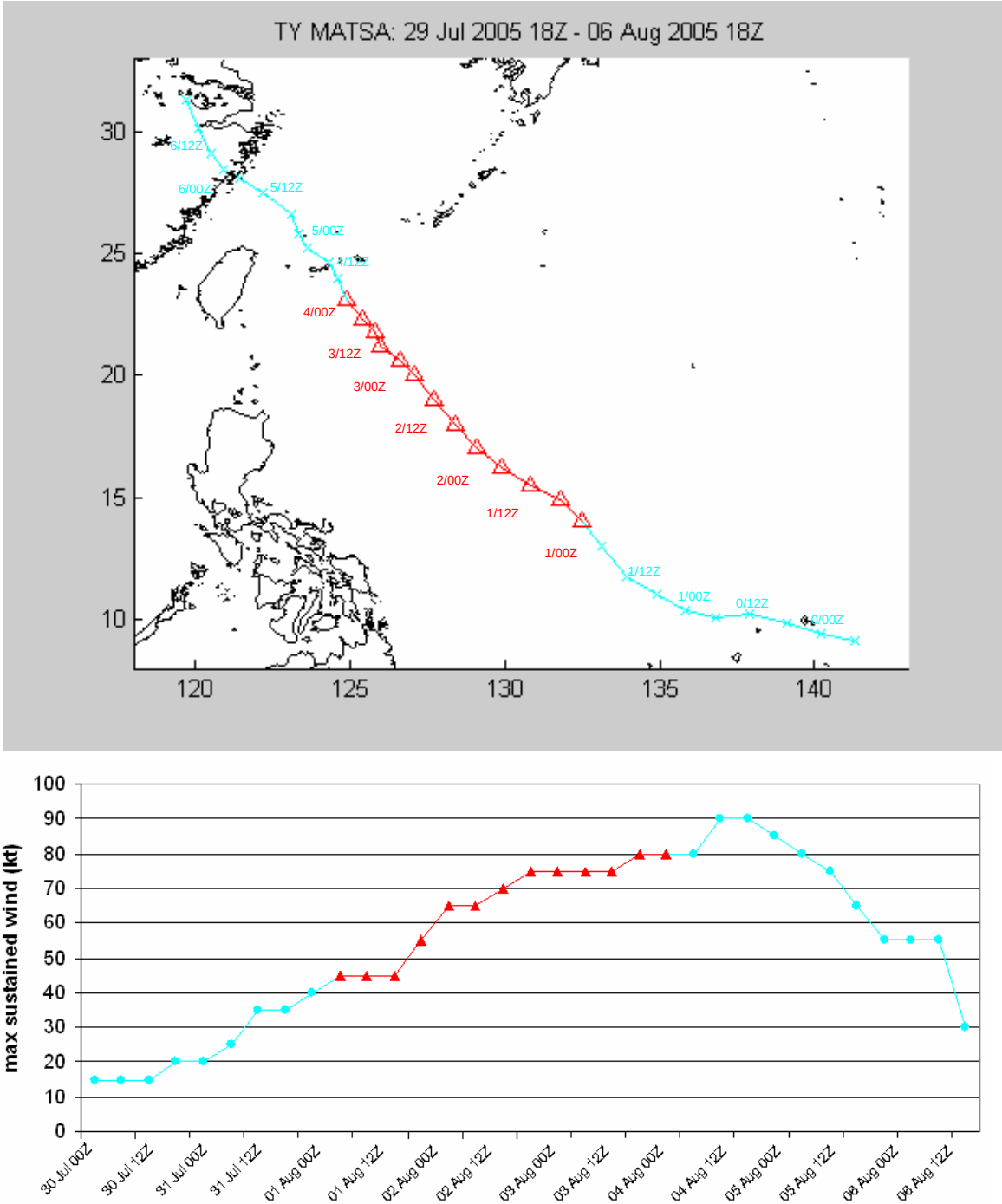

Figure 3.1 Observed track and intensity of Typhoon Matsa. Each point represents a 6-h increment. The triangular points in red indicate the period selected for the 72-h ARW integration.

One ARW integration was made for Typhoon Matsa beginning at 00 UTC 1 August. During the 72-h period covered by the integration, the storm was under the steering influence of a mid-level ridge to the east, and thus had a northwesterly track toward the coast of China. The storm intensity was constant for 12 h and then intensified by 20 kt in only 12 h to reach typhoon strength (65 kt sustained wind) at 00 UTC 2 August before intensifying more gradually through days two and three. Poleward outflow was inhibited by the presence of the ridge north of the storm, and convection was restricted in this region during days two and three (Figure 3.2).

This case presented as a fairly challenging intensity forecast, with alternating no, slow, or rapid intensification to moderate typhoon strength. The track prediction was less challenging because of the nearly straight trajectory to the northwest.

2. Typhoon Sanvu

Typhoon Sanvu began to develop on 8 August 2005 in a region of convection between Palau and the Philippines. The JTWC issued the first TC warning at 12 UTC 10 August when the circulation center was approximately 500 n mi east of the Philippines (Figure 3.3). The developing storm then moved along the southern periphery of the subtropical ridge (STR) in a west-northwesterly direction.

The 72-h ARW integration was initialized at 00 UTC 11 August, which was the time Sanvu first reached tropical storm strength. As with Typhoon Matsu just over a week before, poleward outflow north of the storm was inhibited by the STR to the north that was firmly in place from the western North Pacific to China. Due to the restricted outflow, Sanvu remained at minimal tropical storm intensity during day one of the ARW integration, although intense convection was still present in and around the eyewall (not shown). The center of the storm passed over the extreme northern edge of Luzon, Philippines, and over 12 in of rain was measured at one station on the small Batanese islands north of Luzon between 00 UTC 11 August and 00 UTC 12 August.

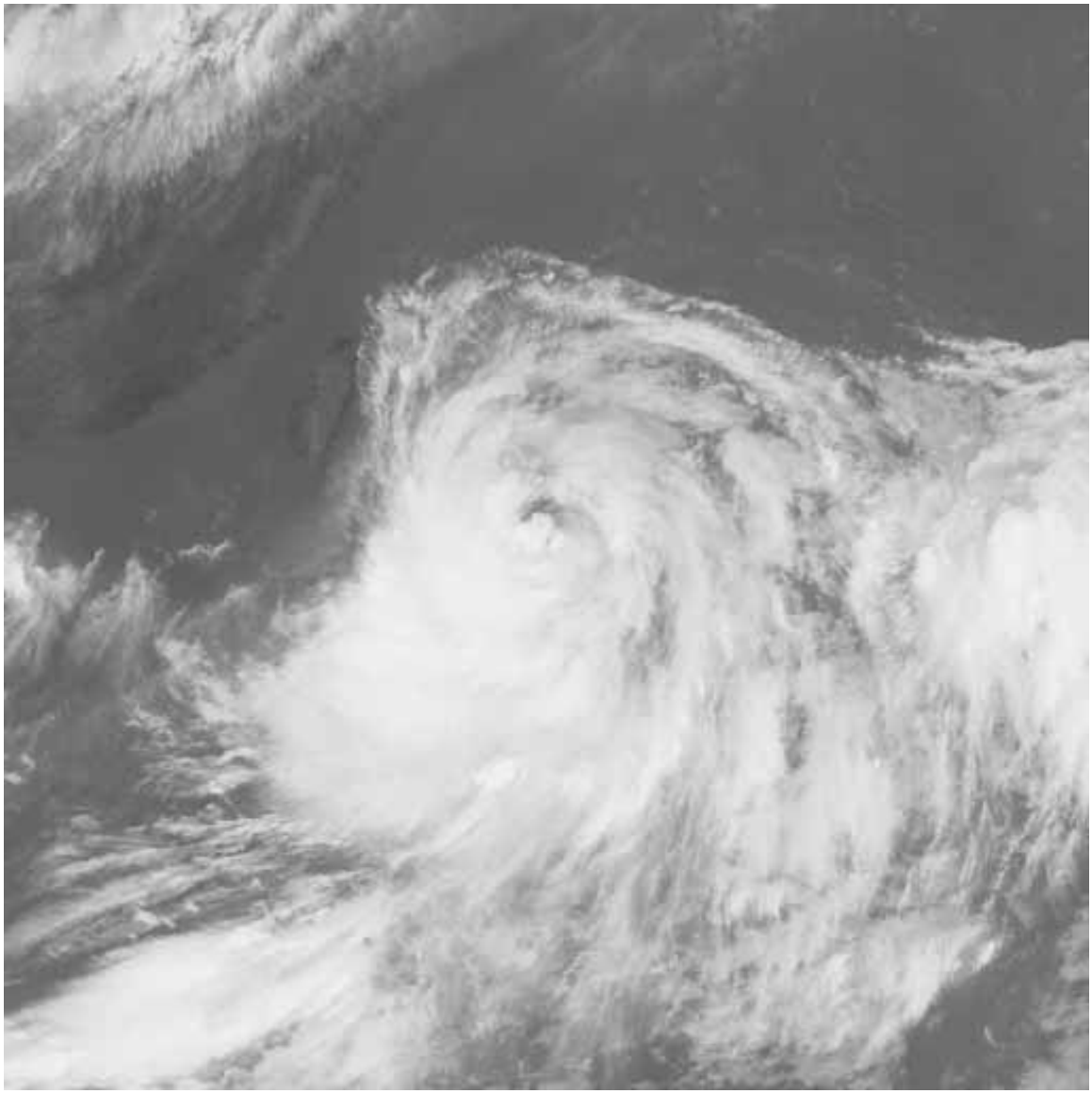

Figure 3.2 (From: Digital Typhoon website) Infrared satellite image of Typhoon Matsa at 03 UTC 3 August 2005. A mid-level ridge to the northeast of the storm likely suppressed convection in the northern half of the circulation and allowed only gradual intensification during this period. [Available online at http://agora.ex.nii.ac.jp/cgi-bin/dt/single2.pl?prefix=MTS105080403&id=200509&basin=wnp&t=0&b=14&lang=en&type=1&size=128 (current as of 31 Jan 2006)].

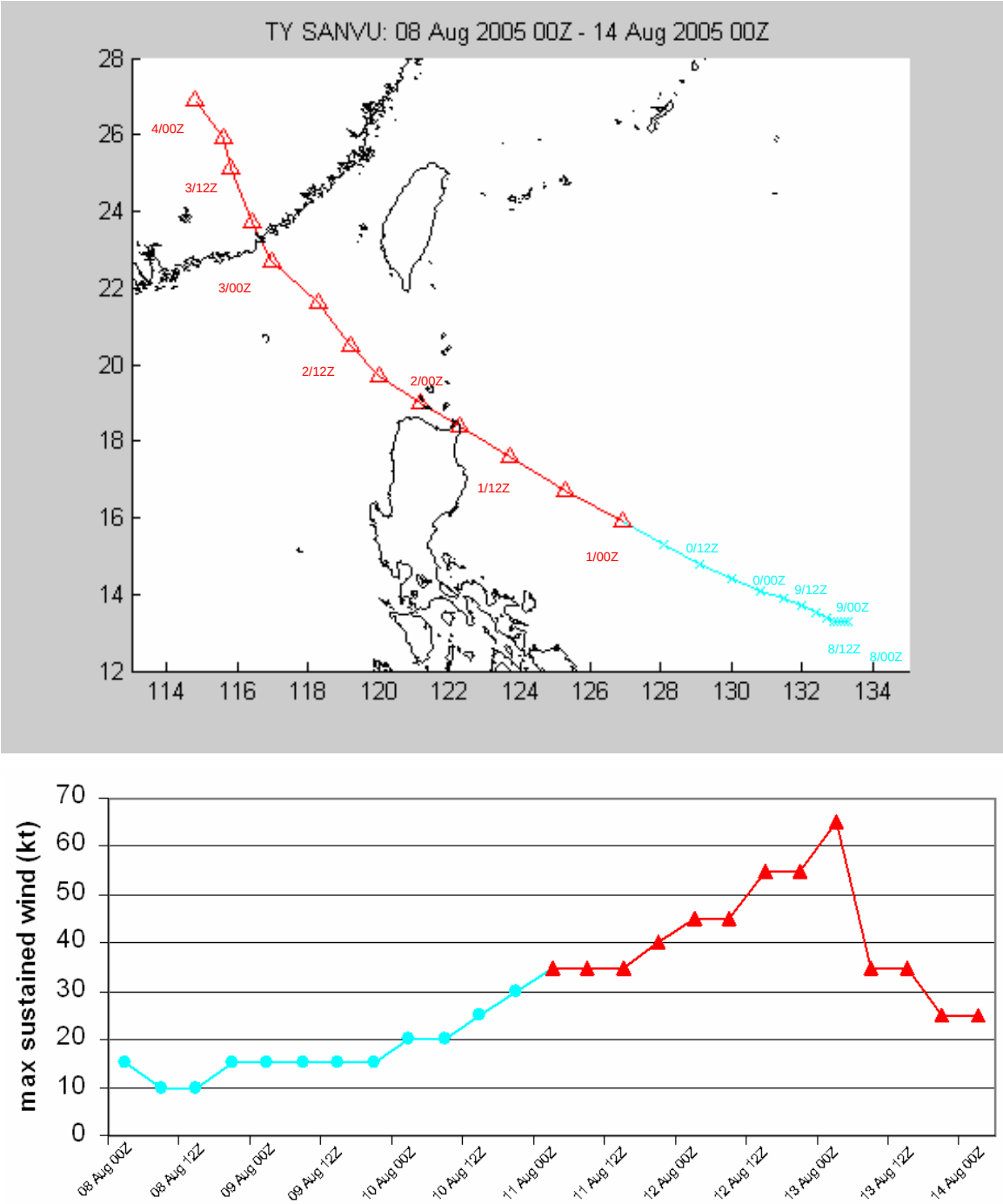

Figure 3.3 Identical to Figure 3.1, except for Typhoon Sanvu. As before, the triangular points in red indicate the period selected for the 72-h ARW integration.

Gradual intensification occurred on 12 August until Sanvu briefly reached typhoon strength at 00 UTC 13 August. It weakened to 55 kt sustained winds as it made landfall approximately 150 n mi east of Hong Kong around 06 UTC 13 August. Although the storm continued to rapidly weaken as it crossed mainland China, about 2,500 homes were flooded and at least two lives were lost.

In summary, the 72-h ARW integration included the intensification period, the “peaking out” of the TC, and the landfall and decay over China. This case differed substantially from the Typhoon Matsa case in that it represents a much slower intensification, and ultimately a much weaker typhoon. However, the track forecast was again easy since the track was nearly straight toward China.

3. Typhoon Mawar

Typhoon Mawar began to develop on 18 August roughly 200 n mi southeast of Iwo-jima. The JTWC issued the first TC warning at 12 UTC 19 August, and the storm reached tropical storm strength 6 hours later. Simultaneously, Tropical Storm Guchol was forming about 600 n mi to the east (Figure 3.4). According to Carr et al. (1997), normal-sized TCs with greater than 324 n mi (600 km) separation are not likely to alter the respective tracks of each other. However, it is possible that the upper-level outflow from the larger, more intense Mawar hindered the early development of Guchol. Eventually, Guchol drifted northeastward and intensified, but never reached typhoon strength. Although Guchol was not selected for this study, it is within the domain of the ARW integration of Typhoon Mawar.

The track and intensity of Typhoon Mawar are shown in Figure 3.5. The storm eventually made landfall near Tokyo, Japan with over 20 in of rain in 24 h and sustained winds of 54 knots (10-min average, which is the standard observing practice in Japan) with a gust of 107 kt. The storm took one life, threatened hundreds of homes with flooding and landslides, and forced the cancellation of 89 commercial flights. The storm was declared extratropical on 27 August.

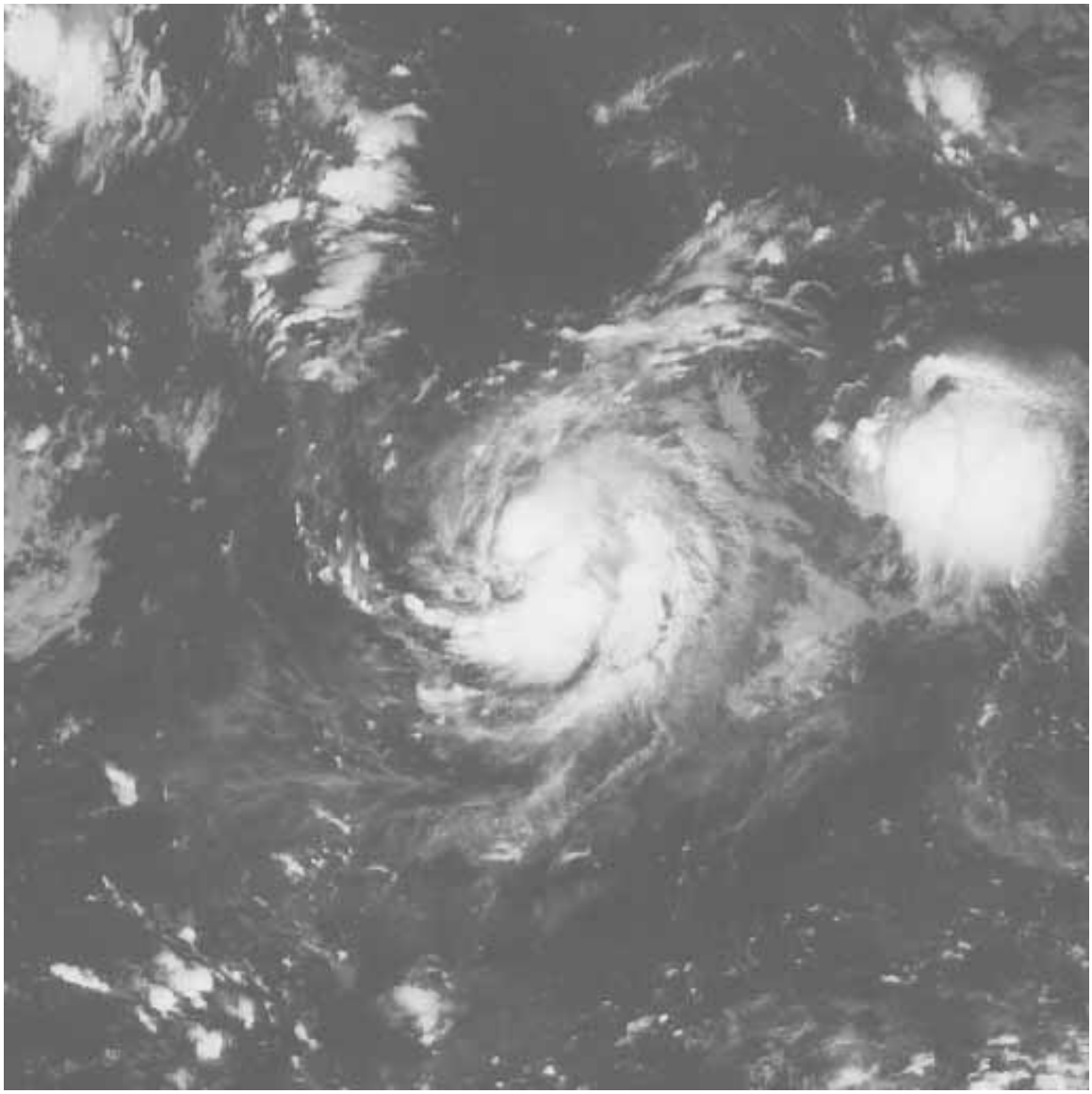

Figure 3.4 (From: Digital Typhoon website) Infrared satellite image of Tropical Storm Mawar (center) and the seedling convection of what would become Tropical Storm Guchol (right side) at 18 UTC 19 August 2005. With a separation of 600 n mi, the two circulations were too far apart to affect the respective tracks of each. [Available online at http://agora.ex.nii.ac.jp/digital-typhoon/summary/wnp/s/200511.html.en (current as of 1 Feb 2006)].

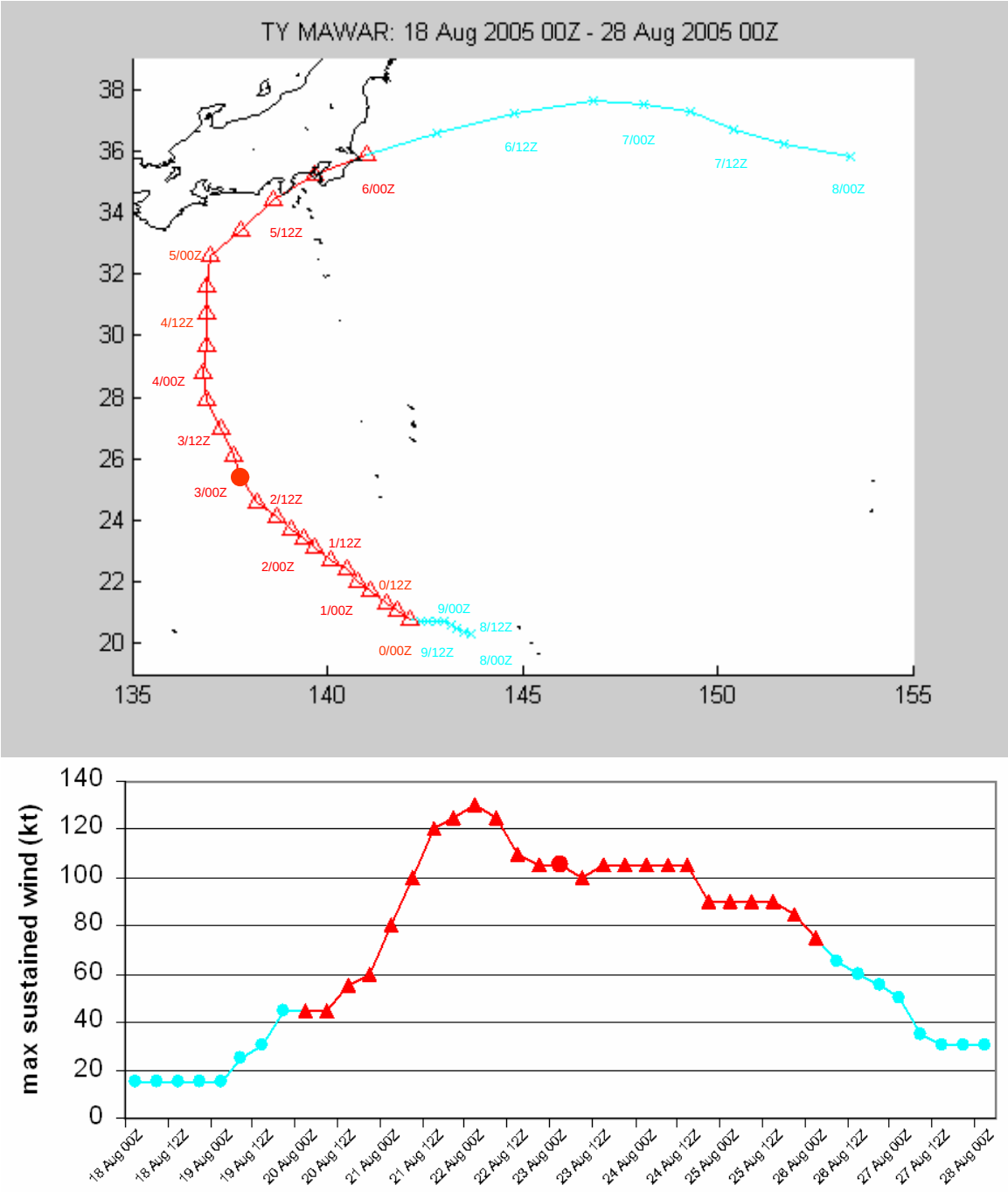

Figure 3.5 As in Figures 3.1 and 3.3, except for Typhoon Mawar. The red triangular points represent the period covered by the two 72-h ARW integrations. The large red dot indicates the ending time of the first integration and the initialization time of the second integration.

Two 72-h ARW integrations were performed for this storm. The first integration was initialized at 00 UTC 20 August and was intended to capture the rapid intensification observed on 21 August. On day one of this integration, Mawar was in a particularly weak steering environment, and was drifting slowly to the northwest along the southwestern periphery of the STR. Intensification began late on day one, and the storm reached typhoon strength at 00 UTC 22 August. Rapid intensification was observed on day two as the storm passed approximately 200 n mi south of Iwo-jima and continued slowly to the northwest. On day three, the storm progressively weakened, but still remained a strong typhoon with sustained winds of 105 kt through the end of the integration.

None of the six intensity prediction techniques included in the study by Blackerby (2005) showed useful skill in predicting rapid intensification. This case was selected to not only test the ARW ability in this regard, but the typhoon also was quite intense as it recurved before finally decreasing in intensity near the end of the integration.

The second integration for this storm initialized at 00 UTC 23 August included the period during which Typhoon Mawar made landfall in Japan around 18 UTC 25 August. On day two of the run, the storm turned to a northward track, and then turned to a northeastward track on day 3.

Although several other cases in this study involved a landfall, this case was noteworthy because it affected large United States military installations near Tokyo. Yokota Air Base west of Tokyo received roughly 3.7 inches of rain over 48 h with sustained winds of 26 kt and a gust of 40 kt. In summary, this second integration involved a recurving, slowly-decaying storm at high latitude that is an important forecast problem when a typhoon may affect large coastal population centers and military installations at latitudes above 30°.

4. Typhoon Talim

The convection in the monsoon trough that eventually developed into Typhoon Talim began approximately 300 n mi east of Guam and persisted for several days before showing signs of organizing into a TC. During the early

stages of development, the storm drifted west-southwestward and passed just south of Guam (Figure 3.6). Eventually the storm would organize, and the JTWC issued the first TC warning at 06 UTC 26 August.

As with Typhoon Mawar, Talim offers several challenging aspects for the ARW predictions, and two 72-h integrations were made. The first integration was initialized at 00 UTC 27 August, which was the time Talim reached tropical storm strength. Talim steadily intensified on day one as it moved northwestward along the southwestern periphery of the STR. It reached typhoon strength on day two (06 UTC 28 August) at about 700 n mi southeast of Okinawa. The storm turned to a more westerly direction late on day two while continuing to intensify. During the final six hours of the integration, Talim was at peak intensity with estimated sustained winds of 125 kt.

In addition to the rapid intensification aspect on both day two and day three, this case also included a challenging track change, which was an opportunity to evaluate the skill of the ARW in predicting changes in steering influences.

The second 72-h integration was initialized at 12 UTC 29 August, which was just prior to the period of peak intensity. Typhoon Talim remained very intense through day one, but began to weaken late on 30 August. Before making landfall in Taiwan around 18 UTC 31 August, it passed just south of the Yaeyama Islands of Japan, where over six inches of rain, sustained winds of 74 kt (10-min average), and gusts to 112 kt were observed. On Taiwan, seven deaths were reported, 1.7 million people lost power, and 48,500 households lost running water due to flooding and wind damage to trees and power lines. Talim was downgraded to a tropical storm at 06 UTC 1 September, and subsequently entered the Chinese mainland, where it took 110 lives including 40 in a massive landslide. Crossing Taiwan and coastal mainland China weakened the storm substantially, and the final warning was issued by the JTWC at 12 UTC 1 September.

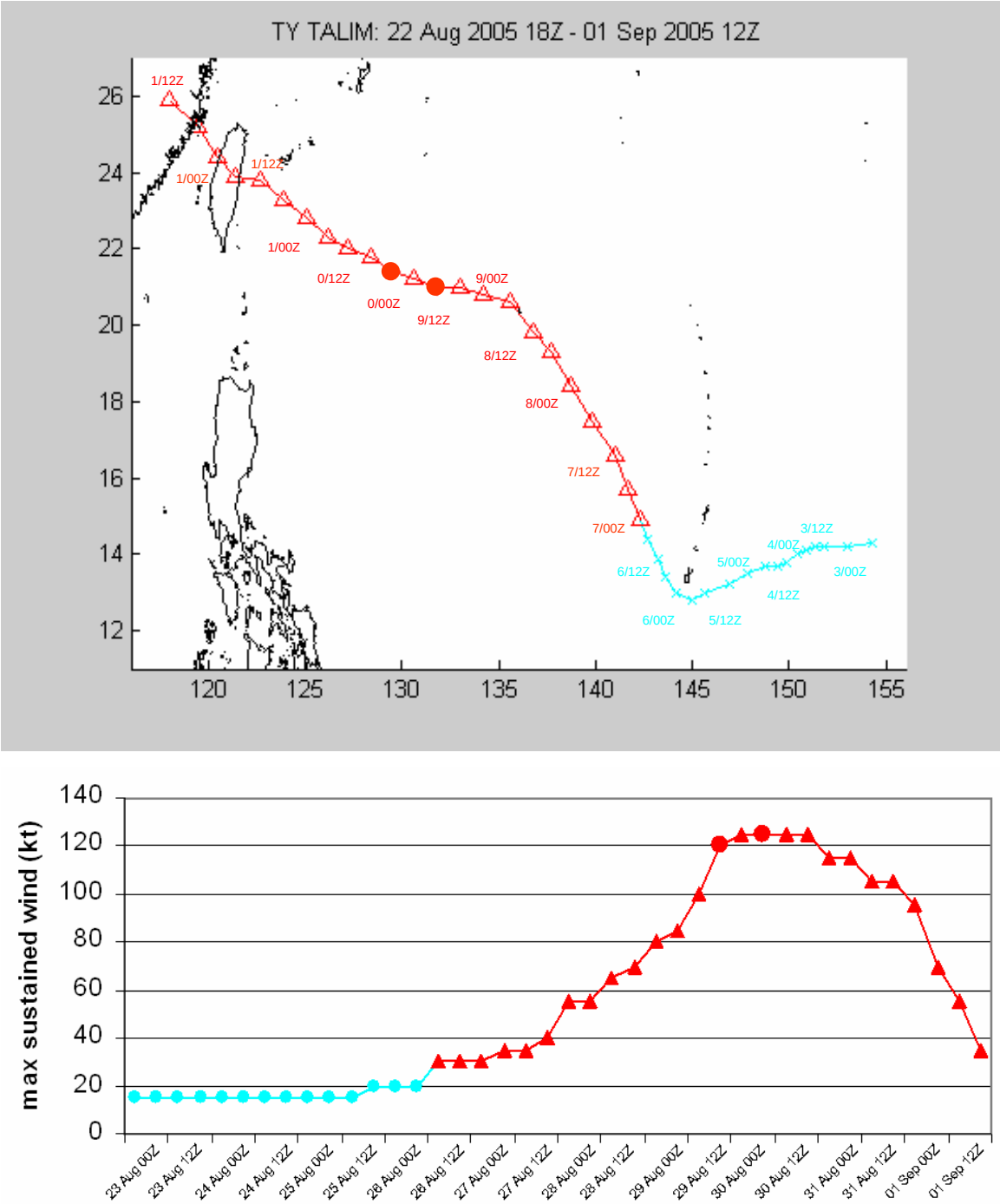

Figure 3.6 As in Figure 3.5, except for Typhoon Talim. The red triangular points represent the period covered by the two 72-h ARW integrations. The first large red dot indicates the initialization time of the second integration. The second large red dot indicates the ending time of the first integration.

The second integration for Typhoon Talim allowed evaluation of AWR skill for a decaying storm. This case was initialized at near peak intensity, and began decaying even before landfall on Taiwan. Rapid decay, which is defined here as a decay rate of at least 30 kt/day (Blackerby 2005), was observed after landfall on Taiwan.

5. Typhoon Nabi

Typhoon Nabi affected the Mariana Islands on 31 August, produced 65 kt sustained winds on Saipan, and dumped over 6 in of rain on Andersen Air Force Base, Guam. Typhoon Nabi had a classic recurvature path through the western North Pacific, which made it another appealing TC for ARW prediction evaluation (Figure 3.7). Ultimately, Typhoon Nabi struck mainland Japan with an intensity of 90 kt.

The seedling convection that became Nabi began approximately 600 n mi east of Guam and drifted westward until the first TC warning from the JTWC at 06 UTC 29 August. Under the influence of a mid-level ridge southeast of mainland Japan, the storm continued to move in the easterly steering flow south of the ridge at 5-10 kt. Nabi reached tropical storm strength at 18 UTC 29 August.

An initialization time of 12 UTC 30 August was selected for the first ARW integration for this storm, which coincided with the time Nabi reached typhoon strength. At this time, the storm was roughly 100 n mi east-southeast of Saipan and was about to turn slightly to a west-northwest heading. At 03 UTC 31 August, Nabi passed less than 50 n mi northeast of Saipan.

Typhoon Nabi had a nearly continuous intensification throughout the first integration period. During day one, the intensity increased 40 kt, which satisfies the definition for rapid intensification. Nabi continued to intensify on day two, although not quite as rapidly as on day one. The storm peaked on day three of this integration and slightly weakend late on 1 September, although still maintaining Supertyphoon intensity (≥130 kt).

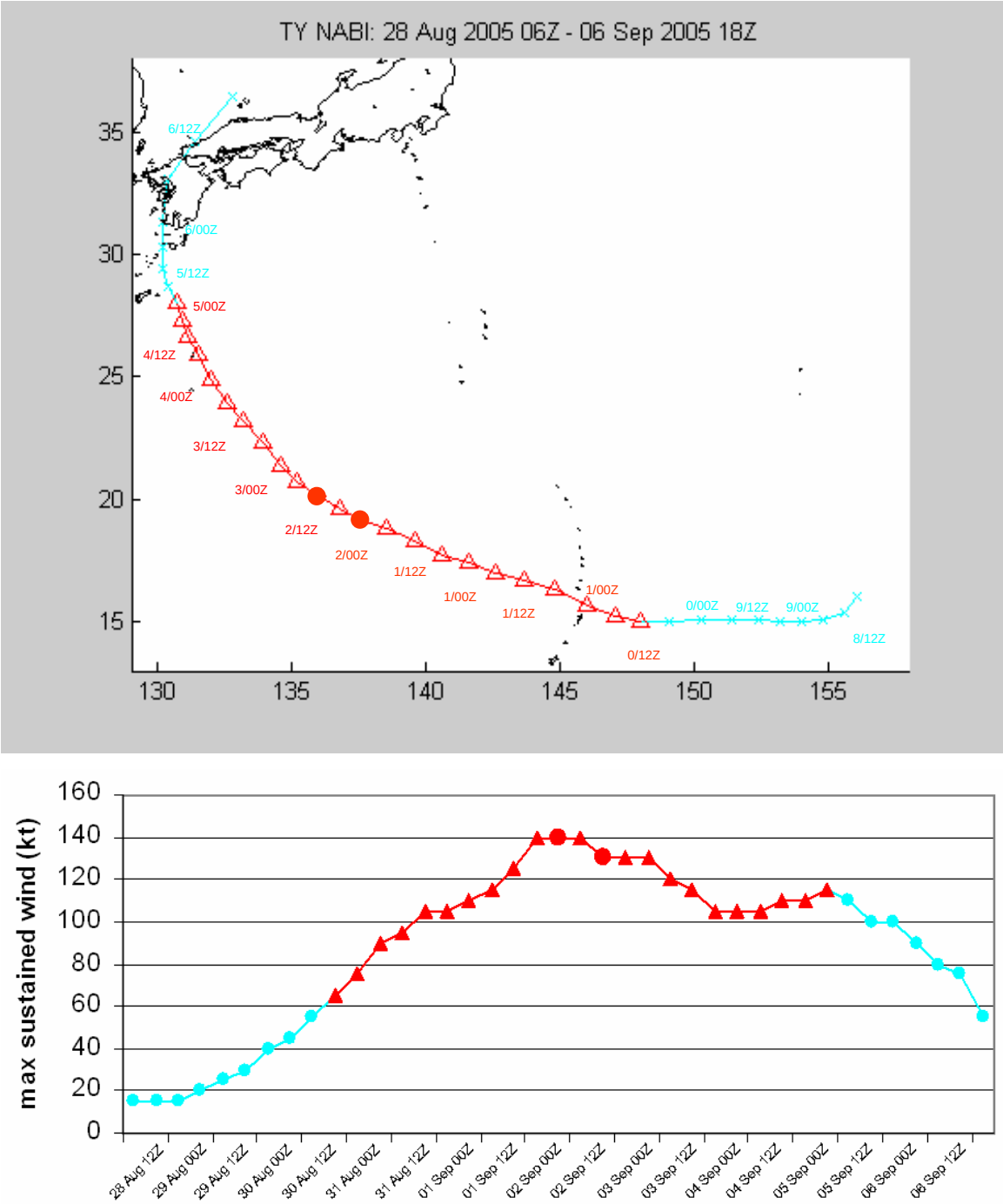

Figure 3.7 As in Figures 3.5 and 3.6, except for Typhoon Nabi. The red triangular points represent the period covered by the two 72-h ARW integrations. The first large red dot indicates the initialization time of the second integration. The second large red dot indicates the ending time of the first integration.

A second ARW integration was selected for this storm with an initialization at 00 UTC 2 September, which was the time of maximum intensity. Nabi gradually weakened on days one and two of this integration before slightly re-intensifying to an intensity of 105 kt late on 3 September. At this time, a mid-latitude trough moving off eastern China forced the mid-level ridge southeast of Japan to retreat eastward. Thus, the steering winds for Typhoon Nabi became northward during day three. The integration ended at 00 UTC 5 September, when the storm was approximately 200 n mi from making landfall on Kyushu Island, Japan.

Whereas one challenge for the second AWR prediction is the directional changes of the TC due to interaction with a mid-latitude feature, another challenge is the slight re-intensification. Blackerby (2005) and Lambert (2005) demonstrated that decay and re-intensification cycles are almost never accurately predicted.

6. Typhoon Khanun

The development and progression of Typhoon Khanun (Figure 3.8) closely resembled that of Typhoon Matsa (Figure 3.1). Similar to Matsa, Khanun originated from convection approximately 600 n mi southwest of Guam and began drifting to the west under the weak steering influence of an upper-level ridge to the north. The first TC warning by the JTWC was on 6 September, and Khanun reached tropical storm strength the same day. Unlike Matsa, Typhoon Khanun struck mainland China with sustained winds of 90 kt and took at least 14 lives.

Some subtle track changes during the slow intensification from 7 September to 10 September were the focus of the first ARW integration, which was initialized at 00 UTC 7 September. Although this subtle weaving pattern with an amplitude of 1-2 d was also apparent with Matsa, Khanun had developed into a more intense storm during this period and had reached typhoon strength at 12 UTC 8 September. The overall intensification of this storm was far from rapid, but it was still an interest along with evaluating the track prediction.

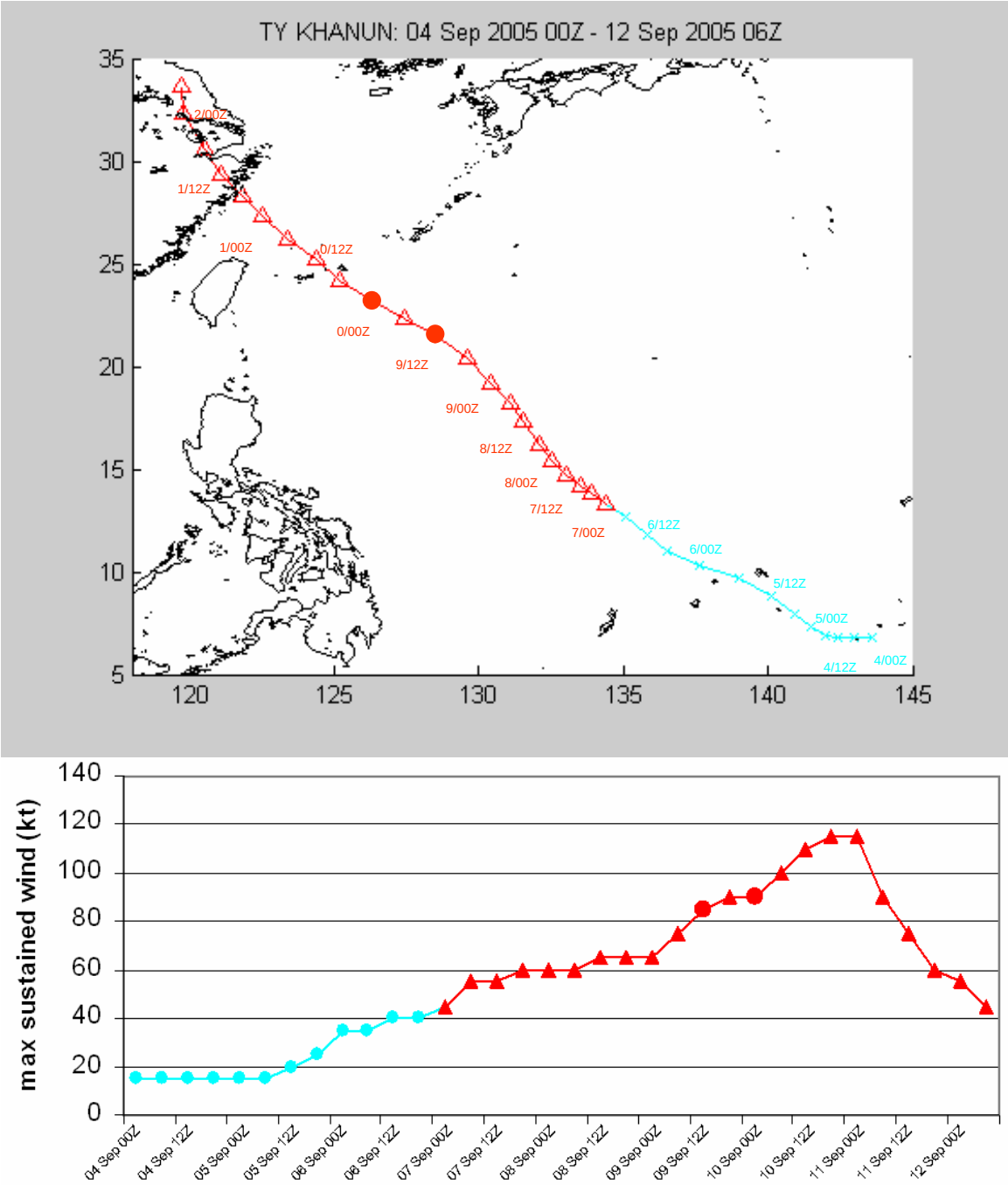

Figure 3.8 As in Figures 3.5, 3.6, and 3.7, except for Typhoon Mawar. The red triangular points represent the period covered by the two 72-h ARW integrations. The first large red dot indicates the initialization time of the second integration. The second large red dot indicates the ending time of the first integration.

A second integration was initialized at 12 UTC 9 September and covered the remainder of the lifecycle of the storm as a TC (the JTWC issued the last warning at 06 UTC 12 September, so the integration was only evaluated for 66h). During this period, Khanun continued to intensify at a moderate rate and reached 115 kt sustained winds late on 10 September just before making landfall in China. This is a significantly more intense storm than the 90 kt peak intensity of Typhoon Matsa, even though they had nearly identical tracks. As indicated in Chapter III.B.1, Matsa began weakening well before making landfall in China as a result of the continued impingement of the mid-level ridge to the north and east. By contrast, convection in the northern half of Typhoon Khanun was not suppressed prior to landfall (Figure 3.9). One objective is to evaluate how well the ARW predicted this lack of a mid-level ridge and continued the intensification.

The second ARW integration continued for 21 h after the typhoon was observed to make landfall and decay rapidly while remaining on a gently curving track toward the north with no abrupt changes. Aside from the Sanvu case (Figure 3.3), which had an irregular track after reaching China, this was the longest period of integration after landfall, and potentially offers the best opportunity for evaluating the ARW predictions for TC decay over land.

C. INITIALIZATION, BOUNDARY CONDITIONS, AND MODEL OUTPUT

1. Initialization

a. ARW

The outer nest, which does not move in time, covers most of the western North Pacific below 50° latitude, and a large portion of Southeast Asia. This domain has 720 gridpoints east to west and 468 gridpoints north to south with a uniform spacing of 12 km. This domain was large enough to keep any of the TCs from approaching the outer boundaries during the integration periods, which was important to avoid the inner nest solution from being contaminated near these boundaries (see Warner et al. 1989).

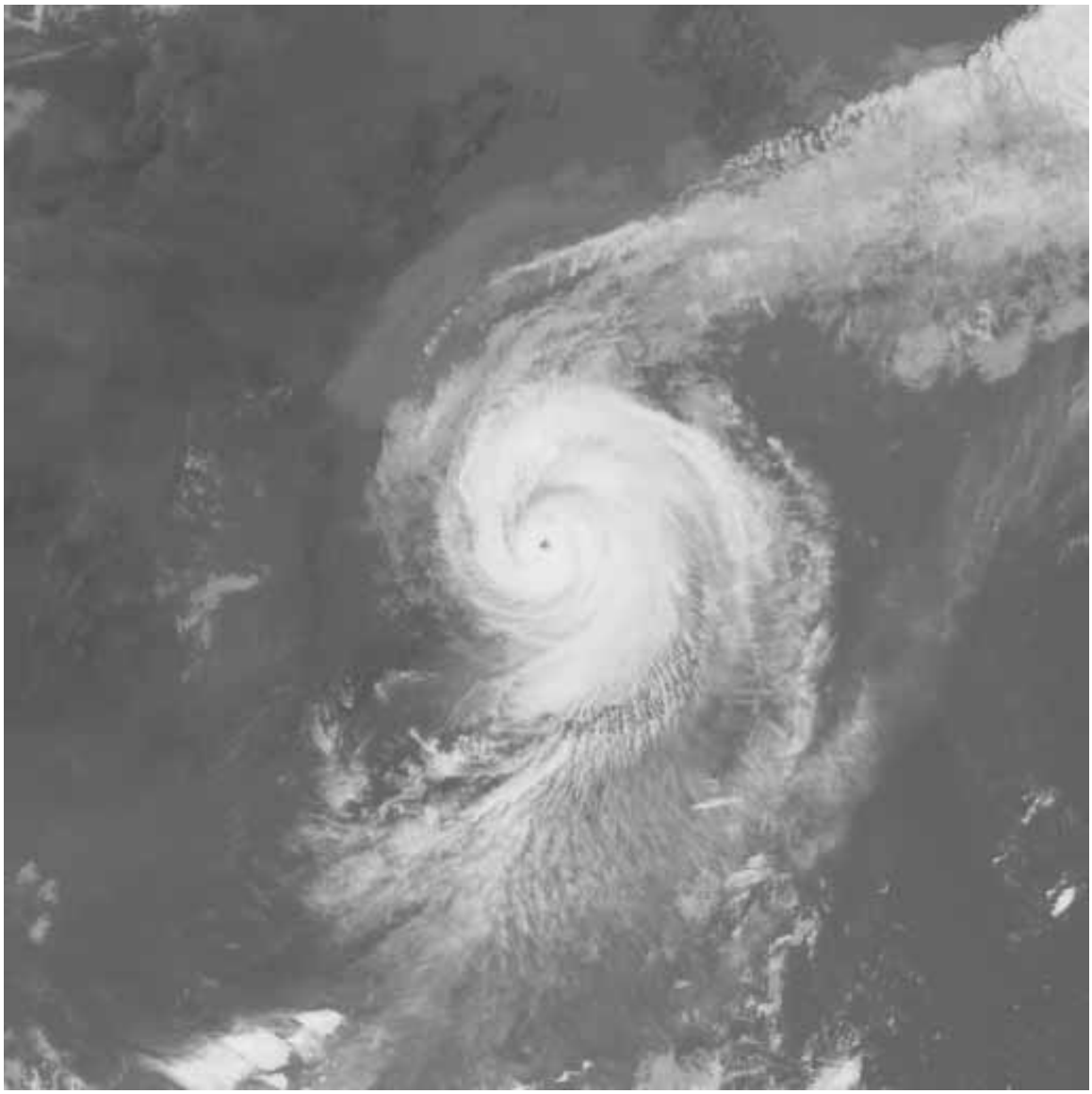

Figure 3.9 (From: Digital Typhoon website) Infrared satellite image of Typhoon Khanun at 03 UTC 11 September 2005. In contrast to Typhoon Matsa in Figure 3.2, convection was not hindered by the presence of a ridge to the north and east, and Typhoon Khanun continued to intensify until landfall in China [Available online at http://agora.ex.nii.ac.jp/digital-typhoon/summary/wnp/s/200515.html.en (current as of 4 Feb 2006)].

The inner nest had a 300 x 300 domain with gridpoint spacing of 4 km. The initial location of the inner nest was centered on the estimated position of the low-level vortex from the JTWC warning. The domains of both grids for the initialization time of the Typhoon Matsa case are shown in Figure 3.10.

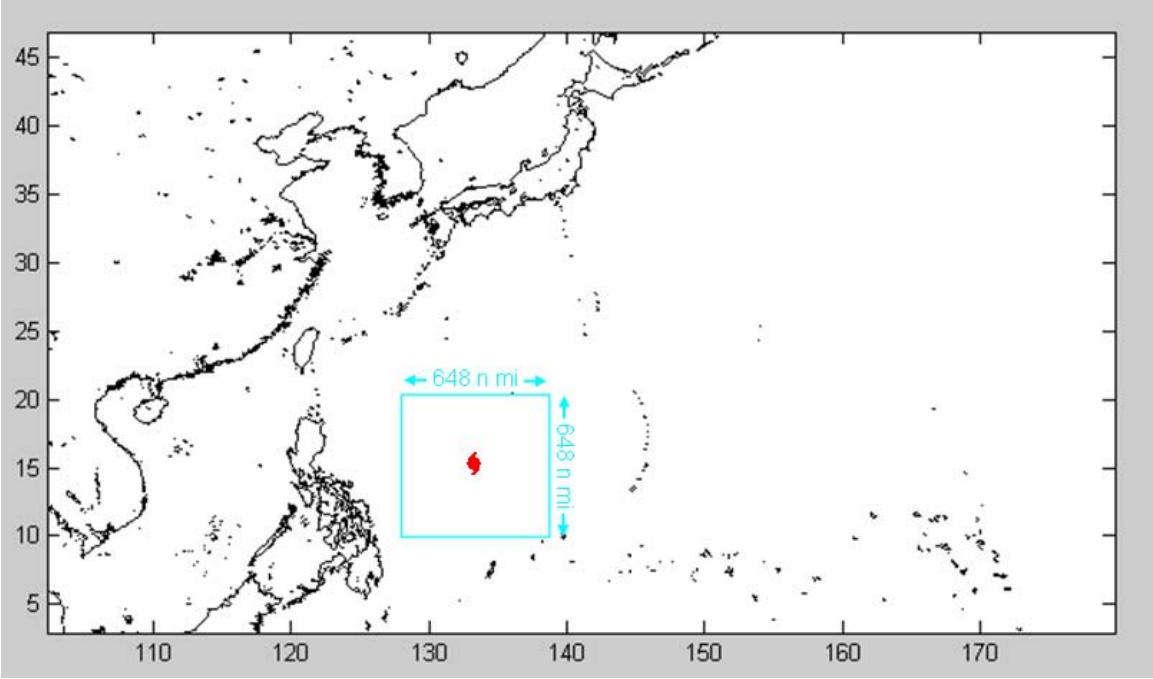

Figure 3.10 The domain of the parent grid, which is stationary, and the nested grid, which is initially positioned manually but then is programmed to automatically follow a vortex, for the initialization of the Typhoon Matsa case. The nested grid was placed in a manner so that it is centered on the storm vortex (red TC symbol).

The ARW was initialized using a “cold start” procedure. That is, the fields from several sources are interpolated directly to the ARW grid at the initialization time, rather than being part of an analysis-forecast-analysis cycle on the ARW grid. The input fields for atmospheric parameters were obtained from the 00-h initial fields of the 1/2° lat./long. resolution NCEP Global Forecast System (GFS). The program “WRF Standard Initialization” (WRF SI) combines the GFS fields with the SST and land-use fields (the origins of the SST and land-use fields are explained in Chapter II.A.2) to obtain the “first-guess” fields for the

ARW. These first-guess fields were updated with observations using a Three-Dimensional Variational Data Assimilation (3DVAR). This 3DVAR incorporates data from radiosondes, aircraft reports, surface observations, and satellite-based measurements valid within one hour before or after initialization time. These observations are blended with the first-guess fields by the 3DVAR technique to achieve the initial ARW fields.

b. MM5

The MM5 predictions used for comparison in this study were from the operational version that is initialized with a "warm start" approach. In this procedure, a preliminary MM5 integration is initialized with a start time 6 h prior to the initialization time for the operational MM5. The first-guess fields for this preliminary integration are obtained from the GFS fields (in this case 1° lat./long. resolution), which are interpolated to the 15 km MM5 grid. However, the GFS wind and mass fields near the TC vortex are replaced with a "bogus vortex" that is "spun-up" from an axisymmetric TC model to achieve the estimated maximum wind speed provided by the JTWC (Low-Nam and Davis 2001). This bogus vortex provides a significant enhancement of storm structure compared to that provided by the low-resolution GFS fields. The position of the vortex is located near the observed position of the TC.

The MM5 fields are combined with the SST and land-use fields, and updated with observations using the 3DVAR. A 6-h integration then provides the first-guess at the desired initial time, and this first-guess is blended with observations using the 3DVAR to provide the initial fields for the operational MM5 integration (personal communication, 3 February 2006, Roy Peck AFWA).

c. Important Differences

Interpolating a lower-resolution GFS analysis to a higher-resolution grid such as the MM5 or ARW may lead to unbalanced mass and wind fields, particularly in areas of large gradients. In most cases, the warm-start approach of the MM5 model is favored over a cold start because these imbalances are geostrophically adjusted during the 6-h pre-integration period. In addition, the

precipitation is “spun-up” during the six hours of integration prior to actual initialization. In a cold start used for the ARW, the imbalances must be geostrophically adjusted and precipitation must be spun-up during the first few hours of the actual model integration. It is generally advantageous to let this model spin-up occur in the preliminary integration rather than during the first few hours of the operational model integration.

In some instances, a cold start may yield superior results [see COMET Module “How Mesoscale Models Work”. Available online at http://meted.ucar.edu/mesoprim/models/print.htm (current at of 3 Feb 2006)]. For example, errors originating during the preliminary integration may not be rectified in regions with sparse observations, and these errors will be continued during the real integration. Although satellite data are available for the western North Pacific, the observational network is very sparse and may favor a cold-start approach. In this study, the GFS fields that are used to initialize the ARW have 1/2° lat./long. resolution, which is twice the resolution of the GFS fields used to initialize the MM5 integrations, and may reduce the possible advantage of a warm start. Finally, cold-start integrations were found to produce admirable track forecasts for Hurricane Wilma in 2005 during preliminary testing in the Gulf of Mexico. As of late October 2005, AFWA is favoring a cold-start configuration when the ARW becomes operational for TC prediction (personal communication, 21 October 2005, Steve Rugg AFWA/DNXM).

Using a bogus vortex is another technique to effectively reduce the spin-up problem of circulations near a TC vortex, which have a scale smaller than can be adequately captured by a lower-resolution initialization model such as GFS (Leslie and Holland 1993). Although use of a bogus vortex (or “synthetic TC observations”) is common in most operational models for TC prediction, AFWA decided not to use a bogus vortex in these ARW integrations. Part of the justification for this decision was that the 1/2° resolution GFS field for the ARW integrations is double that used by the MM5, which might provide a better representation of TC structure, and possibly make a bogus vortex unnecessary.

One of the objectives of this study is to gain insight as to whether a bogus vortex will be required when ARW version 2.1 becomes operational.

One advantage of using a bogus is to more precisely position the TC vortex. Thus, a bogus likely provides a substantial advantage for a short-term position forecast. However, Serrano and Undén (1994) found bogusing actually had a negative effect on medium-range model forecasts, so the European Center for Medium-range Weather Forecasts still does not insert a bogus vortex.

2. Boundary Conditions

A description of the boundary conditions of the inner nest is provided in Chapter II.A.3. Both the ARW and MM5 models receive boundary conditions for the outer nest from the same source as their initial fields (1/2° lat./long. GFS for the ARW, 1° lat./long. GFS for the MM5). These lateral boundary conditions are updated every three hours during the integration. The boundary conditions used in the ARW integration were from the GFS integration initialized at the same time as the ARW integration, and thus do not represent an operationally viable scenario. In the operational MM5 approach, the lateral boundary conditions are interpolated from a prior GFS integration so that no delay is necessary to await the completion of the GFS integration to begin the MM5 integration. Using “on-cycle” boundary conditions, as in the ARW, is not believed to provide an appreciable advantage for TC prediction (Vigh et al. 2003). However, the higher horizontal resolution of the boundary conditions for the ARW may provide a better forecast.

IV. RESULTS

A. LARGE ERRORS ARISING FROM NEST MOVEMENT ALGORITHM

In most numerical models, the vortex tracker algorithm is used simply to extract the latitude and longitude of a TC within the model domain. However, the tracking algorithm in the ARW also determines the movement of the high-resolution inner nest that is necessary to keep the TC and its large gradients near the center of the nest. The GFS and MM5 have vortex tracker algorithms that mainly use low-level features to identify the TC location (Marchok 2002, Hausman 2001). In the COAMPS, which has a moving-nest feature, the vortex tracker and nest position are based entirely on the sea-level pressure field (Liou and Jin 2004).

The mature TC structure will have a vertically stacked configuration. If all TCs had this structure, the ARW algorithm that links the movement of the nest to the 500-mb geopotential height minimum would seem to be adequate (for a complete description of the ARW nest-moving algorithm, see Chapter II.A.3).

In three of the 10 cases in this study, the ARW algorithm based on the 500-mb height minimum failed to appropriately move the nest with the TC and lost track of the storm vortex. This situation is depicted in Figure 4.1 for one of the three cases (first Typhoon Mawar integration). At the start of this integration, an area of unorganized convection existed well to the southeast of Typhoon Mawar near 9°N, 149°E (indicated by a “D” in Figure 4.1). About halfway through the integration, the ARW began developing this convection into a TC. Eventually, this spurious TC was predicted to develop into a typhoon-strength TC and move to the northwest (location depicted in Figure 4.1 as a purple TC symbol). The inner nest (teal squares in Figure 4.1) correctly followed Typhoon Mawar for the first day or so, but by day three the nest was being incorrectly moved southward toward the stronger spurious TC to the south. By the end of the integration, Typhoon Mawar was completely outside the domain of the inner nest.

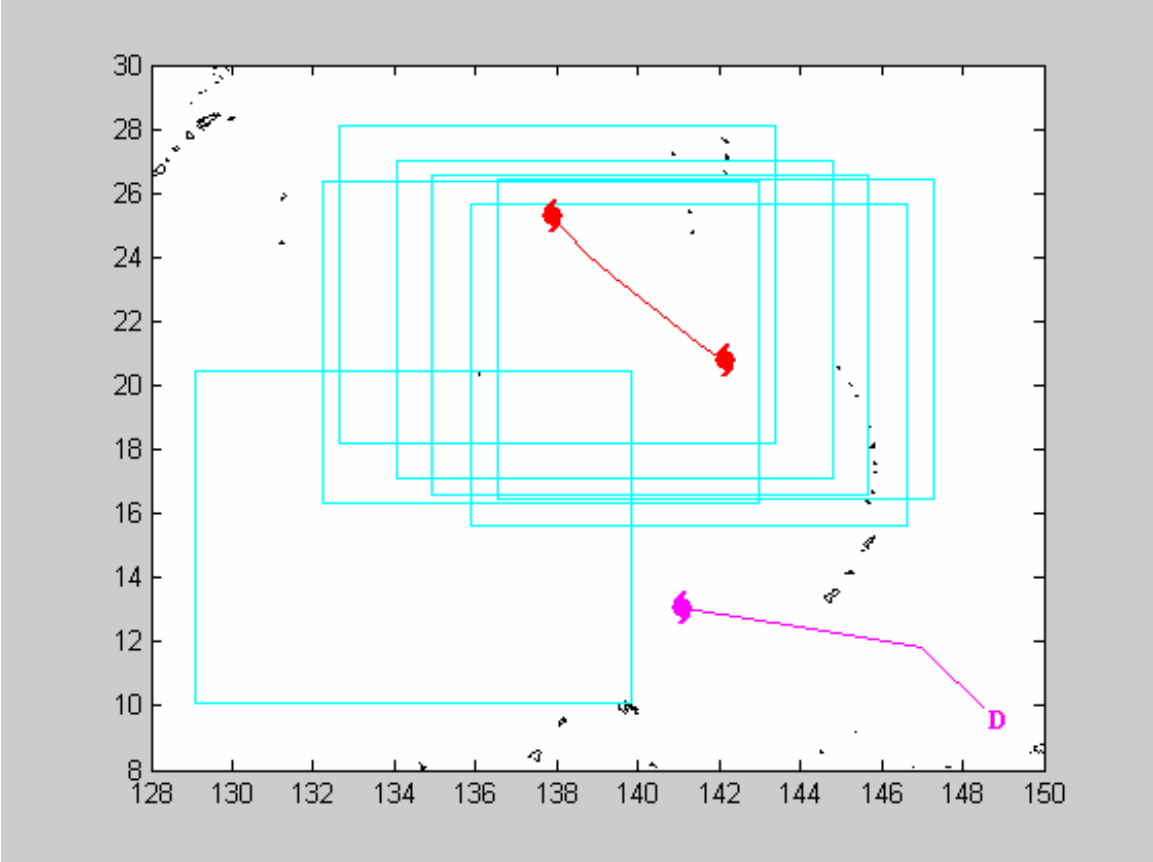

Figure 4.1 Depiction of the erroneous drifting of the ARW nest during the first Typhoon Mawar case that was initialized at 00 UTC 20 August 2005. The red TC symbols indicate the beginning (center right) and ending (upper left) position of Typhoon Mawar during the 72-h integration. The purple TC symbol indicates the ending position of a spurious TC that was generated during the integration. The inner nest, whose boundaries are shown in teal squares in 12-h increments, was drawn towards the stronger TC to the south and eventually became displaced from Mawar. The nest position in the lower left corresponds to the end of the integration.

Although the erroneous movement of the nest in this case may not have happened if it was not for the spurious TC development to the south, this scenario illustrates a limitation of the ARW nest movement algorithm that could occur in similar situations, whether the secondary TC is real or not. Even if the nest had been tracking low-level features (such as the minimum sea-level pressure), it may have not prevented the error in this case since the southern TC was significantly stronger. However, a tracking algorithm following the 500-mb

height minimum was especially problematic during the early stages of this integration when Mawar did not have a low pressure center through a deep layer in the atmosphere. At the beginning of this integration, Mawar had an intensity of only 45 kt and did not yet have a large pressure perturbation on the 0.4940 sigma-p level (not shown). Even before the nest moved completely away from the vortex of Mawar, it had been drifting off course, possibly as it was being re-located toward a localized height minimum caused by strong convection occurring nearby. This drifting conceivably could have been decreased if movement of the nest had been tied to the reasonably well-defined sea-level pressure minimum of Mawar, and may not have drifted toward the southern TC and away from Mawar.

The other two cases involving the nest losing the position of the original vortex were the Typhoon Sanvu case (Figure 3.3) and the first Typhoon Khanun case (Figure 3.8), and both of these integrations were also initialized early in the life cycle of the storms when the intensities were only 35 kt and 45 kt, respectively. The erroneous tracks provided by the ARW vortex tracker and the observed TC tracks for all three of these “bad tracker” cases are shown in Figure 4.2. In the Sanvu and first Khanun integrations, the nest drifted away from the intended TC vortex toward an area around the Philippines. This nest movement could be due to a 500-mb low associated with convection occurring there, an interpolation error caused by steep terrain gradients, or some other reason. Regardless of the reason, the experience with these three ARW integrations is that for weak TCs the present ARW nest-moving algorithm needs to be revised.

Wei Wang (personal communication, 5 January 2006) of NCAR confirmed that the nest-moving ARW was designed for well-developed, well-defined TCs, and is not likely to work well with developing storms. Wang also observed that the nest-moving algorithm had difficulty with TCs at high latitudes, which could occur when a TC encounters strong mid- or upper-level mid-latitude winds that cause the 500-mb height minimum to be displaced from the low-level circulation.

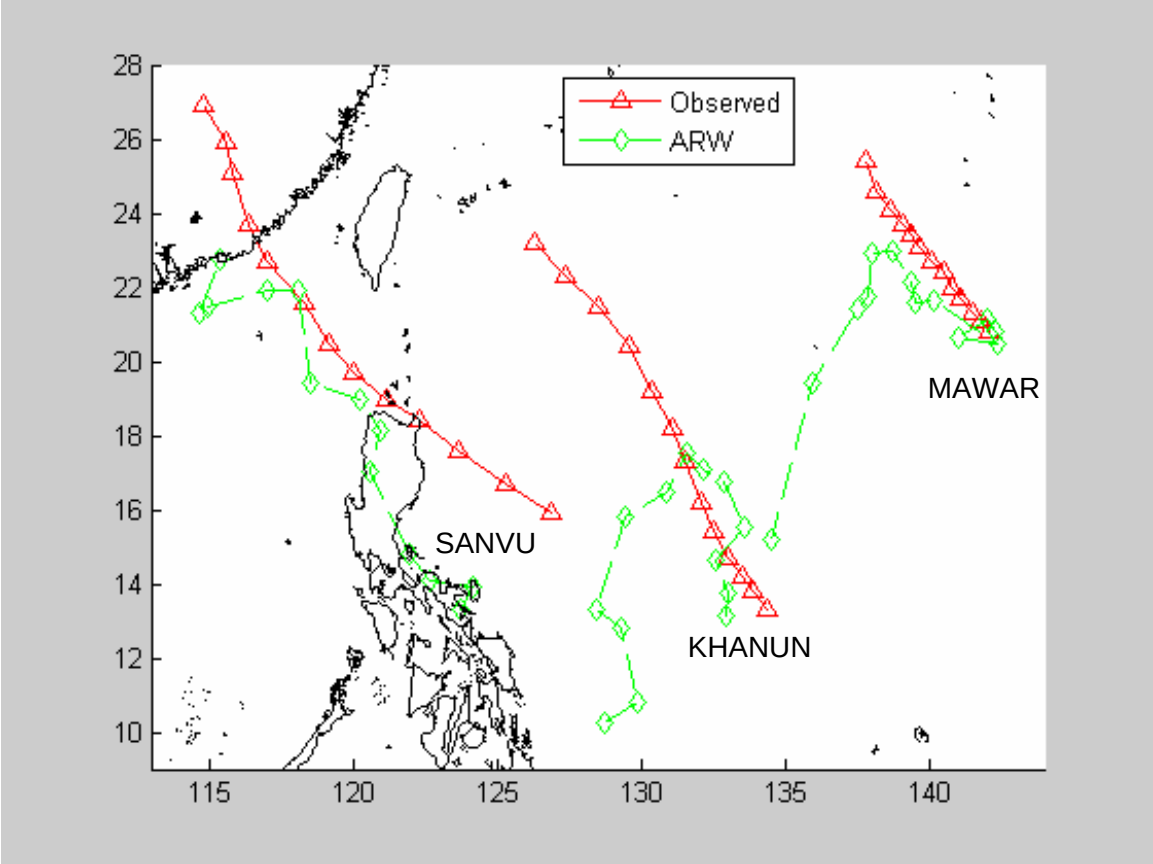

Figure 4.2 The observed tracks (solid red lines with triangles) and ARW vortex tracker-generated tracks (dashed green lines with diamonds) for the three cases when the tracker algorithm failed. The points along the tracks are in 6-h increments. In the Mawar case, the tracker moved towards a spurious TC to the south. In the Sanvu and Khanun cases, the tracker was attracted to the Philippines. All three cases were initialized early in the life cycle of the storm, when estimated TC winds were ≤45 kt.

Since TCs are warm-core lows with a maximum pressure deviation at the surface and maximum wind speeds near the top of the PBL (Elsberry 2006), a nest-tracking algorithm tied to these low-level features instead of the 500-mb height minimum would probably be less likely to have an erroneous nest movement. One such algorithm, which was developed by Professor P. A. Harr at the Naval Postgraduate School and explained in detail in Bower (2004), is the Tropical Cyclone Vortex Tracking Program (TCVTP). The TCVTP uses several parameters to not only track well-formed TCs, but also to identify weak, early-

stage tropical vorticies that have the potential to develop into TCs. In addition, the TCVTP algorithm performs a movement "reality check" on each new vortex position to prevent cases of abrupt speed and/or direction changes that are not realistic for actual TC movement.

Five of the ten cases in this study were initialized when the TC intensity was ≤45 kt, and only two of them had successful nest tracking and are included in the remaining results (except where noted). All five of the cases initialized when the TC intensity was > 45 kt are also included, none of which had nest-moving problems.

B. EVALUATION OF ARW TRACK PREDICTION

1. Overview

The mean TC position error (great-circle distance) of the ARW and MM5 predictions for the seven cases that did not cause failure of the ARW moving nest are shown in Figure 4.3. Overall, the ARW position forecasts were more skillful than the MM5 forecasts at all forecast intervals excluding the initialization time (0-h forecast). The slightly smaller mean error of the MM5 forecasts for the initialization time was likely due to the manual positioning of the bogus vortex during the MM5 preliminary integration (Chapter III.C.1.c). In contrast, the initial position of the vortex in the ARW integrations is determined solely from the non-bogused GFS fields used during the ARW cold-start initialization. The ARW average 72-h position error (173 n mi) was just over half of the MM5 average position error (302 n mi).

Also shown in Figure 4.3 is the mean position error of a CLImatogy-PERsistence (CLIPER) technique for the seven cases. The CLIPER technique is a purely statistical method that uses a combination of regression equations generated from predictors that include past 12-h and 24-h movement, latitude and longitude of the TC, and day of the year (Aberson and Sampson 2003). The CLIPER used in this study for track prediction is often abbreviated C120 because the forecasts are available to 120 h (only the first 72 h were used in this study). The C120

technique was compiled using data from western North Pacific TCs during 1970-1995. Because the C120 involves no meteorological fields, it is often used as a baseline forecast for determining the relative skill of other forecast techniques.

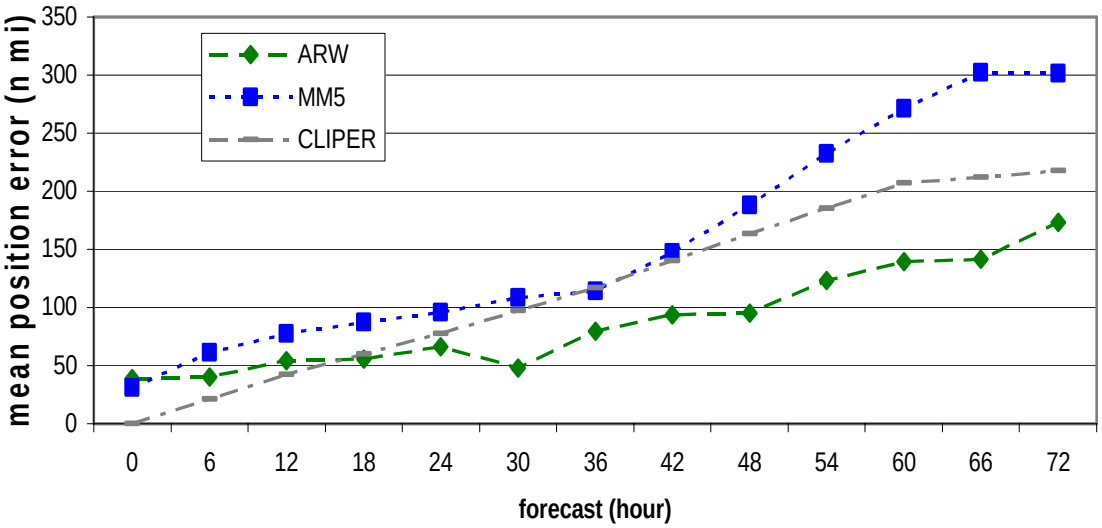

Figure 4.3 The mean TC position errors of the ARW prediction (dashed green line with diamond points), MM5 prediction (dotted blue line with square points), and CLIPER technique (grey dashed-dotted line) for the seven TC cases that did not cause failure of the moving nest algorithm in the ARW integration.

The C120 forecast had a smaller mean position error than both the ARW and MM5 models during the first 12 h of the forecast. This C120 advantage early in the forecast period is due to an initial TC position that precisely matches the observed TC position, which results in a zero position error in the 00-h forecast and very small errors during the first few hours. In addition, the first few forecast hours of the MM5 and (especially) ARW models were often characterized by erratic track changes in response to unbalanced initial conditions. This phenomenon, which is examined further in Chapter IV.B.2, often led to large position errors early in the forecast period.

For the position forecasts beyond the 12-h point, the ARW forecasts outperformed the C120 for the seven cases. In contrast, the MM5 did not

outperform C120 at any forecast hour except for a slight advantage at the 36-h forecast. Therefore, the ARW had skillful track predictions for these seven cases, and the MM5 did not.

2. Track Error Analysis Procedure

Having provided a basic statistical comparison of the overall prediction performance of the ARW and MM5 compared to CLIPER, the following seven sections provide an evaluation of the sources of track errors, as well as more detailed track prediction statistics.

Using SAFA, the track predictions and output fields from up to six other models were examined for the seven cases. These models were the Navy Operational Global Atmospheric Prediction System (NOGAPS), the Geophysical Fluid Dynamics Laboratory Hurricane Prediction System - Navy version (GFDN), the GFS model, the U.K. Meteorological Office global model (UKMO), the Japan Global Spectral Model (JGSM), and the Japan Typhoon Model (JTYM). The SAFA allows easy scrutiny of error mechanisms for TC track forecasts, and similarities were sought between errors identified by SAFA and those observed in the ARW and MM5. The NCEP reanalysis output fields, which do not use a bogus vortex, were also available as “ground truth” for the position and strength of synoptic features.

An attempt is made to distinguish errors due to initialization limitations and those possibly due to deficiencies in physical processes of the model. Intensity errors are evaluated in Chapter IV.C, but in some instances intensity errors were likely related to track errors, and this correlation is discussed when such instances are suspected.

The ARW output for this study was not post-processed, which means only basic variable fields were available and were displayed in sigma-p coordinates as opposed to being interpolated to conventional vertical pressure levels. This difference somewhat complicates a direct comparison of some of these fields to the standard pressure surface (e.g., 500 mb) fields in the SAFA and the NCEP

reanalysis. For example, comparing the ARW and NOGAPS locations of a certain height contour is not feasible. In these cases, qualitative comparisons are possible and still very useful.

Since TC motion is largely determined by the environmental flow surrounding the storm, observational studies have focused on the winds at a distance of 5°-7° latitude (300-420 n mi) from the vortex center (Carr and Elsberry 1990; Franklin 1990). The synoptic-scale features producing the environmental flow near the TC (e.g., monsoon trough, subtropical ridge, baroclinic low) are often thousands of nautical miles away from the storm. Since the moving inner nest is not large enough to include these synoptic features, and barely large enough to include a 5° latitude radius, some of the track errors in the ARW predictions may be somewhat independent of the presence or performance of the moving inner nest. Some exceptions will be noted, such as errors believed to be traceable to intensity errors or other factors originating closer to the TC vortex and within the domain of the inner nest.

The observed and forecast tracks from the ARW and MM5 models for the seven cases are shown in Figure 4.4a-g. To illustrate the approach used to compare track errors of the ARW and MM5 to the track errors of other models in the SAFA program, the SAFA display of five other comparison models for the first Typhoon Talim case is provided as an example (Figure 4.5). A summary of the comparisons between track errors in ARW, MM5, and the six models in the SAFA are provided in the Chapter IV.B.8.

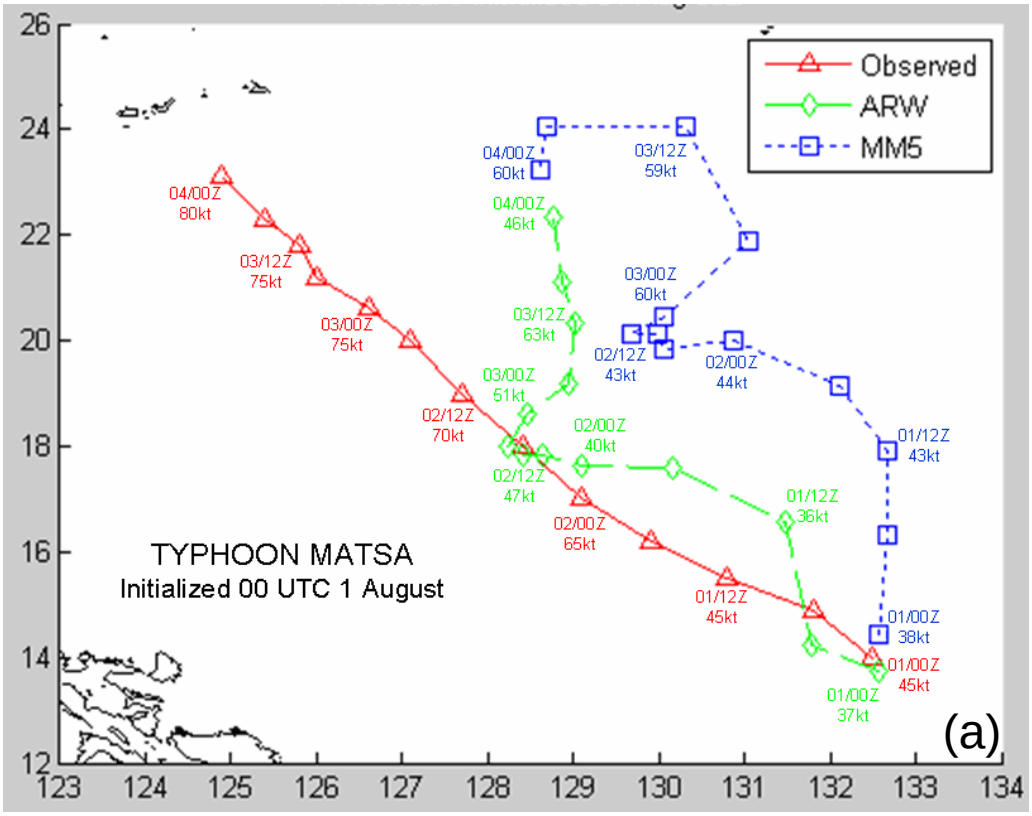
Observed
ARW
MM5
TYPHOON MATSA
Initialized 00 UTC 1 August
(a)
04/00Z 80kt
03/12Z 75kt
03/00Z 75kt
02/12Z 70kt
02/00Z 65kt
01/12Z 45kt
01/00Z 45kt
04/00Z 60kt
03/12Z 59kt
04/00Z 46kt
03/00Z 60kt
03/12Z 63kt
02/12Z 43kt
02/00Z 44kt
03/00Z 51kt
02/00Z 40kt
01/12Z 43kt
02/12Z 47kt
01/12Z 36kt
01/00Z 38kt
01/00Z 37kt

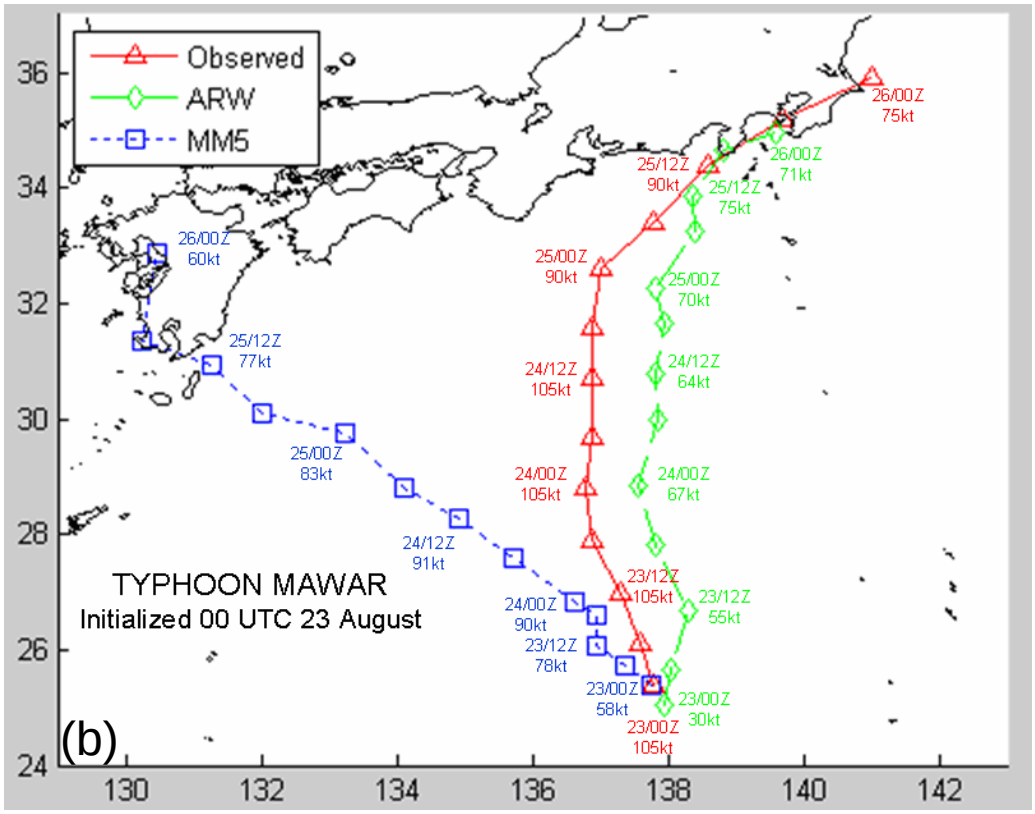
Observed
ARW
MM5
TYPHOON MAWAR
Initialized 00 UTC 23 August
(b)
26/00Z 75kt
25/12Z 90kt
26/00Z 71kt
25/12Z 75kt
26/00Z 60kt
25/00Z 90kt
25/00Z 70kt
25/12Z 77kt
24/12Z 105kt
24/12Z 64kt
25/00Z 83kt
24/00Z 105kt
24/00Z 67kt
24/12Z 91kt
23/12Z 105kt
24/00Z 90kt
23/12Z 55kt
23/12Z 78kt
23/00Z 58kt
23/00Z 30kt
23/00Z 105kt

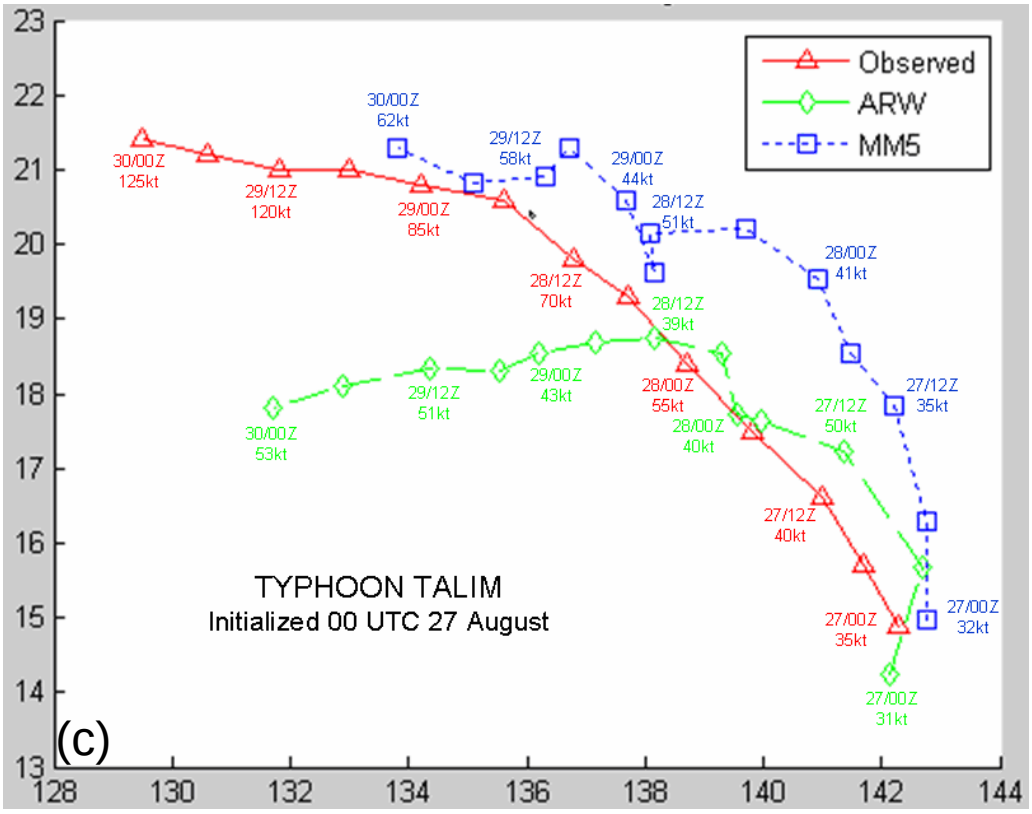
Observed
ARW
MM5
TYPHOON TALIM
Initialized 00 UTC 27 August
(c)
30/00Z 125kt
29/12Z 120kt
29/00Z 85kt
28/12Z 70kt
27/12Z 40kt
27/00Z 35kt
27/00Z 31kt
30/00Z 62kt
29/12Z 58kt
29/00Z 44kt
28/12Z 51kt
28/00Z 41kt
27/12Z 35kt
27/00Z 32kt
30/00Z 53kt
29/12Z 51kt
29/00Z 43kt
28/12Z 39kt
28/00Z 55kt
28/00Z 40kt
27/12Z 50kt

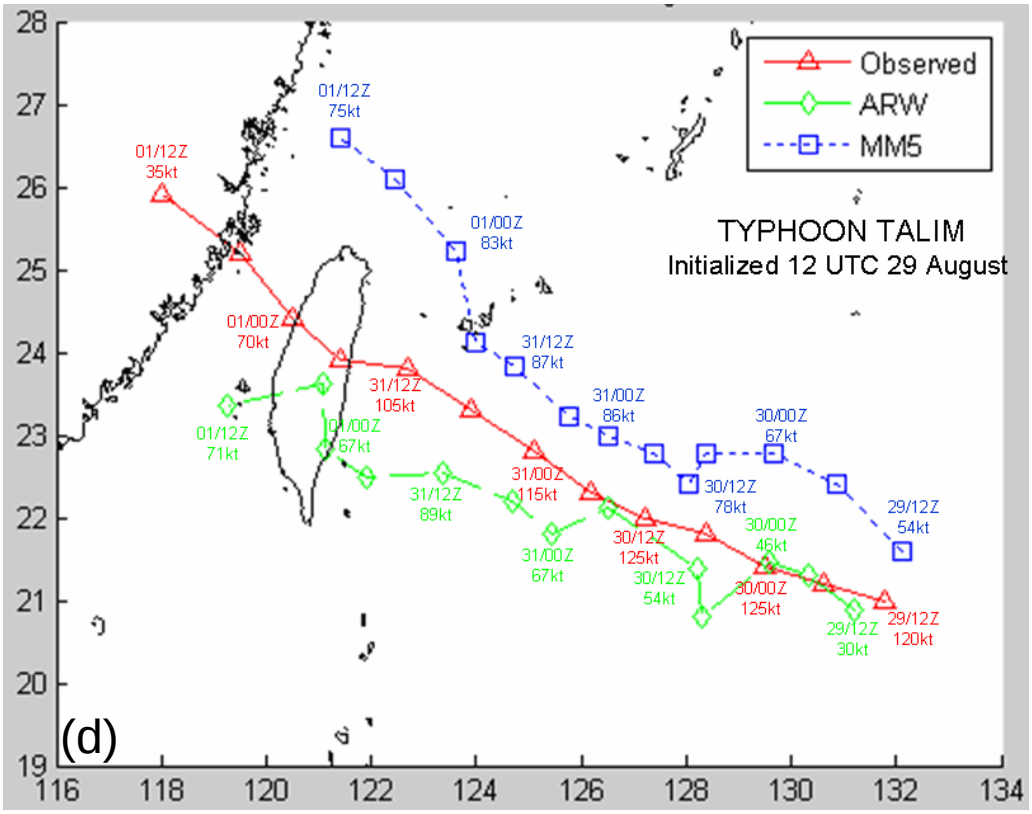
Observed
ARW
MM5
TYPHOON TALIM
Initialized 12 UTC 29 August
(d)
01/12Z 35kt
01/00Z 70kt
31/12Z 105kt
31/00Z 115kt
30/12Z 125kt
30/00Z 125kt
29/12Z 120kt
01/12Z 71kt
01/00Z 67kt
31/12Z 89kt
31/00Z 67kt
30/12Z 54kt
29/12Z 30kt
01/12Z 75kt
01/00Z 83kt
31/12Z 87kt
31/00Z 86kt
30/12Z 78kt
30/00Z 67kt
30/00Z 46kt
29/12Z 54kt

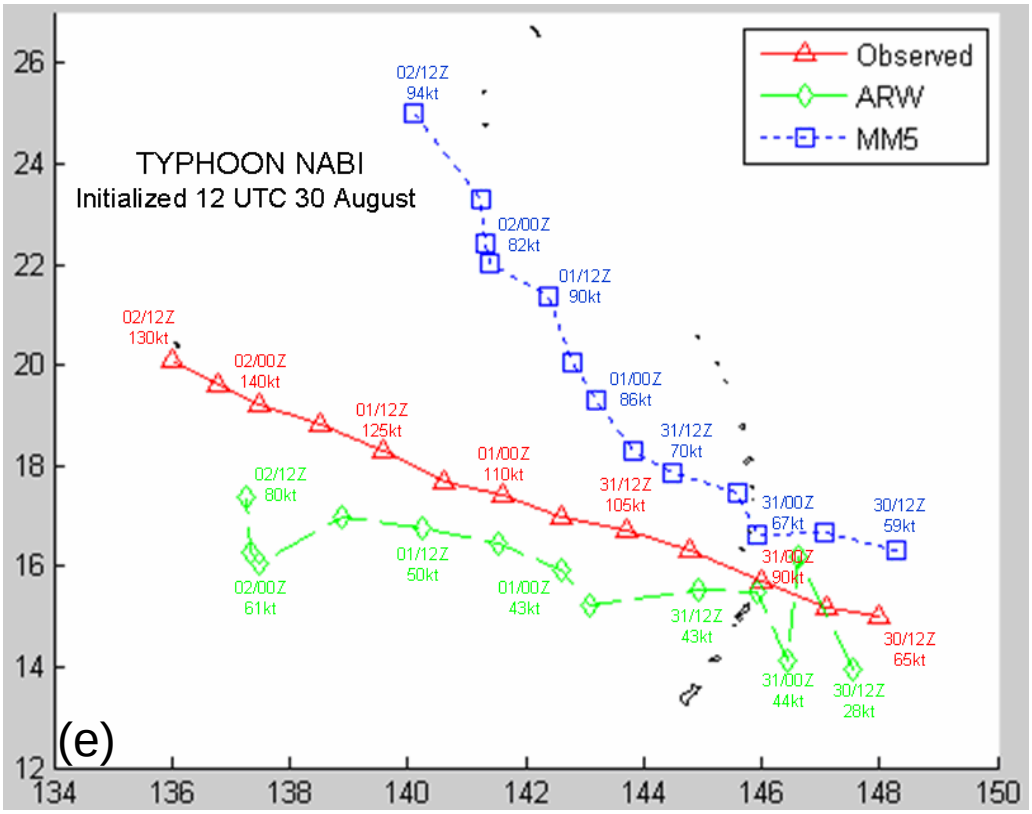
Observed
ARW
MM5
TYPHOON NABI
Initialized 12 UTC 30 August
02/12Z 94kt
02/00Z 82kt
01/12Z 90kt
01/00Z 86kt
31/12Z 70kt
31/00Z 67kt
30/12Z 59kt
02/12Z 130kt
02/00Z 140kt
01/12Z 125kt
01/00Z 110kt
31/12Z 105kt
31/00Z 90kt
30/12Z 65kt
02/12Z 80kt
02/00Z 61kt
01/12Z 50kt
01/00Z 43kt
31/12Z 43kt
31/00Z 44kt
30/12Z 28kt
(e)
26
24
22
20
18
16
14
12
134
136
138
140
142
144
146
148
150

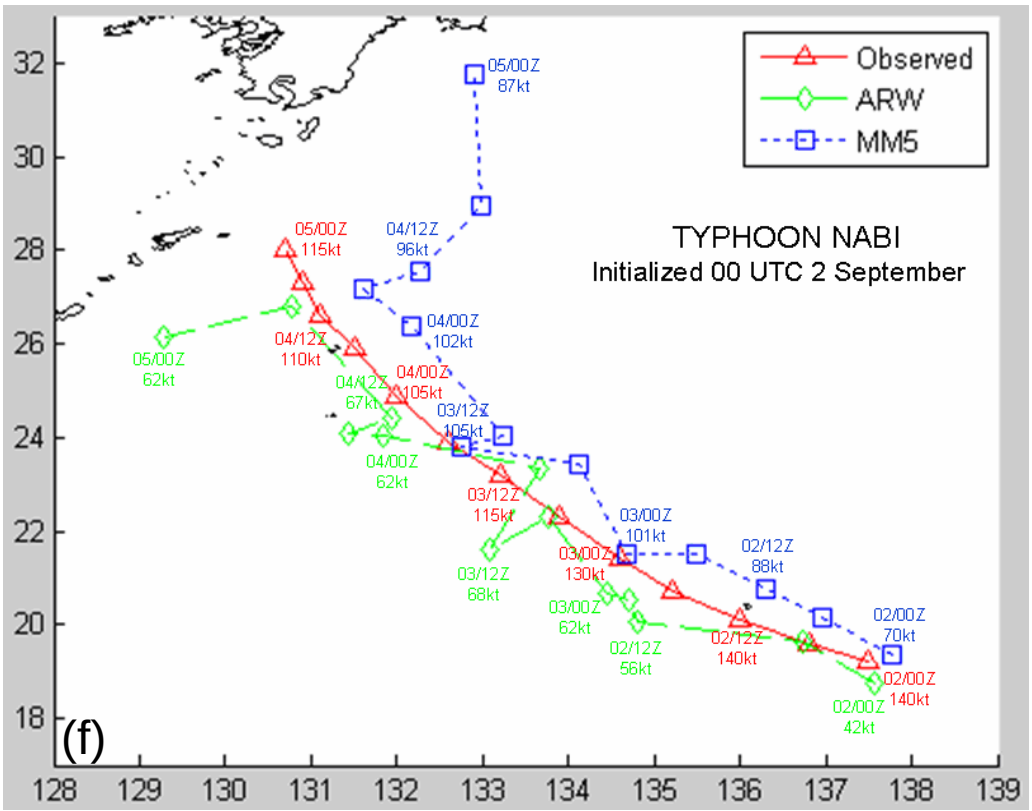
Observed
ARW
MM5
TYPHOON NABI
Initialized 00 UTC 2 September
05/00Z 87kt
04/12Z 96kt
04/00Z 102kt
03/12Z 105kt
03/00Z 101kt
02/12Z 88kt
02/00Z 70kt
05/00Z 115kt
04/12Z 110kt
04/00Z 105kt
03/12Z 115kt
03/00Z 130kt
02/12Z 140kt
02/00Z 140kt
05/00Z 62kt
04/12Z 67kt
04/00Z 62kt
03/12Z 68kt
03/00Z 62kt
02/12Z 56kt
02/00Z 42kt
(f)
32
30
28
26
24
22
20
18
128
129
130
131
132
133
134
135
136
137
138
139

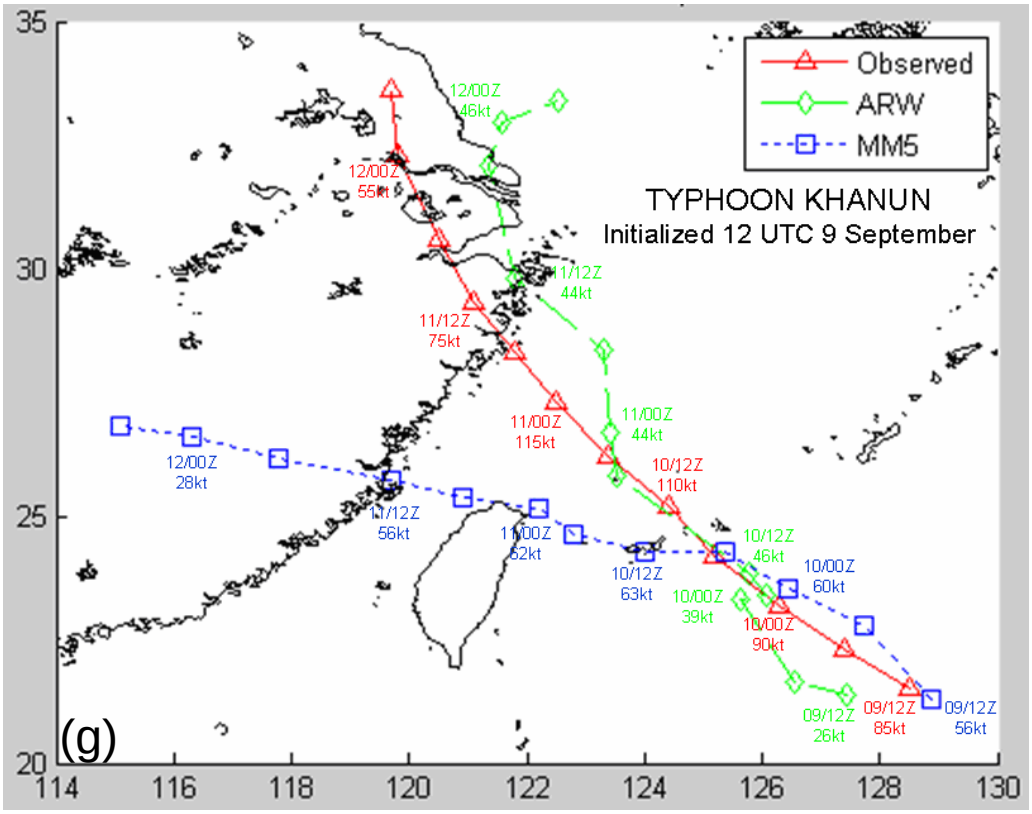

Figure 4.4 Best track (solid red line with triangular points), ARW prediction (dashed green line with diamond points) and MM5 prediction (dotted blue line with square points) for the (a) Typhoon Matsa case; (b) Typhoon Mawar case; (c) first Typhoon Talim case; (d) second Typhoon Talim case; (e) first Typhoon Nabi case; (f) second Typhoon Nabi case; and (g) Typhoon Khanun case. Only the 72-h integration period is shown for each case. Each point represents a 6-h increment. The date, time, and TC intensity forecast (estimated TC intensity for the best track) is labeled every 12 h.

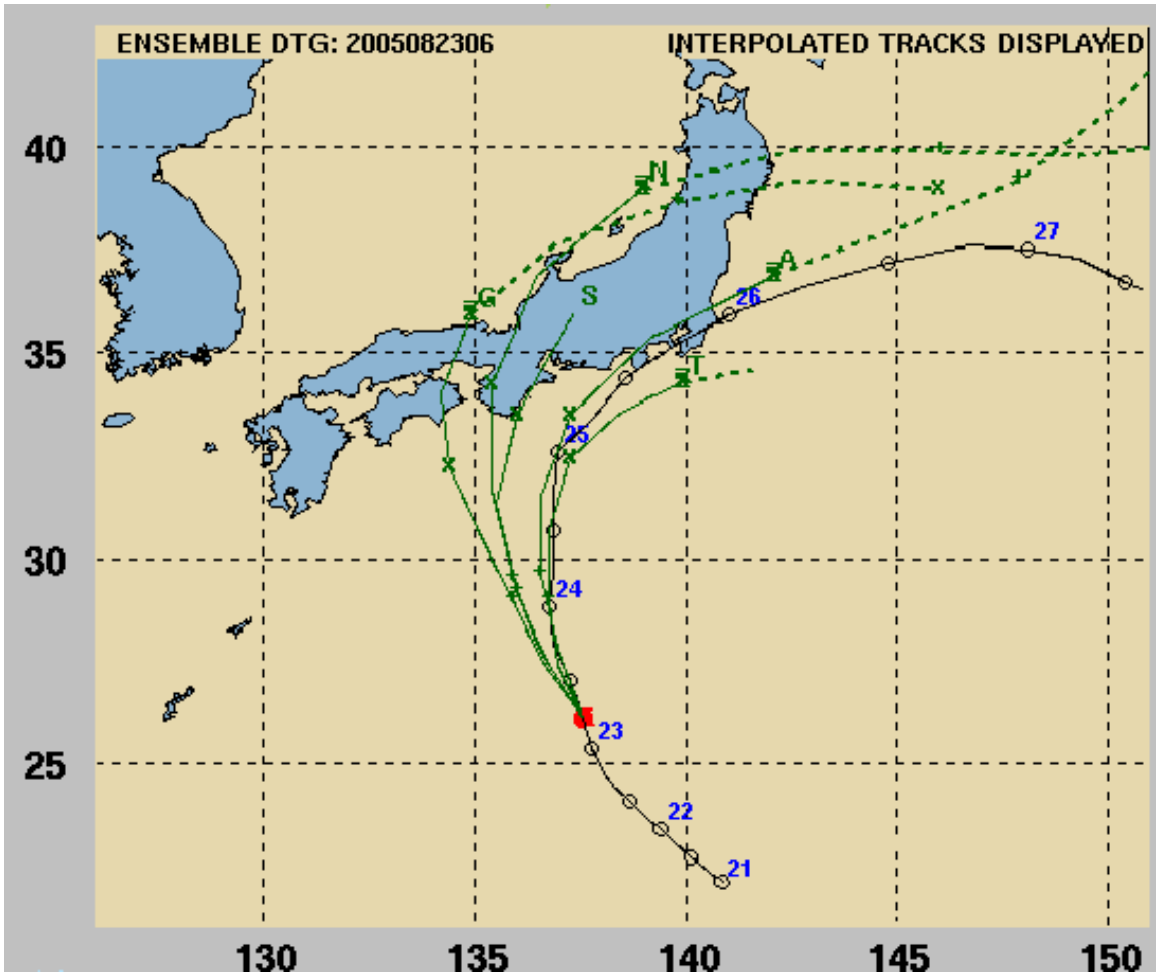

Figure 4.5 SAFA track comparison used for analysis of ARW and MM5 errors in the first Typhoon Mawar case initialized 00 UTC 23 August 2005. The black line with circles each 12 h indicates the best track of Typhoon Talim, and each blue label indicates the 00 UTC position on the indicated date. The 72-h track predictions of five analyzed models are shown in solid green lines. The dotted green lines indicate the track predictions beyond 72 h (out to 120 h). The green "x" marks on the track forecasts are the forecast vortex positions at 00 UTC each day. Each model forecast track is labeled with a green letter: "N" is NOGAPS; "G" is GFDN; "A" is GFS; "S" is JGSM; and "T" is JTYM. The UKMO model was not available for this case.

3. Early Track Errors Due to Model Spin-up

Erratic track changes of various amplitudes were observed during the early hours of all seven cases, and were especially severe in the second Typhoon Talim integration (Figure 4.4d), first Typhoon Nabi integration (Figure 4.4e), and the Typhoon Khanun integration (Figure 4.4g). These track changes were traced to an apparent "wobbling" of the typhoon structure during the early hours of the integrations (Figure 4.6), which often caused the upper-level circulations to be laterally displaced from the low-level circulations by a significant distance. In the first Typhoon Nabi case (Figures 4.4e and 4.6), wobbling of the typhoon was so severe, the low-level circulation passing south of Saipan while the 0.4940 sigma-p level pressure minimum (and the track indicated by the tracker algorithm) passed north of the island.

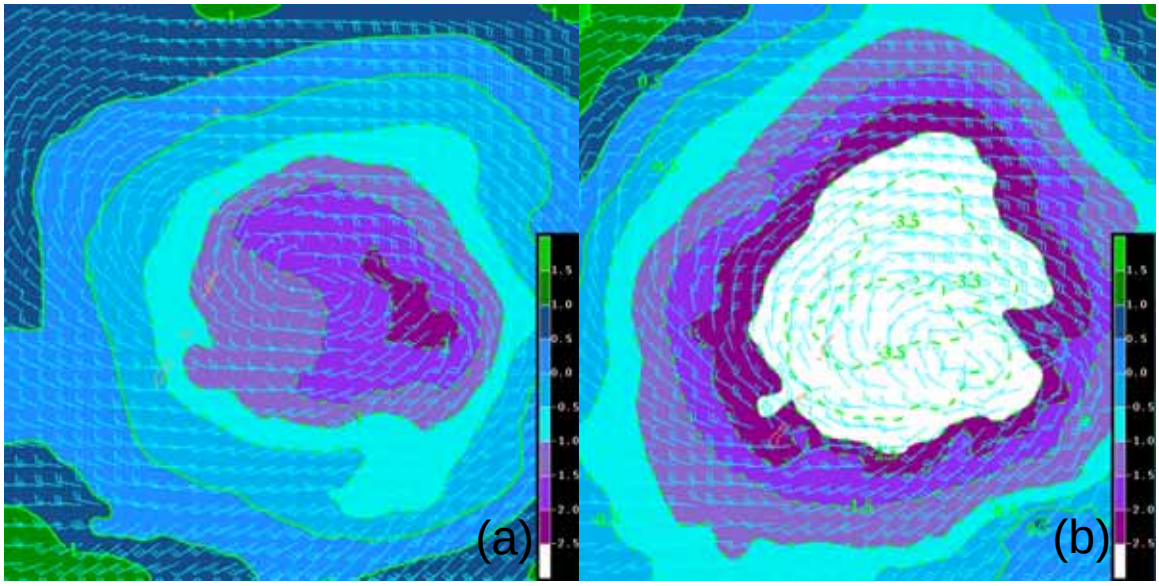

Figure 4.6 Oscillations in the typhoon structure in the ARW inner nest during spin-up of the first Typhoon Nabi integration initialized 12 UTC 30 August 2005. Panels (a) and (b) are the 3-h and 6-h forecasts, respectively. The shaded contours show the 0.4940 sigma-p level pressure perturbation field (difference in pressure from a standard value at the sigma-level, in mb). The wind barbs are the 10 m winds (kt), and are displayed at every tenth grid point. At the 3-h forecast, the low-level circulation is WNW of the mid-level low. At the 6-h forecast, the low-level circulation is ESE of the mid-level low. The wobbling of the TC during spin-up led to erratic track changes in Figure 4.4e.

The cold-start initialization of the ARW leads to mass and wind fields that were not balanced at the start of the integrations. Achieving geostrophic balance during spin-up is complicated by processes such as convection, latent heat release, and precipitation, which are not prescribed as part of the initialization fields and thus must go through a spin-up phase during the early hours of the integration (Figure 4.7a, b) [see COMET Module "The Balancing Act of Geostrophic Adjustment". Available online at http://www.meted.ucar.edu/nwp/pcu1/d_adjust/print.htm (current as of 16 Feb 2006)]. During the spin-up period, oscillations in the mass field were observed (Figure 4.7c,d) as the ARW attempted to correct the unbalanced state of the atmosphere.

The cold-start initialization also resulted in initial intensities that were substantially too low in five of the cases (discussed further in Chapter IV.D). However, the two cases that were integrated with initial intensities within 10 kt of the best-track intensity (Matsa and the first Talim) did not have less wobbling than those that were initialized with intensities that were too low. This suggests the wobbling was mostly tied to the geostrophic adjustment process and not a result of the integrations being initialized with a TC that was too weak.

The chaotic nature of the oscillations in Figure 4.6, which occur at different frequencies at different levels of the model, was the source of the wobbling or "sloshing" of the mass fields at different levels, which created the erratic ARW track forecasts during the early stages of the integrations. These track changes during spin-up were exacerbated by the nature of the ARW vortex tracker since it tracks the 500-mb height minimum. The mid-level height minimums of the TCs generally had larger position oscillations during spin-up than the more identifiable low-level circulations.

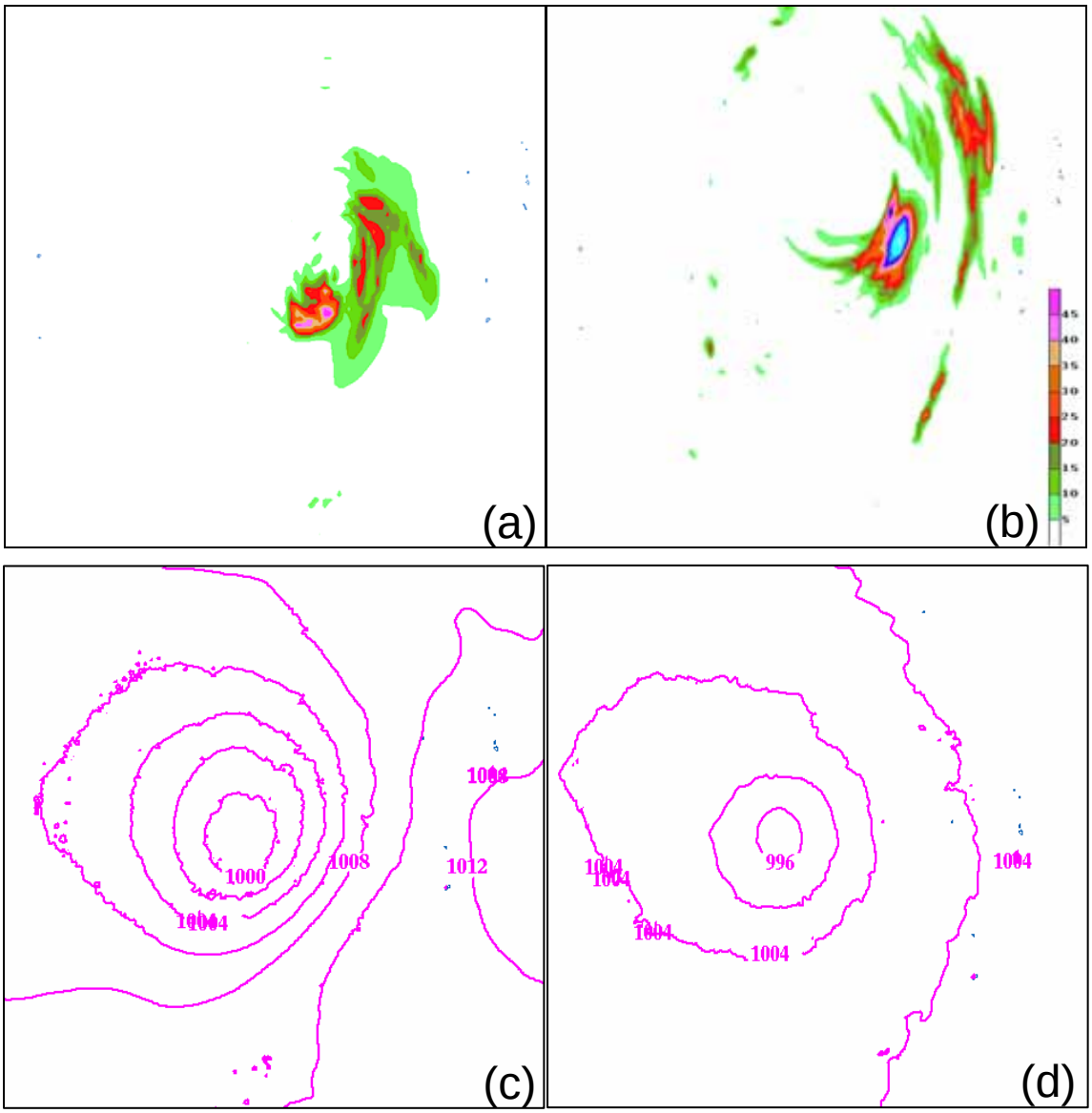

Figure 4.7 Indications of ARW spin-up occurring during the first few hours of the Typhoon Mawar integration initialized 00 UTC 23 August 2005. Panels (a) and (b) are the outer nest 3-h precipitation totals (mm) valid at forecast hour 3 and 12, respectively. The precipitation gradually increased to realistic values during the spin-up period after being initialized with no precipitation occurring. Panels (c) and (d) are the inner nest surface pressure fields (mb) valid at forecast hour 3 and 12, respectively. The high frequency waves in the field contours are an indication of unbalanced conditions. The contours are somewhat smoother near the storm center after 12 h of integration (d), but many waves still exist that indicate the balancing process is continuing.

East-west cross-sections of the ARW-predicted meridional wind components through the center of each storm allow easy identification of the circulation at every level, and the degree of wobbling during spin-up could be assessed. Perhaps the most severe ARW typhoon wobbling was in the Typhoon Khanun case (Figure 4.8). The vortex in the 0-h forecast (Figure 4.8a) is severely contorted. The lateral distance between the circulation center at the surface and the circulation center at 0.80 sigma-p level is roughly 86 km. This contorted vortex is extremely unlikely to be accurate given the Khanun estimated intensity was actually 85 kt at the time. This contorted vortex is mostly corrected in the low levels by the 12-h forecast (Figure 4.8b). However, the ARW prediction continued to have a very disorganized upper-level circulation of Khanun for several more hours of integration, which partially accounts for the erratic ARW track changes of Khanun between 12 h and 24 h (Figure 4.4g). In an operational scenario, these track changes near the Japanese Ryukyu Islands would be particularly troublesome and give the forecaster very little confidence in the ARW model predictions. However, the ARW forecast was excellent after the spin-up period and significantly outperformed the MM5 on days two and three of the integration.

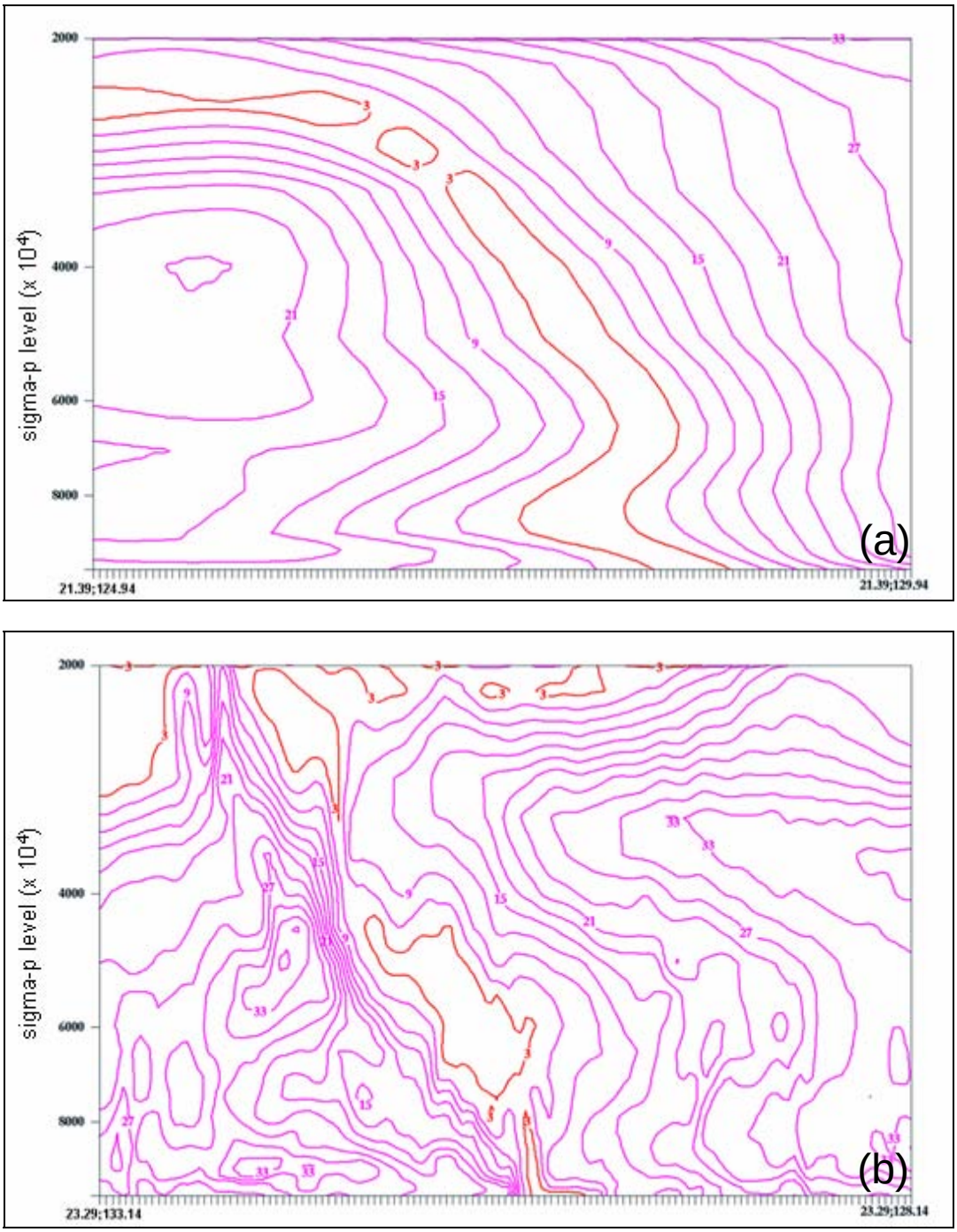

Figure 4.8 West-to-east cross-section of wind speeds (kt) normal to the plane through the center of Typhoon Khanun on the ARW inner-nest at forecast hour 0 (a) and 12 (b). The 3-kt isotach is highlighted to indicate the center of the circulation. The ARW clearly had an extremely contorted vortex at the initial time. By 12 h, the vortex had become reasonably aligned in the lower and middle levels. The horizontal interval is approximately 2.2 n mi.

The MM5 forecasts had fewer abrupt track changes than the ARW, which suggests the benefits of a warm-start initialization (in addition to a vortex tracker based on low-level features). Additionally, the smaller 00-h position error of the MM5 compared to the ARW provided by the MM5 vortex bogus often gave an advantage that may have large implications in an operational scenario. A good example of this is the Khanun case (Figure 4.4g). The integrations were started when Khanun was less than 24 h from passing the Ryukyu Islands, and the ARW was *starting out* with an error of 60 n mi. In this case, the forecaster may favor the MM5 forecast based solely on the MM5 00-h error being only 24 n mi. However, the relocated vortex in the MM5 did not always result in a better initial position than the ARW. The ARW had a slightly smaller 00-h error than the MM5 (68 n mi versus 80 n mi) in the first Typhoon Nabi case, which was initialized 15 h before the typhoon passed the Mariana Islands.

Several of the cases had an ARW track forecast that had a very small cross-track error, although the along-track movement was too slow. To evaluate whether there was a slow bias in the model, the average along-track error (with sign) for all seven cases was calculated (Figure 4.9). Both the ARW and MM5 had a large slow bias, with the MM5 having a much larger slow bias beyond the 42-h forecast (it should be noted that the MM5 also had much larger overall error beyond 48 h, and the along-track error increases when the cross-track error increases even if the forecast translation speed is correct).

The ARW slow bias progressively increases during the early hours of the integrations before temporarily leveling off after 24 h. It was hypothesized that typhoon wobble and erratic track changes (see Figure 4.4) during ARW-spin up may have interfered with the forward progress of the TC during this period and accounted for the growing slow bias. Instances of ARW integrations with early track changes followed by small cross-track error with a slow bias were the Matsa, Mawar, second Talim, and first Nabi cases. To evaluate this hypothesis, the mean along-track errors for the CLIPER forecasts were also calculated and compared to the ARW along-track errors for all seven cases (Figure 4.9). During

the spin-up period (roughly the first 24 h of the integration), the CLIPER forecasts had a slow bias that was larger than the ARW. This result indicates the TCs in this study moved significantly faster than the climatological norm and makes it difficult to explain whether the ARW slow bias was due to spin-up or conventional model forecast error not related to spin-up.

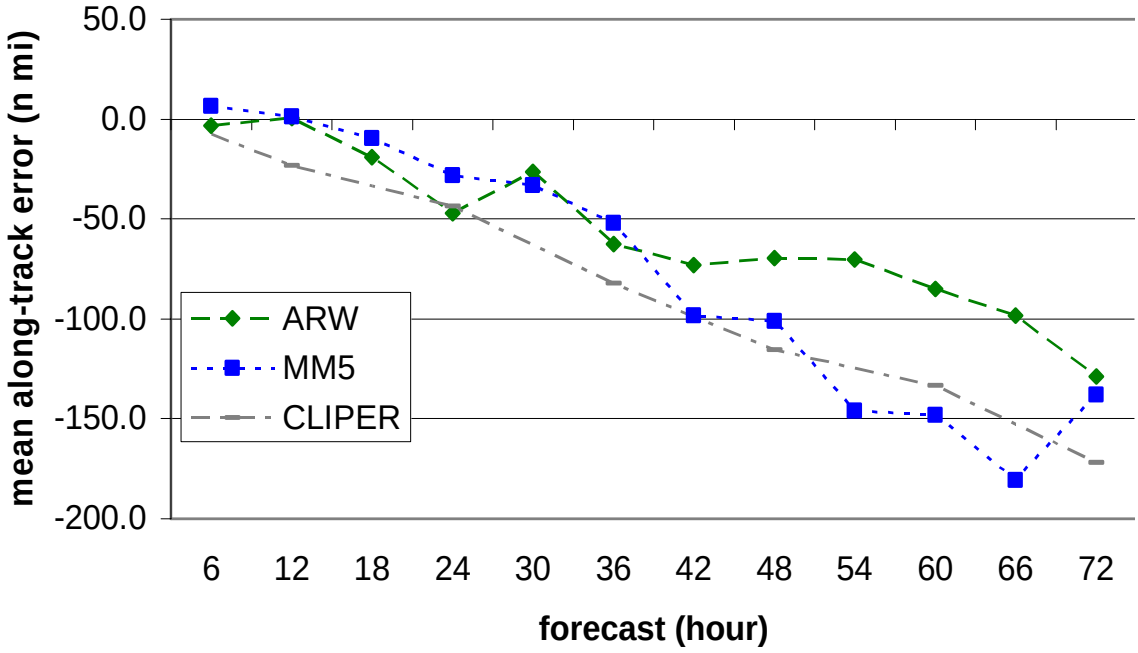

Figure 4.9 Mean along-track error of the seven ARW predictions (dashed green line with diamond points), MM5 predictions (dotted blue line with square points), and CLIPER technique (grey dashed-dotted line) for the seven cases. Positive values are forecast positions ahead of the observed position, and negative values are forecast positions behind the observed positions. Beyond 12 h, all three techniques had predictions significantly behind the observed storms.

4. Tracker Error

The mid-level vortex tracker algorithm of the ARW helped to amplify early track changes due to typhoon wobble, but erratic track changes were also observed later in the ARW integrations that probably cannot be attributed solely to spin-up. Even the MM5 forecasts, which were derived from a tracker based on

low-level features, occasionally had abrupt and unrealistic directional changes that were more likely a result of an imperfect tracker than actual model error.

In these ARW integrations, the tracker algorithm provided output in 15 min intervals. A continuous track connecting all of these fixes (not shown) has excessive high-frequency track changes and would be only marginally useful compared to a track with a much smoother 12-h interval. When the tracks are plotted with longer increments between points, these tracker errors become smoother and are less obvious. For example, The National Hurricane Center best-tracks that are based on six-hourly estimates of TC positions are "subjectively smoothed" to avoid the erratic motion implied by simply connecting the fix locations [Available online at http://www.nhc.noaa.gov/aboutgloss_text.html (current as of 18 Feb 2006)]. An interval of 6 h (used in this study) provides reasonably smooth tracks without completely removing the abrupt changes inherent in the output of each tracker.

The erroneous nest movements due to the ARW tracker were described in Chapter IV.A. A few additional instances of noteworthy ARW tracker errors occurred in these seven integrations, although not severely enough to cause the moving inner nest to "lose" the TC from its domain. One of these was associated with the abrupt westward movement during the final hours of the second Typhoon Nabi integration (Figure 4.4f). The ARW track forecast was very accurate for this case despite the abrupt turn to the west between the 66-h and 72-h forecasts. This turn was due to shearing of the storm, which caused the upper-level circulation to become displaced to the west (Figure 4.10). In the ARW 72-h forecast, the lateral distance between the circulation center at the surface and the circulation center at sigma-p level 0.50 is roughly 77 n mi. Whereas the tracker followed the circulation at roughly sigma-p level 0.50, the low-level circulation in the ARW forecast continued on a fairly accurate track through the end of the integration.

Interestingly, shearing between the surface and sigma-p level 0.50 was not observed in the ARW forecasts for the two TCs reaching the mid-latitudes:

Typhoons Mawar and Khanun. The ARW track forecasts for these runs were better than the MM5 and CLIPER, with 72-h forecast error below 100 n mi in the Mawar case and below 150 n mi in the Khanun case. Had these storms exhibited low- or mid-level shearing, tracker errors may have been substantial, and possibly even resulted in failure of the inner nest to keep the TC surface circulation inside the inner-nest domain.

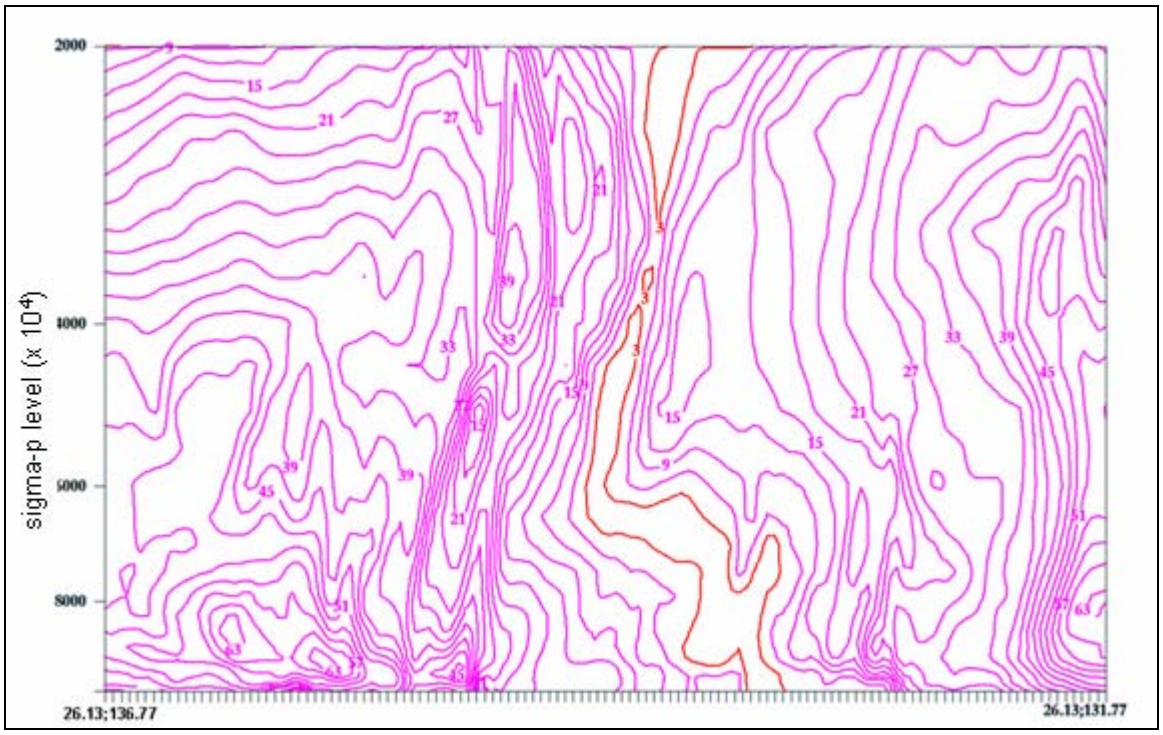

Figure 4.10 West-to-east cross section of normal wind component (kt) for the 72-h ARW inner nest forecast from the second Typhoon Nabi integration. Shearing of the storm caused the upper-level circulation center to be displaced from the low-level circulation center, which resulted in a significant error of the ARW vortex tracker. The horizontal interval is approximately 2.2 n mi.

The other notable ARW track change due to tracker error was over Taiwan during the second Typhoon Talim integration (Figure 4.4d). An abrupt turn to the north is indicated by the ARW tracker despite the surface pressure center remaining on a relatively smooth course to the WNW. A similar behavior occurred near the high terrain of the Philippines in the Sanvu integration and

Khanun integration that are not included in these results due to complete tracker failure (Chapter IV.A). As in those cases, the tracker error over Taiwan could have been due to a terrain interpolation error or localized convection to the north that caused a minimum in 500 mb heights. Since the fields in this study were displayed in terrain-following vertical coordinates, it was not possible to detect height minima over the mountainous terrain. However, the precipitation field (not shown) indicated intense convection occurring north of the vortex, and this convection was probably enhanced by the strong easterly flow rising up the eastern slopes of the mountains. In addition, channeling by the terrain caused multiple small-scale eddies in the low-level wind fields (Figure 4.11), which may have temporarily helped lower the 500-mb heights on the mesoscale. Furthermore, the TC vortex appeared to have weakened and become a bit disorganized while crossing the mountains, which also could have contributed to the tracker straying off course. In the ARW 72-h forecast, Typhoon Talim was in the Taiwan Strait, and the upper-level circulation (and tracker) once again was aligned with the low-level circulation.

5. Steering by the Subtropical Ridge

The subtropical ridge (STR) is a dominant circulation in the western North Pacific during June-September, and is often a primary factor in the environmental flow of a TC. All seven cases were affected by the STR circulation to some degree during the integrations, and several model track errors were traced back to errors in the position of the STR.

Of particular interest was the initialization of the Typhoon Khanun case (Figure 4.4g). Prior to the integration, Khanun was on a north-northwest course toward Okinawa. Just prior to initialization of this run, the STR began to build from the northeast and Khanun turned toward the northwest. Despite the relatively low-resolution GFS fields used to initialize the MM5, the first few hours of the MM5 integration had low track error. The ARW forecast, which was initialized with the 1/2° lat./lon. resolution GFS fields but with a cold start, also

had a fairly accurate track during the first 24 h. In this case, the 1/2° lat./lon. resolution GFS was sufficient to resolve subtle changes in the STR during the ARW cold-start initialization.

Figure 4.11 10 m wind barbs (kt) over Taiwan from the 66-h ARW inner nest forecast of the second Typhoon Talim integration. The winds are displayed at every grid point. The vortex center of Talim is in the lower left of the image, just off the west coast of Taiwan. Several mesoscale circulations were created by the terrain in the ARW, and may have helped create 500-mb height perturbations wthat caused an error in the vortex tracker algorithm.

The interaction of the STR with a mid-latitude trough was the focus of the track forecast in the second Typhoon Nabi integration (Figure 4.4f). The ARW, MM5, and all six models in SAFA handled the gradual veering of the steering flow very well and had 72-h position errors <300 n mi. The MM5 was the only model that recurved Nabi too quickly, although the early recurvature was not significant until the 60-h forecast. The MM5 early recurvature could have been due to movement of the trough that was too fast, which may have caused the

STR to retreat eastward too quickly. In contrast, the gradual turning motion in the ARW integration was very accurate throughout (the abrupt direction change at 66 h is due to a tracker error – see Chapter IV.C.2). The gradual retreat of the ridge and veering of the steering flow in the ARW outer nest is shown in Figure 4.12.

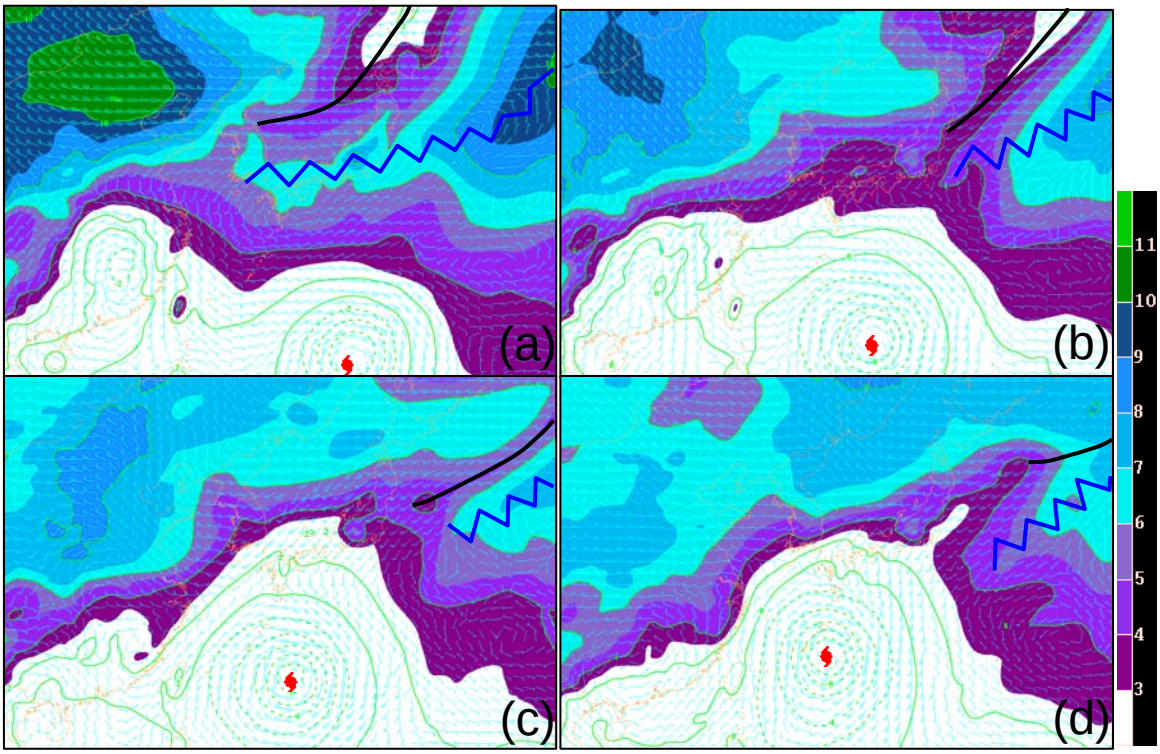

Figure 4.12 The (a) 0-h, (b) 24-h, (c) 48-h, and (d) 72-h ARW outer-nest forecasts for the second Typhoon Nabi integration initialized 00 UTC 2 September 2005. Contours and shading are the 0.50 sigma-p level pressure perturbation (mb), and the barbs are the 0.50 sigma-p level winds (kt) displayed at every tenth grid point. As the mid-latitude trough (black line) forced the STR (blue crimped line) to retreat eastward, the steering flow for Typhoon Nabi (red typhoon symbol) gradually became northward. This ARW forecast verified very accurately.

On day one of the first Typhoon Talim case (Figure 4.4c), the STR in the ARW forecast appeared to be quite weak to the northeast of the storm. Since ARW height fields were not available for display, this observation was made by comparing the position of mid-level pressure perturbation contours with the

pressure perturbation contours from the other integrations. The NCEP reanalysis fields on day one of the first Typhoon Talim case did not have an anomalously weak STR northeast of the TC. The weak STR in the ARW may account for the cross-track error to the right on day one of the integration, although the error was not substantially larger than the day one error for the SAFA models. The MM5 track forecast during day one was also to the right of the track, and the MM5 error was larger than any of the six models in SAFA.

Another major focus of the Typhoon Khanun case (Figure 4.4g) was at the end of the integration, when the TC was gently recurving after making landfall in China. The ARW forecast did not have erratic track changes after landfall, although the track error was increasing during the final 18 h of integration in part due to an erroneous position of the STR. During this period, the STR was to the east at about 34°N latitude (not shown). Once (the remnants of) Khanun crossed this latitude, it turned to the northeast and eventually struck the Korean Peninsula (after the integration period). The ARW forecast was for a turn to the northeast approximately 18 h too early due to the STR axis being at around 32°N. The GFS, NOGAPS, and GFDN models had very similar early recurvature errors. The MM5 forecast on days two and three of this integration was not similar to any of the other models, and had a 72-h forecast error of 472 n mi.

Early recurvature error was also observed on day three of the Typhoon Matsa case (Figure 4.4a) in the ARW integration and possibly in the MM5 integration. In this case, the STR to the northeast of Matsa in the ARW integration became severely eroded due to a spurious TC that was predicted to form between Matsa and the center of the subtropical high (not shown). Satellite imagery on day three of this case had an area of disorganized convection near the location of the spurious TC formation (not shown), but the convection never developed into a TC. Although the MM5 error to the right of the track may have also been due to a similar mechanism as the ARW error, the uncharacteristically erratic track forecast from the MM5 suggests a vortex tracker problem or spin-up.

The GFS was the only model in SAFA that had a similar excessive recurvature error for this case. The GFS model fields were not available for this case, so it could not be determined if a spurious TC between Matsa and the subtropical high was responsible for the GFS error. For the 72-h forecasts, the ARW, MM5, and GFS errors were between 200 n mi and 225 n mi. The other five models in SAFA had smaller errors for this case, which was expected to be one of the easier track forecasts.

6. Subtropical Ridge Modification

Modification of the STR as a TC steering mechanism is a result of planetary vorticity advection by the TC (Carr and Elsberry 2000a). Small values of planetary (and absolute) vorticity equatorward of the TC are advected to the northeast (Northern Hemisphere) by the TC circulation, which creates an anticyclone to the southeast of the TC that is called the peripheral anticyclone. Similarly, anomalous positive vorticity is created to the northwest of the TC. For a TC that is moving westward south of the STR, the peripheral anticyclone can merge with the subtropical high and cause the dominant ridge axis to become reoriented so that it passes southeast of the TC (Figure 4.13). Thus, the environmental flow around the TC becomes northward and causes the TC to move in a more poleward direction. In addition, poleward motion is further enhanced if the positive vorticity anomaly northwest of the storm creates a col zone or “break” in the STR.

This STR modification is more likely for large TCs because the winds at larger radii bring low values of planetary vorticity farther northward and create a stronger peripheral anticyclone. In addition, TCs at higher latitudes are also favorable for STR modification because the plantery vorticity gradient is larger, which allows more intense anticyclonic vorticity advection and a stronger peripheral anticyclone (Carr and Elsberry 2000a).

STR modification was evident in the NCEP reanalysis fields from the first Typhoon Talim integration (Figure 4.4c). The peripheral anticyclone gradually strengthened during the period of this integration as Talim increased in intensity

(and size) and moved to higher latitudes. The small ARW track error on day one of this integration was more likely due a slight under-forecast STR strength as opposed to STR modification error (see Chapter IV.C.3), but the ARW error during the final 36 h of this case appeared to be due to insufficient STR modification. The NCEP reanalysis fields valid at 36 h (Figure 4.14a) had evidence in the mid-levels of a significant ridge modification, as well as evidence of a weak break in the STR to the north. Such a ridge modification was consistent with the northwestward track of the TC through day two (Figure 4.4c) of the case. However, the storm gradually turned more westward on day three as it encountered the strong ridge over the Ryukyu Islands. In contrast, the ARW forecast had less ridge modification during this case (Figure 4.14b), and the ARW forecast had Talim turning to the west late on day one after it encountered the ridge over the Ryukyu Islands. The insufficient ridge modification led to an increasing error on days two and three as the ARW track forecast was a little south of west while the actual storm track was to the west-northwest.

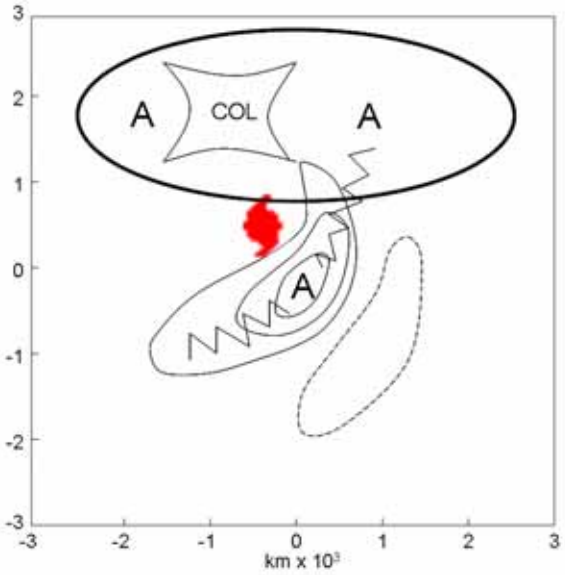

Figure 4.13 (After: Carr and Elsberry 2000a) Schematic of subtropical ridge modification due to a peripheral anticyclone. The reorientation of the ridge to the southeast of the TC creates a poleward steering flow.

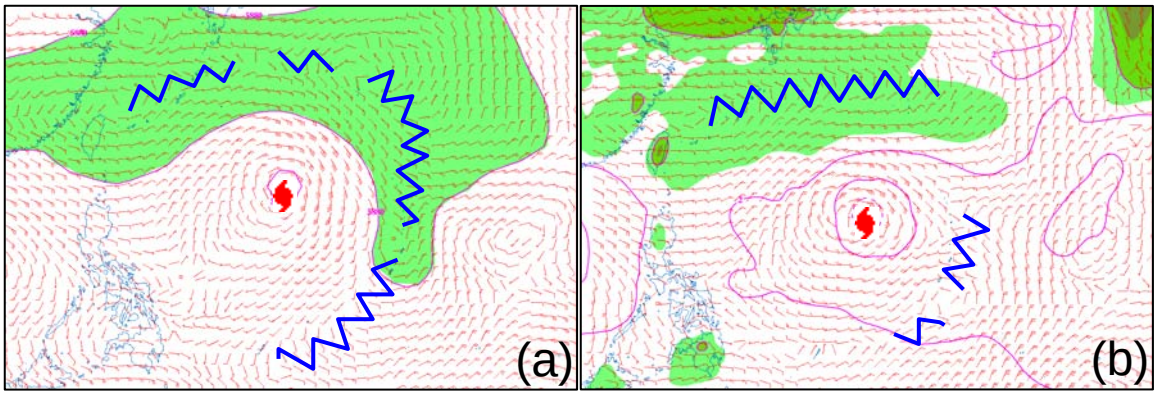

Figure 4.14 ARW insufficient ridge modification during the first Typhoon Talim case. The panels are from (a) the 500 mb NCEP reanalysis and (b) 36-h ARW outer nest forecast at the 0.4940 sigma-p level valid at 12 UTC 28 August 2005 (36 h into the integration). The shaded contours are the height fields (pressure perturbation field in the ARW). Winds are in kt, and in the ARW are displayed at every tenth grid point. In the ARW field, the STR is not modified, which keeps Talim on a westward track.

Even though the intensity of Talim was about equal in the NCEP reanalysis and the ARW fields at 36 h (10-m winds were about 40 kt – not shown), the JTWC estimated Talim to have an intensity of 70 kt at this time (recall the NCEP reanalysis does not have a bogus vortex). In addition, the ARW significantly under-forecast the size of Talim on days two and three. This size error may have been the primary factor for the insufficient ridge modification. All six models 72-h forecasts in SAFA outperformed the ARW and the MM5, and the UKMO was the only other model that had too little poleward movement on days two and three. The MM5 and NOGAPS track forecasts did not have the premature westward turning despite also significantly under-forecasting the intensity (and size in the case of NOGAPS) of the storm. In the MM5, the majority of the error was due to a slow bias (Figure 4.4c).

Insufficient STR modification by the ARW was not observed in all cases. At the end of the end of the first Typhoon Nabi integration (Figure 4.4e), the ARW forecast had a very pronounced STR modification (Figure 4.15b). In this case, the STR modification was more pronounced than in the NCEP reanalysis on day

three (Figure 4.15a), but this was unlikely to have caused the (relatively small) ARW cross-track error. The cross-track error in the ARW in this case is more likely a result of negative along-track errors (forward progress too slow) early in the integration, which allowed time for the steering flow ahead of the TC to slightly change direction. The UKMO had a similar track forecast as the ARW, but was not quite as slow. The abruptness of the poleward turn of the ARW forecast during the final 6 h suggests a tracker error.

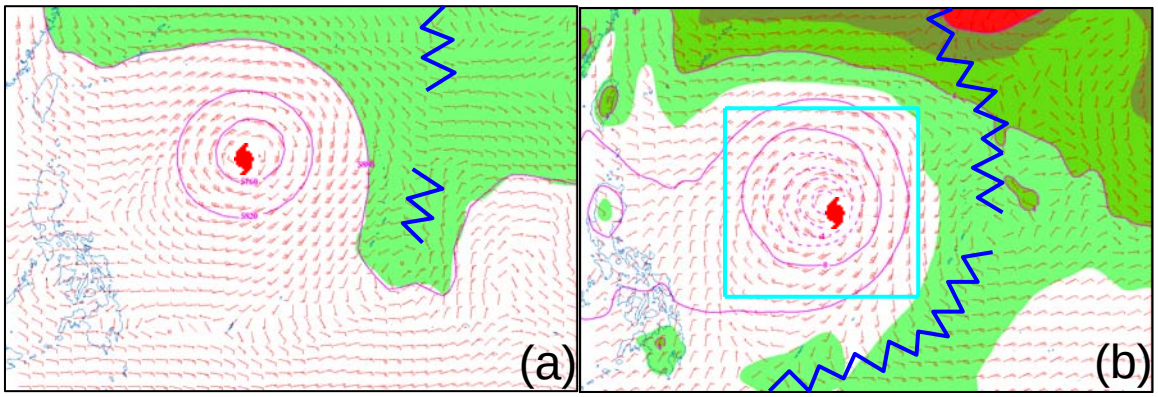

Figure 4.15 As in Figure 4.14, except for the first Typhoon Nabi case valid at 12 UTC 2 September 2005 (72 h into the integration). The pronounced ridge modification in the (a) ARW forecast is slightly stronger than in the (b) NCEP reanalysis.

The MM5 and GFS forecasts had small along-track errors early in these Typhoon Nabi integrations, but both had excessive poleward propagation throughout the entire integrations. Only the GFS model was similar to the MM5, but the MM5 by far had the largest 72-h position error (372 n mi) of all the models. Since the GFS is used to initialize the MM5, the similarity of the forecast errors suggests a TC vortex that is too large, and thus causes excessive ridge modification. If this is the case, the ARW integration would not have the same error since spin-up severely contorted the vortex early in the forecast.

Although the feedback from the inner nest to the outer nest could have an effect during the ridge modification process, the peripheral ridge, vorticity advection, and col zone in the ridge modification scenarios were generally outside the domain of the ARW inner nest (the relative size of the inner nest is

included in Figure 4.15d for reference). However, STR modification errors in the ARW integration were not likely due low model resolution since the 12 km resolution of the outer nest is sufficient to resolve the features involved in STR modification.

7. Erroneously Strong Anticyclone in China

As Typhoons Talim and Nabi approached the Ryukyu Islands roughly four days apart, an erroneously strong anticyclone in China was observed in the ARW integrations. The anticyclone produced erroneously strong northeasterly flow in the mid-levels, which is what ultimately sheared Typhoon Nabi in the ARW forecast and caused a tracker error just before reaching Kyushu Island (see Chapter IV.C.3, also Figure 4.10). All six models in SAFA had similar track errors to varying degrees, with the ARW, UKMO, GFDN, and NOGAPS having the largest error to the left of the observed track.

Typhoon Talim also encountered this anticyclone near the end of the second integration for this storm (Figure 4.4d), although the anticyclone was farther west at this time and did not cause noticeable track error in the ARW forecast. If the ARW forecast had not had large negative along-track error (forecast too slow), the TC would have reached mainland China and likely have been subjected to stronger northerly steering flow in the region than what was observed in most of the other models. The JTYM forecast was the only model that had track error to the south for Talim after it reached the Taiwan Strait.

8. Similarities with the SAFA Models

The track forecasts of the ARW, which were shown in Chapter IV.B.1 to have skill compared to CLIPER, had only one significant error (defined as position error >100 n mi at 24 h, >200 n mi at 48 h, and >300 n mi at 72 h) at any 24-h interval during the seven integrations (Table 4.1). The MM5 forecasts had significant errors in nine of the 24-h periods. Since the MM5 fields were not available, it is difficult to determine the error mechanisms of the MM5 track forecasts in these cases.

Table 4.1 Summary of ARW and MM5 significant track errors for each 24-h period of the seven cases, where a significant error is defined >100 n mi at 24 h, >200 n mi at 48 h, and >300 n mi at 72 h. Since the MM5 model fields were not available, the MM5 error mechanisms are not included in the table. The Typhoon Khanun case was 66 h long.

			ARW		MM5
		Track Description	Error Mechanism	Models with Similar Error	Models with Similar Error
MATSA	24-H	NW along STR			GFS
	48-H	NW along STR			
	72-H	NW along STR			
MAWAR	24-H	NW along STR			GFDN
	48-H	N entering recurvature			GFDN
	72-H	NE recurvature			GFDN
TALIM I	24-H	NW along STR			NOGAPS, GFS, JGSM, JTYM
	48-H	NW along STR			
	72-H	WNW along STR			
TALIM II	24-H	WNW along STR			
	48-H	WNW along STR			
	72-H	WNW along STR			
NABI I	24-H	WNW along STR			
	48-H	WNW along STR			JTYM
	72-H	WNW along STR			JTYM
NABI II	24-H	WNW along STR			
	48-H	WNW along STR			
	72-H	NW entering recurvature			
KHANUN	24-H	WNW along STR	Spin-up/Tracker	None	
	48-H	NW along STR			GFDN
	66-H	NNW entering recurvature			GFDN

The significant MM5 errors did not have any clear positive correlation with the errors of any of the other models. Interestingly, there appeared to be a negative correlation between cross-track errors of the MM5, and those of the ARW and UKMO (e.g., when the MM5 error was left-of-track, the ARW and UKMO errors were right-of-track). However, the small number of cases in this study precludes a statistically significant analysis of these possible correlations.

9. Landfall

A summary of the track forecast errors for all instances of landfall (Table 4.2) highlights the performance of each model for the period when the TCs were most likely to affect large populations and/or military installations. Except for the timing of the Typhoon Nabi landfall (defined as the time it crossed the Mariana Island archipelago – see Figure 4.4e), the ARW forecasts were equal or superior to the MM5 forecasts for landfall prediction.

Table 4.2 Summary of ARW and MM5 position and timing errors for all instances of landfall in the seven cases. Positive timing errors are forecasts that had landfall occur after observed landfall; negative timing errors are forecasts that had landfall too early. For the first Typhoon Nabi case, "landfall" is considered to be when the TC passed the Mariana Islands archipelago, even though the storm did not make direct landfall on any of the islands during the integration.

	Observed Landfall			ARW		MM5	
	Location	Time	Hours into Integration	Location Error	Timing Error	Location Error	Timing Error
MAWAR	Miura Peninsula, Japan - just south of Tokyo	1730 UTC 25 August	65.5	48 n mi SW	within 1 h	505 n mi SW, on Kyushu Island	-2.5 h
TALIM II	near Hualien, Taiwan	18 UTC 31 August	54	66 n mi S	+6 h	no landfall	N/A
TALIM II	near Fuzhou, China	06 UTC 1 September	66	no landfall	N/A	no landfall	N/A
NABI I	no landfall, but passed Mariana Archipelago 35 n mi NE of Saipan	00 UTC 31 August	12	13 n mi S	+12 h	55 n mi N	0 hr
KHANUN	near Jinqing Town, China	07 UTC 11 September	43	69 n mi N	+4 h	195 n mi S	+5 h

In one prominent example, the ARW landfall forecast for Typhoon Mawar (which occurred over 65 h after initialization) had a location error of only 48 n mi, and a timing error of less than one hour. In contrast, the MM5 forecast had very large location error of over 500 n mi, (making the otherwise impressive timing error nearly irrelevant). The ARW landfall forecast on Taiwan of Typhoon Talim was not as precise, but still outperformed the MM5, which forecast the TC to miss the island completely. Neither model forecast Talim to make landfall on mainland China.

As with possible correlations between models, the small sample size used in this study may not represent the performance of the models over a longer period. All that can be determined definitively is that the ARW landfall forecasts were usually more accurate than the MM5 landfall forecasts for these seven cases.

C. EVALUATION OF ARW INTENSITY PREDICTION

1. Overview and Methodology for Evaluation

The mean intensity errors of the ARW, MM5, and CLIPER techniques for the seven cases are shown in Figure 4.16. The CLIPER technique used for comparison of the ARW and MM5 intensity forecasts is the Statistical Typhoon Intensity Forecast 5-Day Model (ST5D) developed by Knaff et al. (2003) using data from western North Pacific TCs during 1967-2000. The MM5 had a lower mean intensity error than the ARW at all forecast intervals, and the MM5 errors were substantially lower than the ARW errors during the first 54 hours.

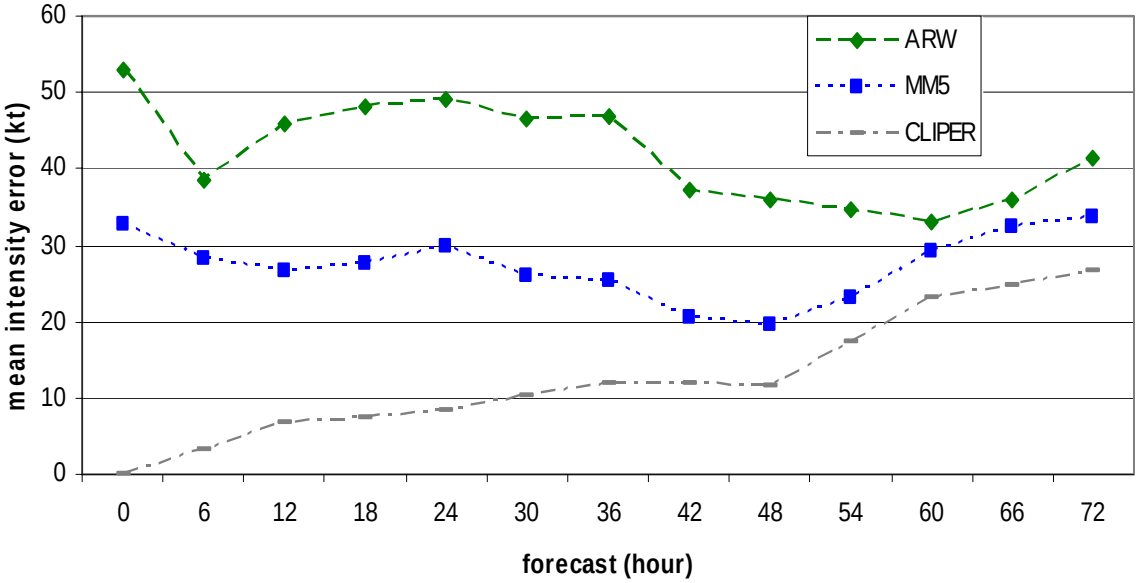

Figure 4.16 The mean absolute intensity (sustained surface winds) error of the ARW prediction (dashed green line with diamond points), MM5 prediction (dotted blue line with square points), and CLIPER technique (grey dashed-dotted line) for the seven TC cases that did not cause failure of the moving-nest algorithm in the ARW integration.

Because the initial intensity errors were so large, the errors decreased in time to 48 h (60 h) for the MM5 (ARW), which is contrary to what would be anticipated since model error is expected to grow in time. Later in the forecasts, the error growth was similar to that for the large sample of TCs included in the

climatology and persistence forecast ST5D. As in the C120 track forecasts, the ST5D technique had zero error at the 00-h forecast because the initial intensity is an input in the technique. In contrast to the track forecasts, the CLIPER-type intensity technique ST5D had smaller mean intensity errors than the ARW and MM5 at all forecast intervals. The superior performance of the ST5D indicates the ARW and MM5 did not have skill for the intensity prediction of these seven cases.

The main reason for the large TC intensity errors is a strong negative bias at all forecast hours for both the ARW and MM5 (Figure 4.17). Furthermore, intensity errors for both models had a negative bias at nearly all forecast intervals for each of the seven TCs in this study. The very strong negative bias and large mean error (Figure 4.16) of the ARW at initial time may be attributed to the initial vortex from the first-guess GFS field, which does not have a bogus vortex or high-resolution model spin-up prior to initialization. In most cases, the vortex intensified during the the first six hours of the integration, which is evident in the immediate decrease in ARW model error (Figure 4.16) and corresponding decrease in model error bias (Figure 4.17) between 0 h and 6 h. A similar evolution was observed for the first 12 h of the MM5 forecasts, although the change was not nearly as strong as in the ARW. Beyond the first several hours of the ARW and MM5 integrations, factors other than model spin-up are more likely to contribute to the negative intensity bias than they are early in the integrations. These factors, along with the relationship between model spin-up and intensity errors, are examined in the following sections.

In the remaining results, the ARW intensity errors are evaluated by interrogating the storm structure, including the mass and moisture distribution, thermal structure, wind fields, and precipitation. Attention was given to the entire low-level wind field as opposed to only the maximum wind, as the circulation around the storm center covers a large area and is of high importance to the

protection of military and civilian assets. Since the NCEP reanalysis fields do not use a bogus vortex, the storms are almost always too weak and thus are of limited value for evaluating intensity errors.

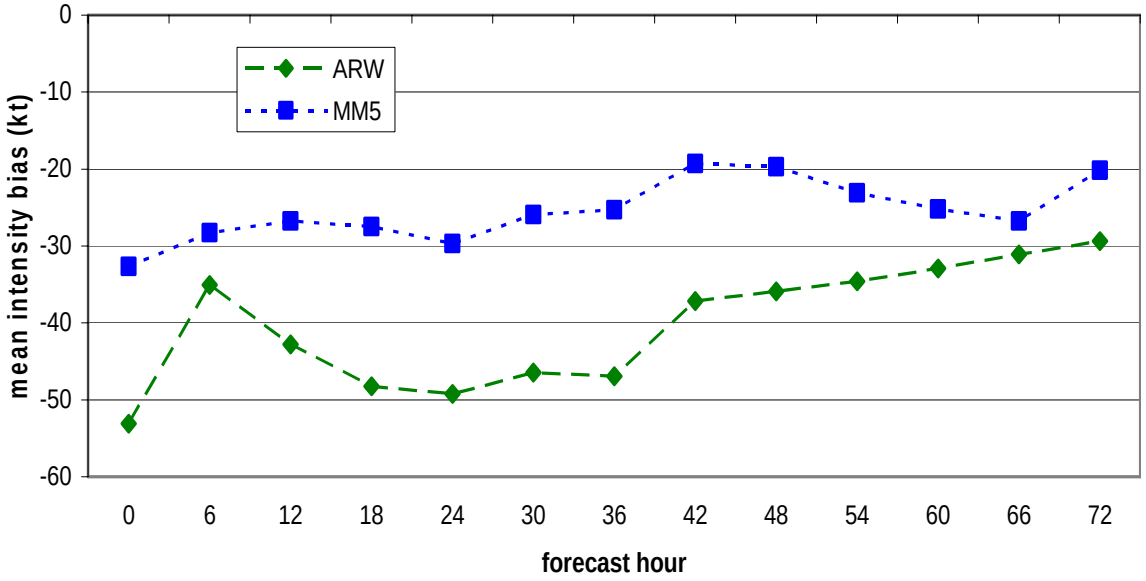

Figure 4.17 The mean intensity error bias (sustained winds) of the ARW predictions (dashed green line with diamond points) and MM5 predictions (dotted blue line with square points) for the seven TC cases that did not cause failure of the moving nest algorithm in the ARW integration.

2. Intensity Errors Due to Initialization and Spin-up

The observed TC intensities at the initial time for the ten ARW runs (including the three cases that had nest failure) ranged from 35 kt to 140 kt. Since the ARW initial conditions were provided by the lower resolution, non-bogused GFS fields, the initial TC intensities in the ten ARW integrations were never greater than 42 kt. Furthermore, the initial intensities in the ARW integrations had virtually no correlation with the observed TC intensities, while the MM5 initial intensities were slightly higher for the more intense storms (Figure 4.18). Although both the ARW and MM5 usually had an initial intensity that was too weak, the bogus vortex, warm-start procedure used in the MM5 produced a stronger initial TC for the stronger storms. In contrast, the ARW essentially initialized the storms with an intensity around 30 kt, regardless of the

actual storm intensity. This "homogeneous intensity initialization" not only produced large intensity errors for the stronger TCs, but also conceivably increased the chances for moving-nest failure for the strong TCs since the 500-mb height minimum may have been significantly unresolved and underdeveloped. Even so, the three nest failure cases in this study were with observed TC intensities ≤45 kt (see Chapter IV.A).

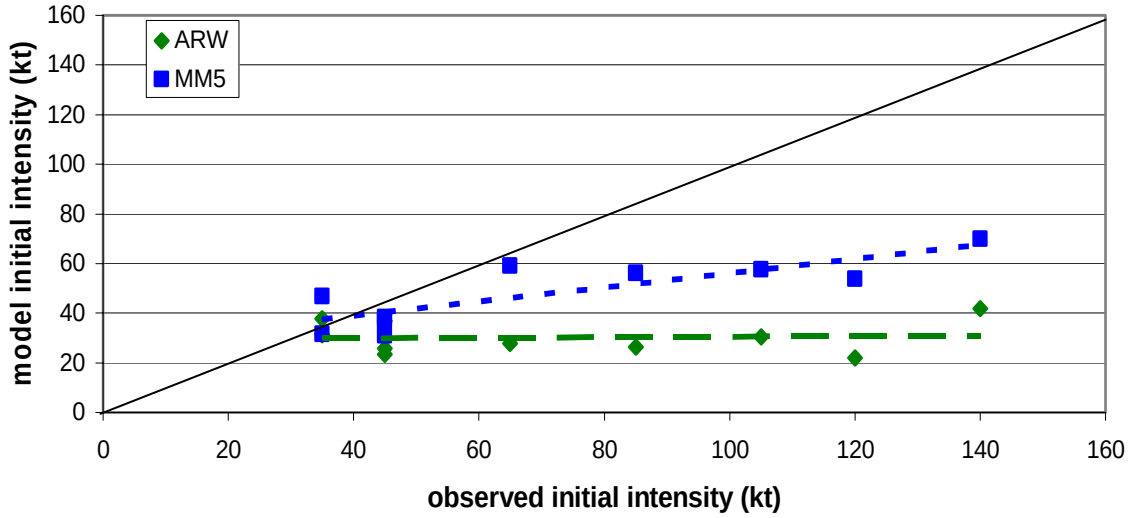

Figure 4.18 Scattter plot of observed TC intensity at initialization of all ten cases (includes three cases with moving-nest failure) versus the initial TC intensity indicated in the ARW (green diamonds) and MM5 (blue squares) models. The diagonal black line represents an accurate initial intensity. Least-squares regressions for each model are indicated by the dashed green (ARW) and dotted blue (MM5) lines. The initial TC intensity in the ARW model had virtually no correlation with the observed intensity.

Of the seven ARW integrations that did not have a moving-nest failure, two had initial observed TC intensities near 30 kt, and thus were initialized with accurate intensity by the ARW. These two cases were the first Talim integration (Figure 4.19) and the Matsa integration (Figure 4.20). Since the other five ARW integrations had initial intensities that were more than 35 kt too low, it was hypothesized that these two integrations would have the smallest storm structure irregularities due to spin-up.

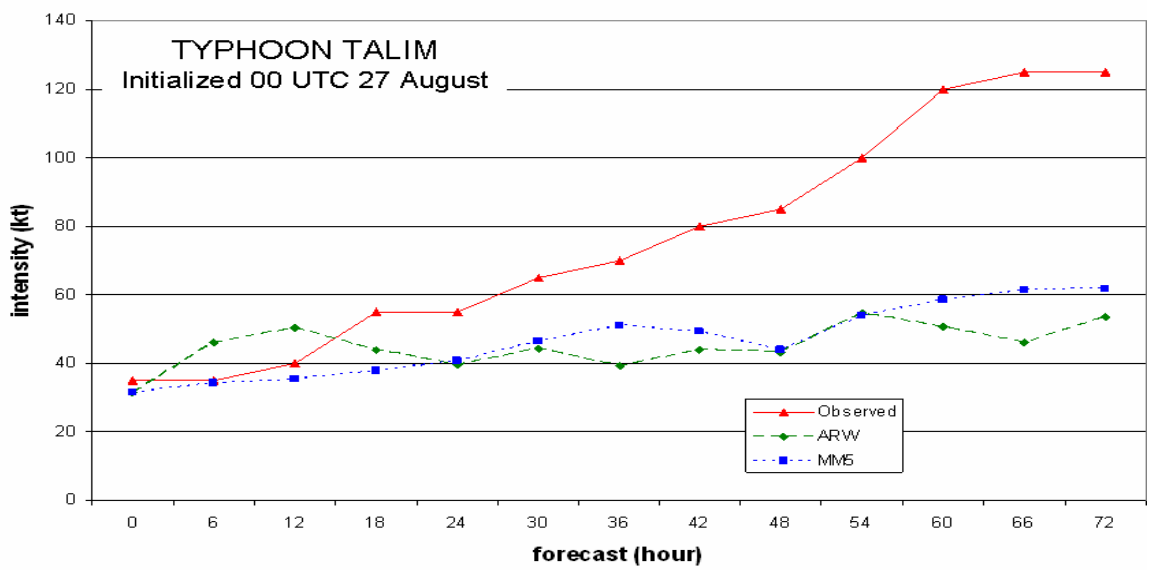

Figure 4.19 Observed and forecast intensity for the first Typhoon Talim case initialized at 00 UTC 1 August 2005.

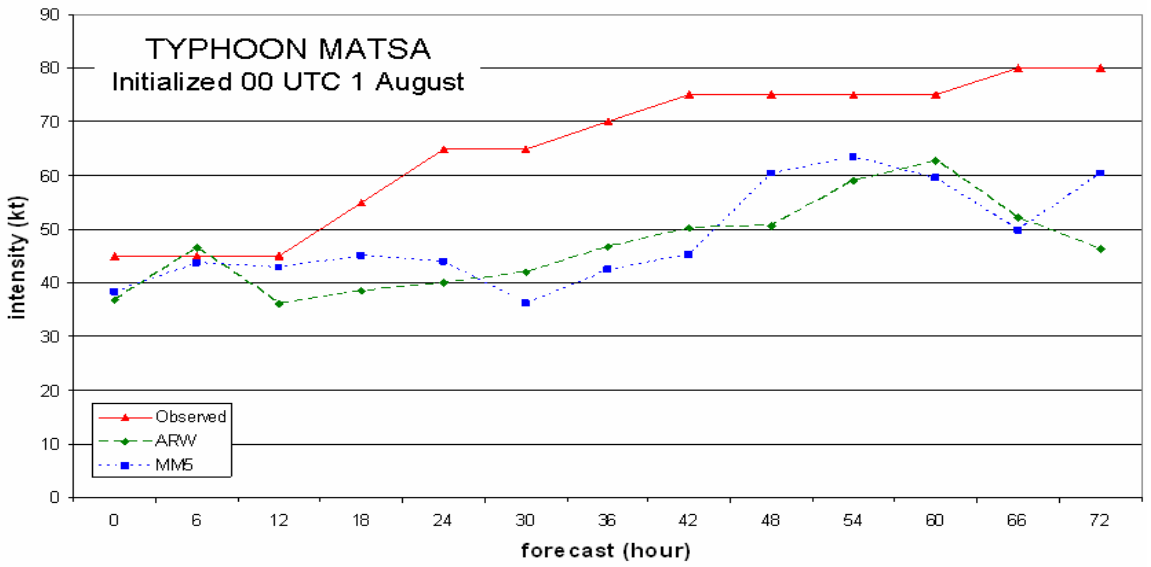

Figure 4.20 Observed and forecast intensity for the Typhoon Matsa case initialized at 00 UTC 27 August 2005.

The ARW initial conditions for the first Typhoon Talim integration (Figure 4.21) had a radius of maximum low-level winds of roughly 110 n mi, and a vortex that was severely tilted with height. Since Talim was in reality a weak tropical storm at this time (estimated sustained winds were 35 kt), this large radius of maximum winds in the initial conditions might not be unreasonable. Satellite imagery on 03 UTC 3 August (not shown) indicated Talim had a ragged eye structure with a radius of approximately 100 n mi. However, the tilted nature of the vortex was not likely to be realistic. Other unrealistic aspects were the maximum eyewall winds at an altitude of roughly 450 mb (0.45 sigma-p level), and virtually no warm core existed near the center of the vortex at any level. Neither of these conditions, which were also observed in the Matsa initial fields, is consistent with the structure of a developing tropical cyclone, which should have the maximum winds near the top of the PBL and warming in the eye due to subsidence (Elsberry 2006).

After 9 h of ARW integration in the first Talim case (Figure 4.22), the radius of maximum surface winds slightly decreased, and the intensity of the low-level winds did increase. However, the maximum winds in the storm were still well above the boundary layer, and the overall structure of the TC had become rather contorted. High-frequency oscillations of the surface pressure (not shown), wind, and potential temperature fields indicated the mass and wind fields were not in balance and TC development was being hindered by significant model spin-up. A contorted TC structure was also present in the Matsa case during the first 12 h of integration (not shown).

The cases that were initialized with a TC intensity 35 kt or more below the observed intensity had similar effects of spin-up as those in the second Talim and Matsa cases. Typhoon Mawar, which had an initial bias of over 70 kt (Figure 4.23), had a similar pattern of a slight eyewall contraction and increase in surface winds during the first 6 h, followed by a “breaking down” of the TC structure for several subsequent hours. This phenomenon could be observed in the

precipitation field, which has a small contraction of eyewall convection between 3 h and 6 h (Figure 4.24a, b), followed a dilation and fragmenting of the eyewall convection (Figure 4.24c).

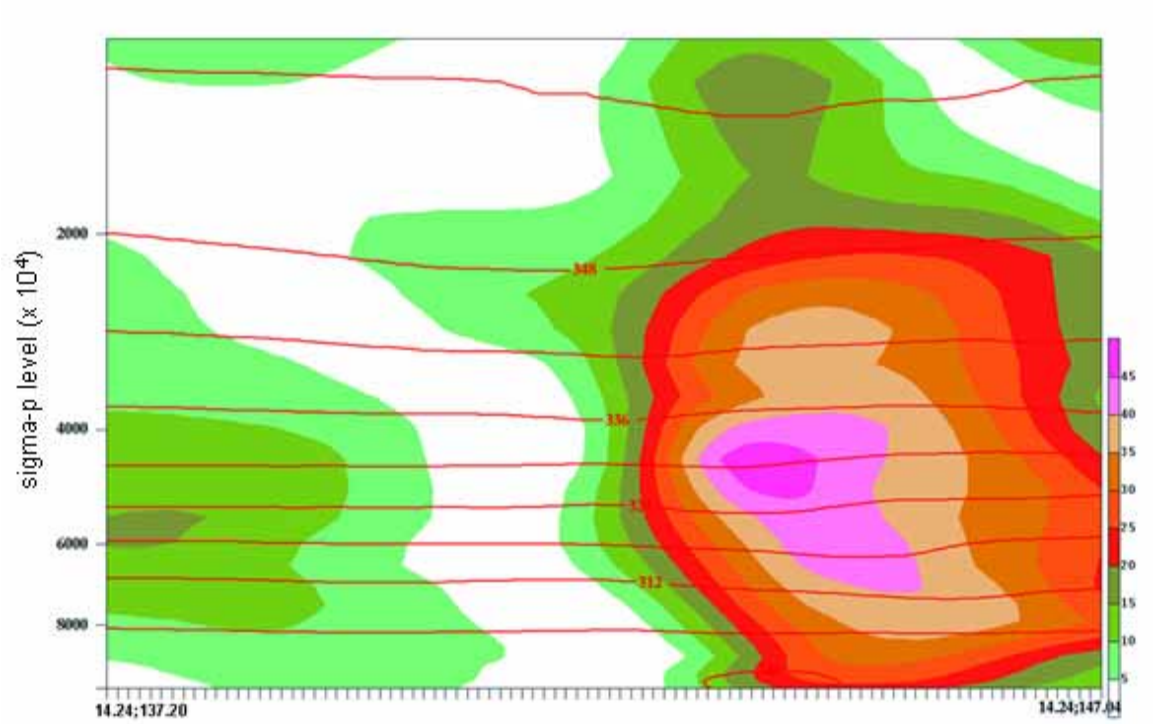

Figure 4.21 West-to-east cross-section of the initial ARW meridional winds (shading, in kt) and potential temperatures (contours, in K) through the center of Tropical Storm Talim from the first integration for this storm at 00 UTC 27 August 2005. The cross-section is from the inner-nest fields. The horizontal interval is approximately 4.4 n mi.

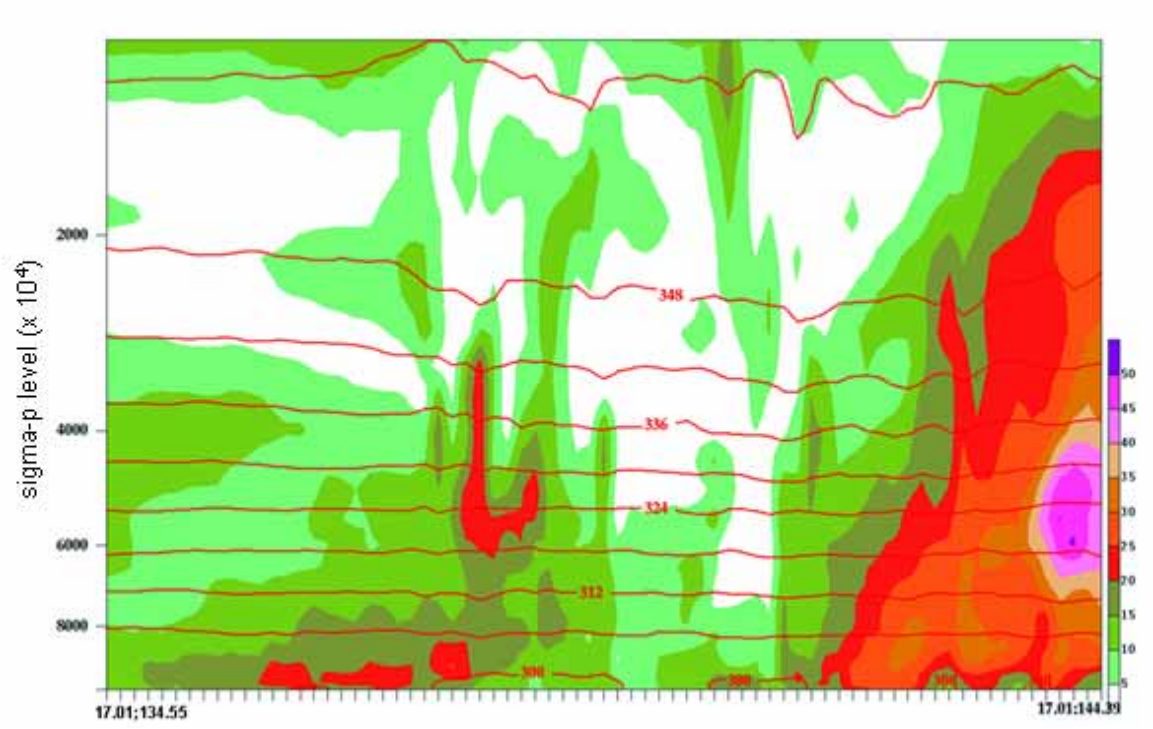

Figure 4.22 As in Figure 4.21, except for the ARW 9-h forecast.

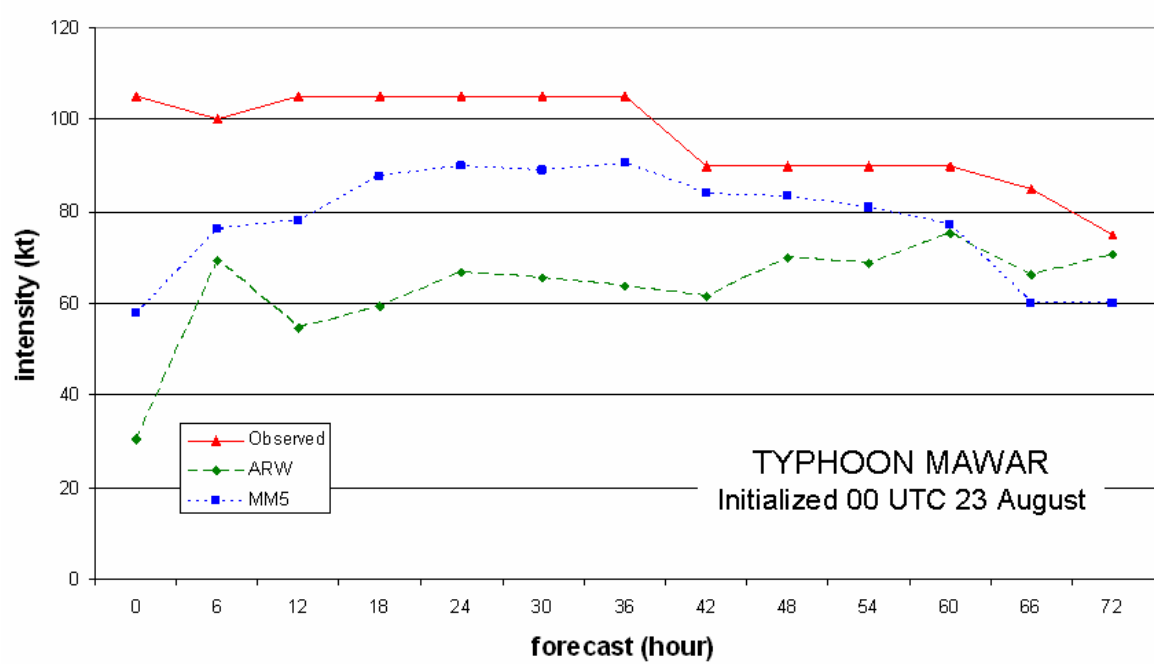

Figure 4.23 Observed and forecast intensity for the Typhoon Mawar case initialized at 00 UTC 23 August 2005.

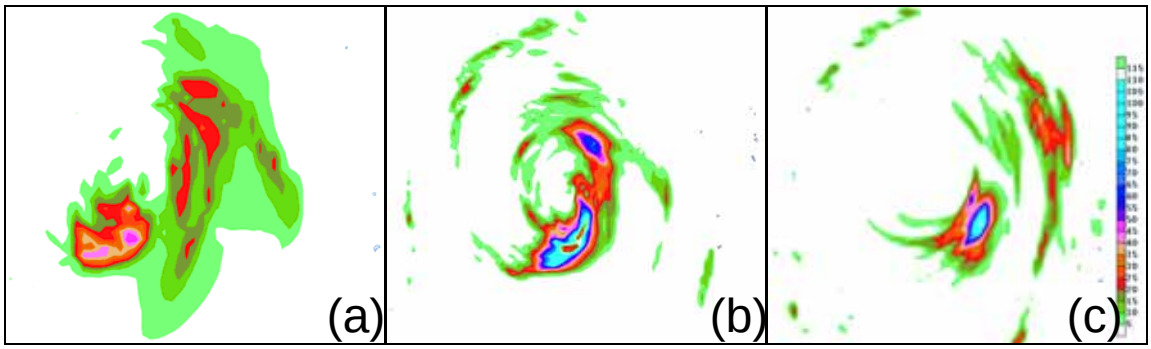

Figure 4.24 Outer-nest 3-h accumulated precipitation (mm) for the (a) 3-h forecast, (b) 6-h forecast, and (c) 9-h forecast of the Typhoon Mawar case. After bogusing with an initial vortex that was too large, the eyewall slightly contracted from 0-6 h, then dilated and fragmented by 9 h. Incremented inner-nest precipitation fields were not available in this study, but feedback from the inner-nest and outer-nest allowed a fair assessment of inner-nest precipitation location by viewing the outer-nest precipitation.

The ARW-predicted changes during spin-up were particularly severe in the first Typhoon Nabi integration (Figure 4.25). After the initial small contraction of the vortex and corresponding increase in intensity, the typhoon structure remained severely imbalanced and disorganized until 48 h. The strongest winds in the storm remained well above the boundary level, which limited the air-sea fluxes of heat and moisture necessary for development. In contrast, spin-up in the second Typhoon Talim integration (Figure 4.26) caused less disorganization of the TC, despite this case being initialized with an intensity 91 kt too low. The structure of Talim was relatively balanced by the 18-h forecast. The drastic differences in these two cases were related to the character of the initialization fields (Figure 4.27). The initial vortex structure in the Nabi case was severely asymmetric and required a prolonged period of spin-up before reaching balance and being able to intensify. In the Talim case, the initial vortex was already reasonably symmetric and required a shorter adjustment period.

In all seven cases, the severity of spin-up adjustments after an initial small contraction appeared to depend on the structure of the vortex in the initial fields

and not on the intensity accuracy of the initial vortex. Even in the first Talim and Matsa cases, which were initialized with accurate vortex intensity, spin-up adjustment and corresponding vortex disorganization were significant.

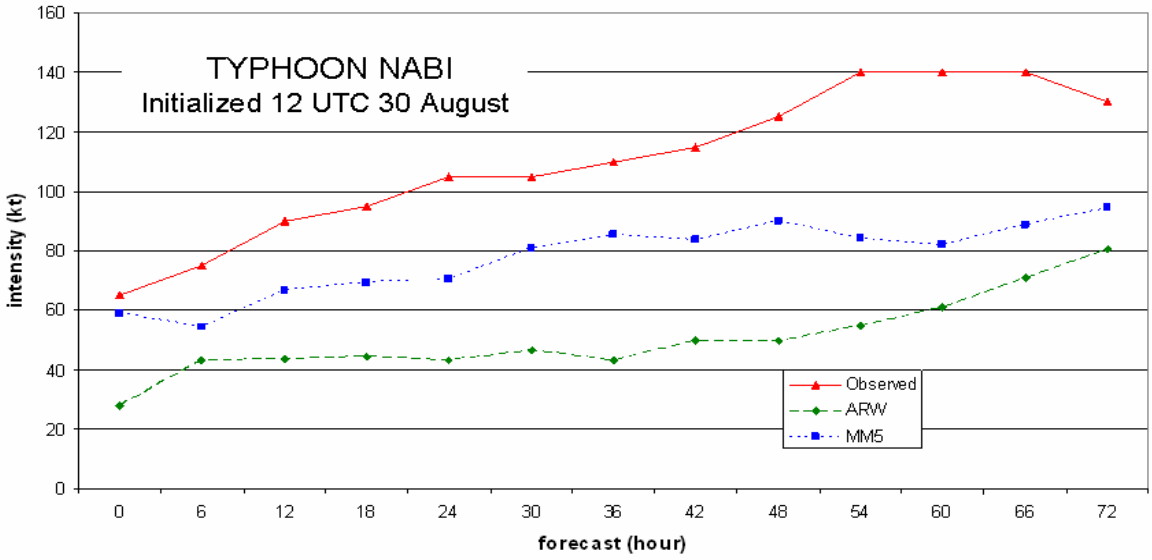

Figure 4.25 Observed and forecast intensity for the first Typhoon Nabi case initialized at 12 UTC 30 August 2005.

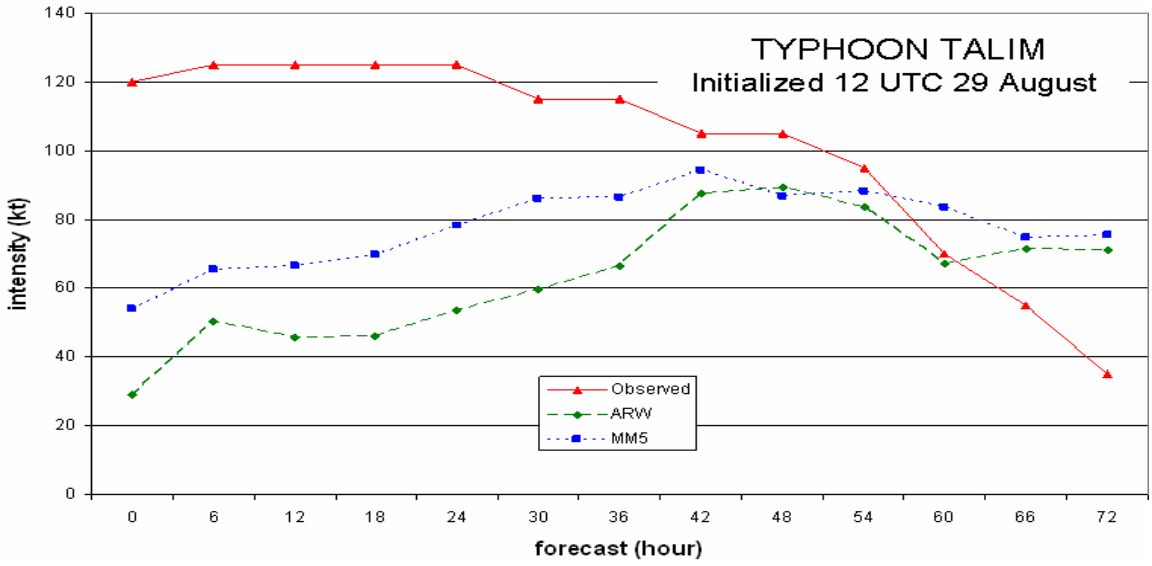

Figure 4.26 Observed and forecast intensity for the second Typhoon Talim case initialized at 12 UTC 29 August 2005.

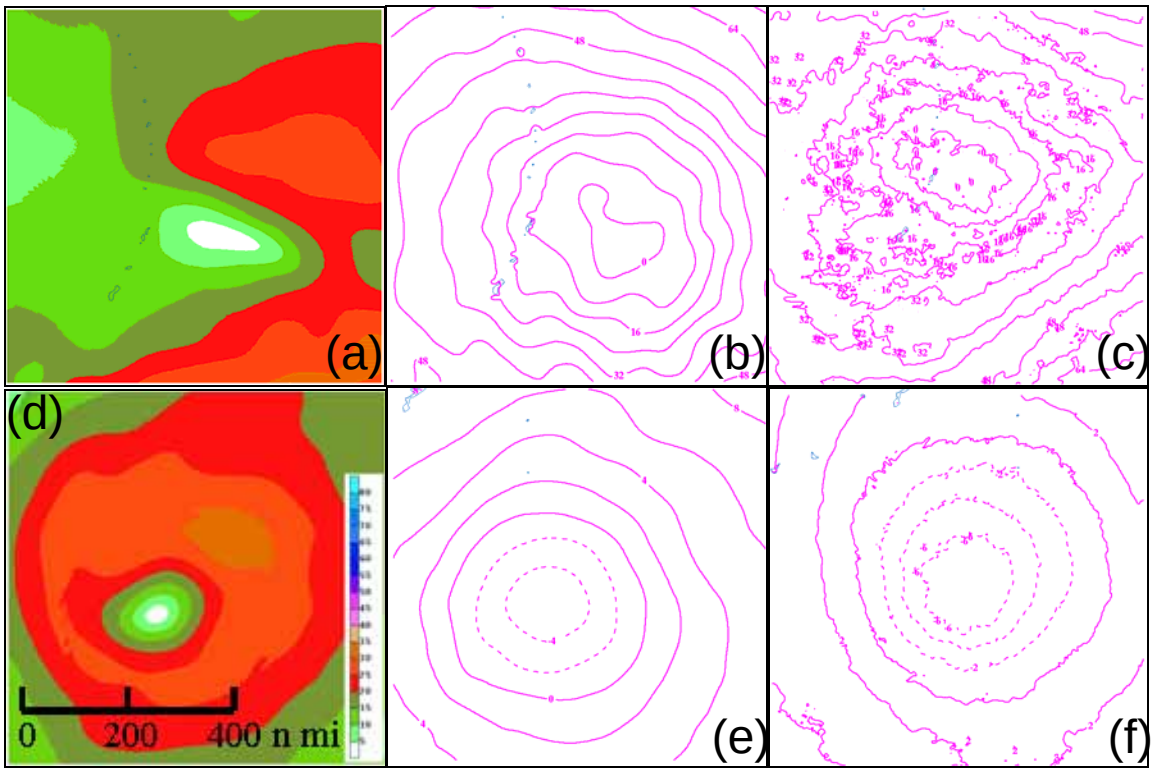

Figure 4.27 Comparison of inner-nest ARW initial conditions in the first Nabi integration (top row) and second Talim integration (bottom row). (a) and (d) are 0.988 sigma-p level isotachs (kt) from the initial wind fields, (b) and (e) are the corresponding initial 0.988 sigma-p level pressure perturbation fields (mb), and (c) and (f) are the same fields after 12 h of integration. Compared to the relatively symmetric vortex structure in the initial fields of the Talim case, the Nabi case had an irregular, asymmetric vortex that was still undergoing extensive spin-up adjustments after 12 h.

In several of the cases in this study (i.e., those with a severely flawed initial vortex structure), spin-up is likely to have affected the intensity forecasts well beyond the first few hours of the integrations. In many cases, this complicated the ability to discern intensity errors due to spin-up from those due to other causes. One example is in the Typhoon Khanun case (Figure 4.28), which had a reasonably well-defined vortex structure in the low levels after only 12 h but had a severely contorted upper-level vortex at this time (Figure 4.8). The upper levels of this storm remained severely disorganized in the ARW integration until 54 h. Thus, the TC did not have a sufficient organization or upper-level

outflow to intensify as did the storm, which reached an intensity of 115 kt. According to JTWC, the radius of tropical storm-force winds at the time of peak intensity was 85 n mi in all four quadrants (in this context, JTWC uses 34 kt for tropical storm force winds, which is the definition used hereafter in this text. By most definitions, tropical storm force winds are actually 35 kt). In the ARW integration, the peak surface winds were only 44 kt, so the storm structure was quite different. If the ARW track forecast had been poor in this case, the lack of upper-level outflow in the ARW may have been attributable to TC interaction with a ridge or midlatitude system and subsequent shearing of the structure. However, the track forecast was excellent (Figure 4.4g) and no significant errors in position or amplitude of other synoptic features were apparent in the ARW fields. Consequently, prolonged effects of spin-up is proposed as the primary cause of the disorganized upper levels in the Khanun case.

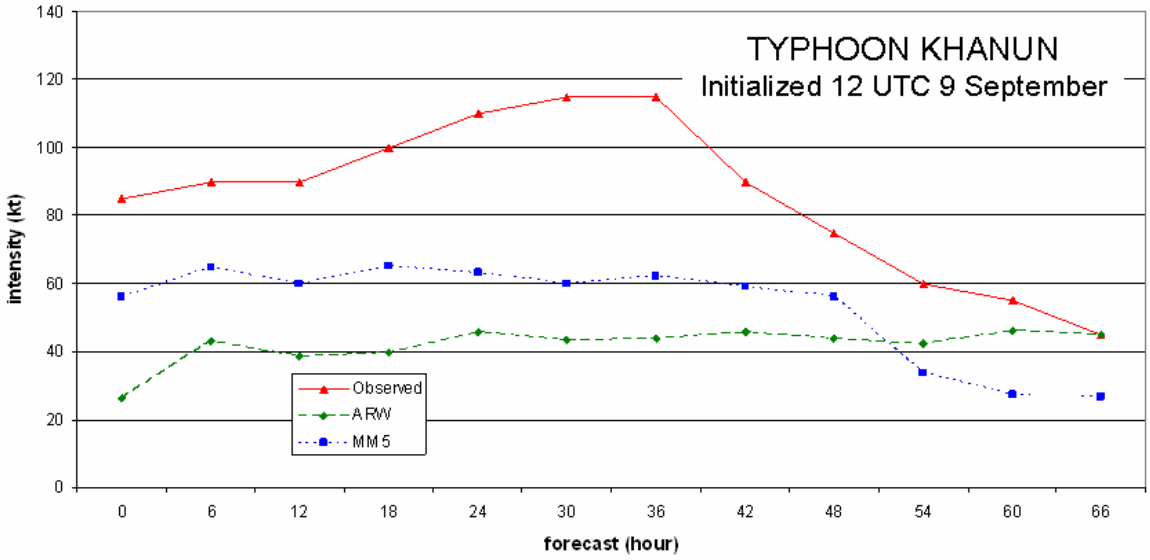

Figure 4.28 Observed and forecast intensity for the Typhoon Khanun case initialized at 12 UTC 9 September 2005.

A summary of all cases of significant intensity errors (defined as intensity error >10 kt at 24 h, >20 kt at 48 h, and >30 kt at 72 h) for the ARW and MM5 in all seven cases is provided in Table 4.3. The duration of the ARW spin-up effects on the vortex structure in each case was subjectively determined. The

ARW predictions had significant error in all but three of the intervals. Since the ARW intensity forecasts had a large negative initial bias in five of the cases and suffered from considerable spin-up effects in all the cases (sometimes for days), intensity error mechanisms are not assigned. It is assumed that initialization and/or spin-up greatly contributed to all significant errors. For the remaining sections of this chapter, intensity prediction performance of the ARW is evaluated during significant events in a mostly qualitative manner.

Table 4.3 Summary of ARW and MM5 significant intensity errors for each 24-h period of the seven cases, where a significant error is defined >10 kt at 24 h, >20 kt at 48 h, and >30 kt at 72 h. The duration of the spin-up effects on the ARW vortex were determined subjectively by examination of the model fields. The Typhoon Khanun case was 66 h long.

		Intensity Description	ARW		MM5
			Duration of Spin-up	Significant Error	Significant Error
MATSA	24-H	Intensification to 65 kt	12 h	X	X
	48-H	Intensification to 75 kt		X	X
	72-H	Intensification to 80 kt		X	
MAWAR	24-H	Steady at 105kt	21 h	X	X
	48-H	Decay to 90 kt		X	
	72-H	Landfall, decay to 75 kt			
TALIM I	24-H	Rapid intensification to 55 kt	48 h	X	X
	48-H	Rapid intensification to 85 kt		X	X
	72-H	Rapid intensification to 125 kt		X	X
TALIM II	24-H	Intensification to 125 kt	18 h	X	X
	48-H	Rapid decay to 105 kt			
	72-H	Landfall, rapid decay to 35 kt		X	X
NABI I	24-H	Rapid intensification to 105 kt	48 h	X	X
	48-H	Rapid Intensification to 125 kt		X	X
	72-H	Intensification, then decay to 130 kt		X	X
NABI II	24-H	Decay to 130 kt	27 h	X	X
	48-H	Decay to 105 kt		X	
	72-H	Reintensification to 115 kt		X	
KHANUN	24-H	Intensification to 110 kt	54 h	X	X
	48-H	Landfall, rapid decay to 75 kt		X	
	66-H	Over land, rapid decay to 45 kt			

No attempt was made to account for specific MM5 intensity errors since the MM5 fields were not available for this study. Based on several forecasts of intensification by the MM5 shortly after initialization, it did not appear the vortex structure was hindered by spin-up problems as often or to the same extent as in

the ARW integrations. Perhaps the best example of this was in the second Typhoon Nabi integration (Figure 4.29). Although the ARW and MM5 had initial intensities well below the observed intensity in this case, the MM5 forecast had rapid intensification beginning shortly after initialization, which is something the ARW did not forecast in any of the 10 cases. It should also be pointed out that the MM5 had a particularly straight track forecast during this period (Figure 4.4f), which further indicates the absence of appreciable initial imbalances. The lower initial intensity error and fewer indications of spin-up in the MM5 integrations contributed to the MM5 forecasts having significant intensity errors in only 13 of the 21 intervals.

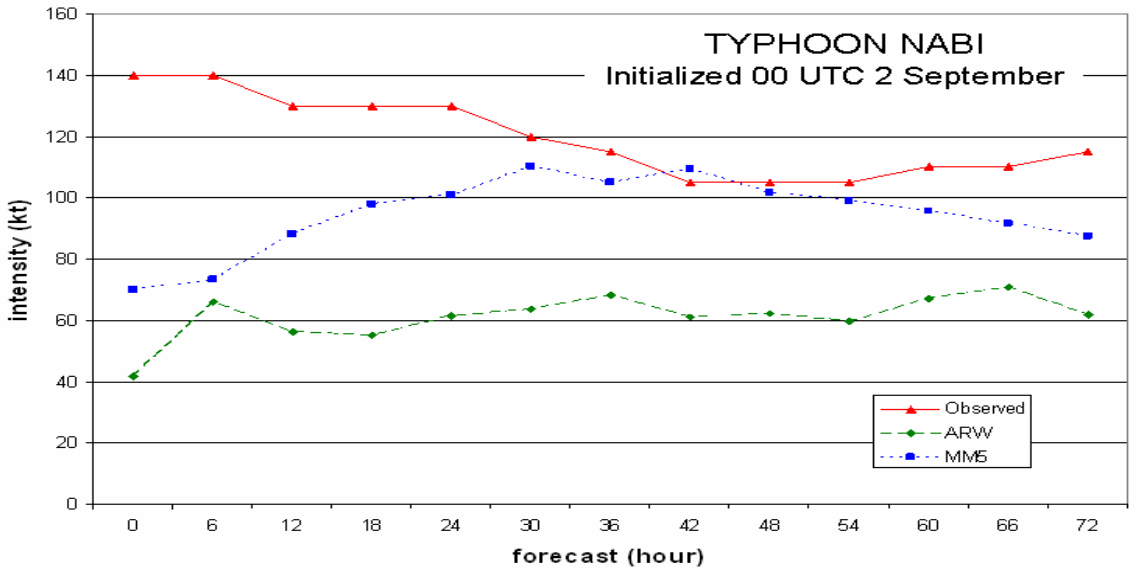

Figure 4.29 Observed and forecast intensity for the second Typhoon Nabi case initialized at 00 UTC 2 September 2005.

It is certainly the case that the spin-up perturbations observed in the ARW integrations were tied to the resolution of the GFS initial fields and the cold-start, non-bogus initialization procedure. Another potential source of small spin-up perturbations could be related to the resolution of the SST data (1/4° lat./lon.), which was higher than the GFS initial fields (1/2°lat./lon.), but still far below the inner-nest resolution (4 km, or roughly 1/28° lat./lon.). In NWP experiments with a winter storm over the North Atlantic, the low resolution GFS was found to

perform better than the mesoscale NCEP Eta model because the resolution of the SST data more closely matched that of the GFS [see COMET Module “Ten Common NWP Misconceptions”. Available online at http://www.meted.ucar.edu/norlat/tencom/p02 (current as of 27 Feb 2006)]. Since the intensification and sustenance of a TC relies on latent heat flux from the ocean (which is mostly a function of SST), it is possible the 1/4° resolution SST data also induced fluctuations in the low levels of the model and contributed to spin-up effects.

3. ARW-Predicted Structure during Formation and Intensification

After the roughly 12-h spin-up period in the ARW Typhoon Matsa integration (Figure 4.20), the ARW forecast a gradually strengthening storm that had a rate of intensification on day two that closely matched the observed rate of intensification. The 60-h forecast peak intensity was 63 kt, and at this time the model had a tight, vertical vortex with the maximum winds near the surface at a radius only 15 n mi (Figure 4.30). Anticyclonic flow above the 0.20 sigma-p level provided upper-level outflow during this time.

As Khanun made landfall late on day 2 in the ARW integration, the intensity was not affected in the forecast (Figure 4.28), which was roughly the same time that the upper portions of the vortex were finally becoming organized and aligned with the low-level vortex (Figure 4.31). Warming in the vortex core (Figure 4.31), especially in the upper levels, was first observed at this time, and convection on the east side of the storm (which was still over water) intensified and moved closer to the eye. Perhaps the typhoon maintained a weak tropical storm intensity after landfall because the constructive effects of a properly structured vortex counteracted the destructive effects of being (partially) over land.

The second Typhoon Talim ARW integration (Figure 4.26) had a reasonable vortex structure at the initial time (Figure 4.27d, e), and after a comparatively brief spin-up period, appeared balanced, vertically stacked, and had a warm core in the 18-h forecast fields. For the next 30 h, the ARW forecast

maintained a well-formed vortex (Figure 4.32) and predicted a rapid intensification to 89 kt, which was the most intense ARW forecast in this study.

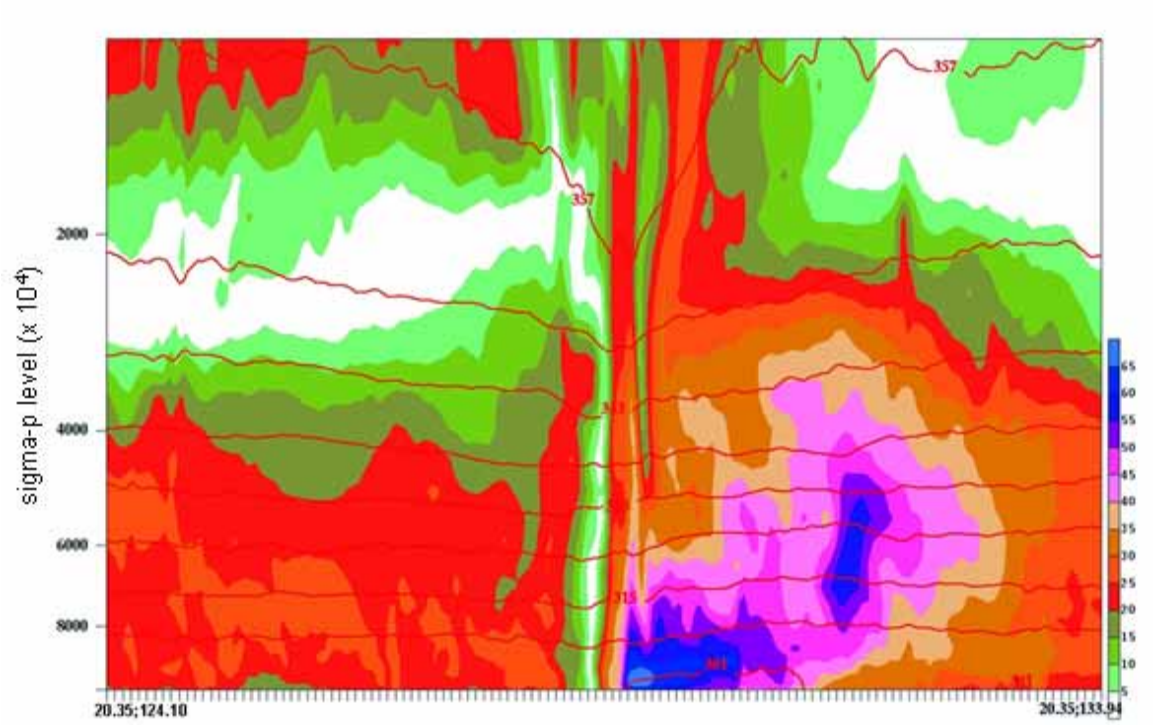

Figure 4.30 As in Figure 4.21, except for the ARW 60-h forecast of Typhoon Matsa. The broad horizontal white band at roughly 0.20 sigma-p level is the transition from cyclonic flow below to anticyclonic flow aloft.

During the period of rapid intensification in the ARW forecast, the actual intensity was 120 kt before beginning to decay from the impacts of land to the west. Since Talim was in a favorable environment for an intense TC, the ability of the ARW model to forecast a rapid intensification of this storm was encouraging. Very high values of surface latent heat flux were predicted over a broad region in this integration (Figure 4.33a) compared to the Mawar case in which a less favorable environment existed and the TC was actually decaying (Figure 4.33b). Even after Talim crossed Taiwan and decayed, the ARW predicted a reintensification of the TC over the warm waters of the Taiwan Strait.

Carr and Elsberry (1997) proposed a tangential wind profile that first increased approximately linearly and then more rapidly to the maximum winds near the eyewall. The outer wind structure in the second Talim ARW forecast did not become larger during intensification in the model, but instead it closely matched the size of the outer wind structure analyzed by the JTWC (Figure 4.34). This agreement suggests the negative intensity bias errors of the ARW in this case were not due to the overall storm being too small, but were instead due to an eye that was too large. The ARW structure does not exactly match the observed structure (the ARW winds extended slightly farther ahead, or northwest of, the TC, and not quite as far behind, or southeast of, the TC as in the JTWC analysis). However, the two structures are fairly close, and the since the environmental steering flow and beta-effect propagation depend on the outer wind structure of a TC, the accurate size in the ARW forecast for this case also may account for the accurate track forecast (Figure 4.4d).

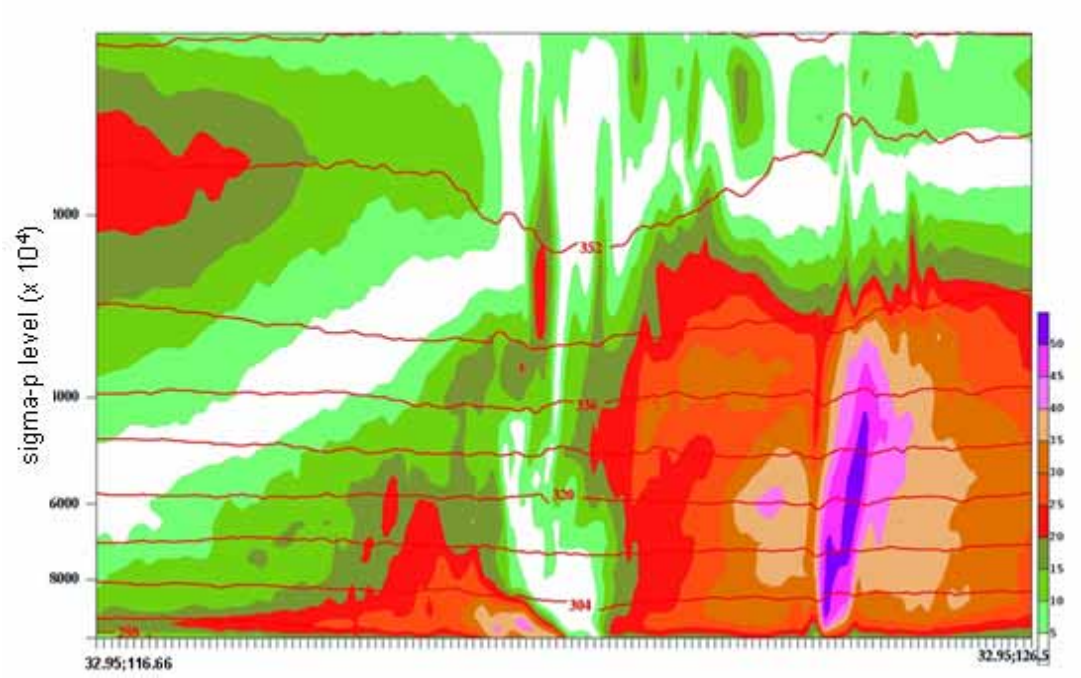

Figure 4.31 As in Figure 4.21, except for the ARW 60-h forecast of Typhoon Khanun. The upper-level outflow eventually became aligned with the low-level vortex. A warm core was evident at 54 h.

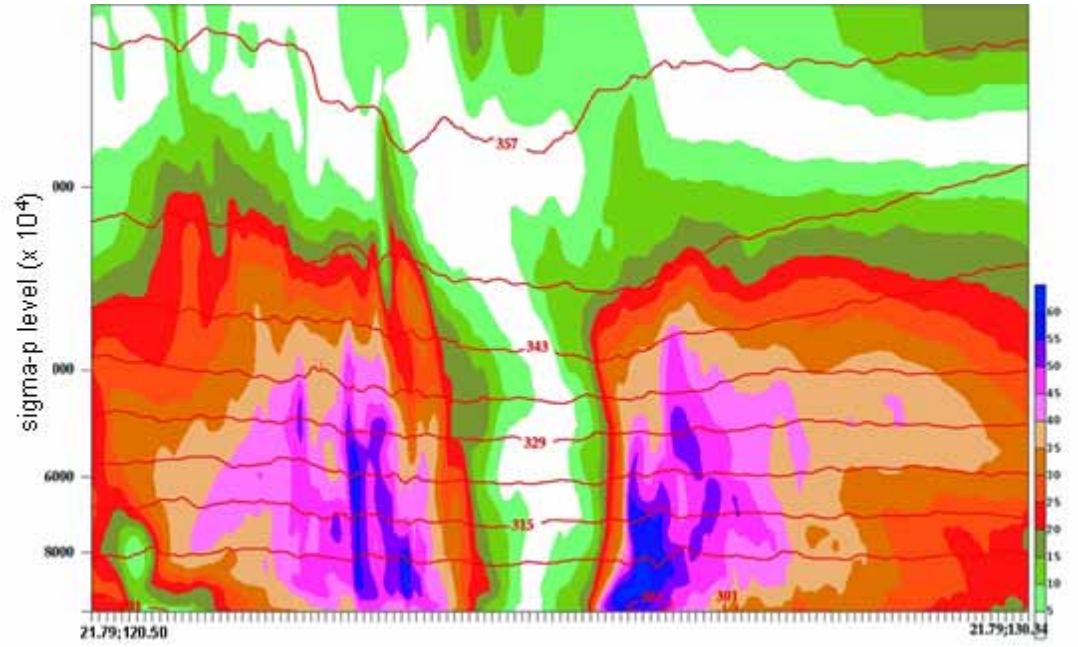

Figure 4.32 As in Figure 4.21, except for the ARW 36-h forecast from the second Talim case. The vortex was well-formed, and the forecast was a rapid intensification at this time.

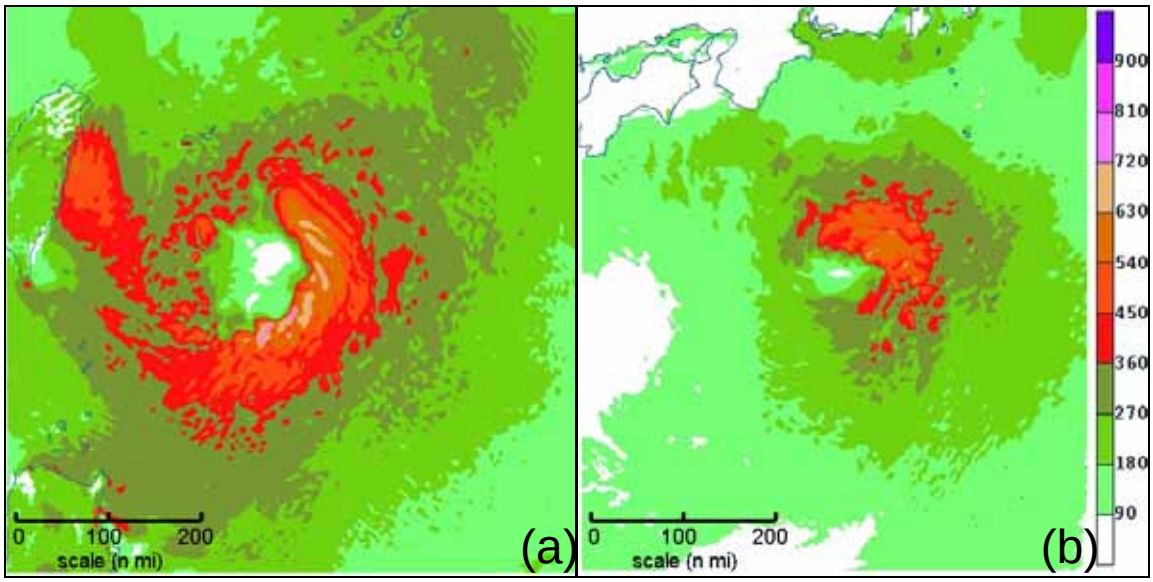

Figure 4.33 Surface latent heat flux (W/m^2) from the 36-h ARW inner-nest forecasts from the (a) second Talim integration and (b) Mawar integration. The ARW forecast intensity was 65 kt for both storms at this time, but Talim had a much larger area of latent heat flux, which led to rapid intensification in the model. The scale in each panel is approximate.

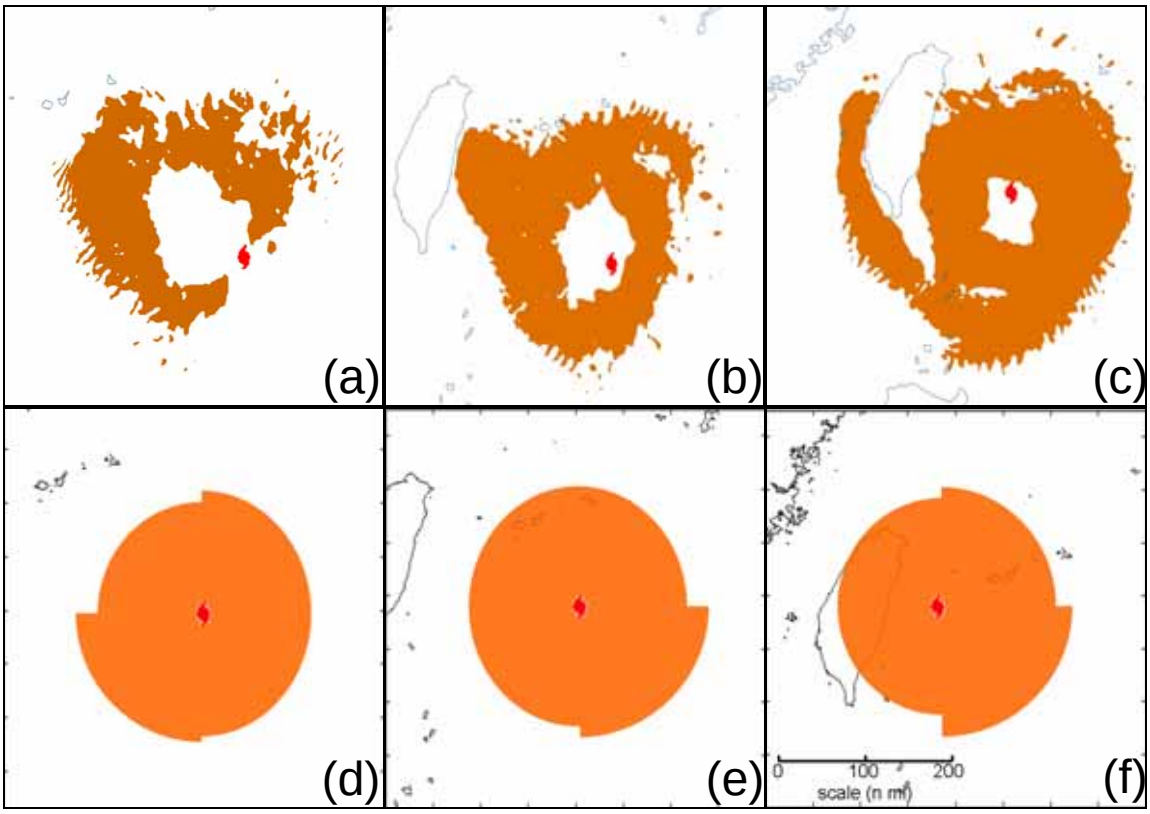

Figure 4.34 Region of tropical storm force winds (34 kt) in the inner-nest ARW forecast (top row), and as estimated by the JTWC (bottom row) valid at (a, d) 24 h, (b, e) 36 h, and (c,f) 48 h in the second Typhoon Talim integration. The region of tropical storm-force winds in the JTWC analysis does not account for terrain effects or weaker winds in the eye. The scale in each panel is approximately the same.

Not all of the TCs had an accurate outer wind structure in the ARW forecasts, and storms that were too small did not rapidly intensify regardless of how much the size of the eye decreased. The radius of maximum winds in the Typhoon Mawar ARW forecast was 40 n mi at 48 h, and 21 n mi at 60 h (Figure 4.35a-c). Despite the contraction of this eye, the forecast intensity was too low throughout day three, which was likely attributable to an under-forecast of the overall size of the TC (Figure 4.35). In particular, the forecast size of Mawar was especially too small on the west side of the storm.

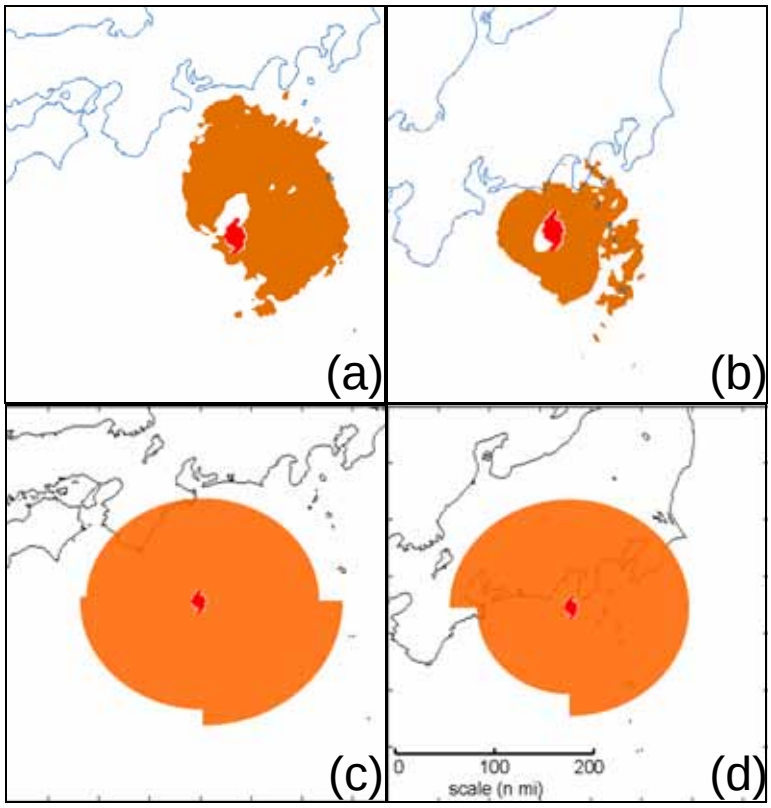

Figure 4.35 As in Figure 4.34, except for the Typhoon Mawar case valid at (a, c) 48 h and (b, d) 60 h. The ARW forecast size was too small, which resulted in an under-forecast of the intensity despite a very small eye.

An accurate TC size and marked shrinking of the vortex were forecast during the rapid intensification on day three of the first Typhoon Nabi integration in the ARW (Figure 4.36). Between the 42-h and 60-h ARW forecasts, the radius of maximum winds decreased from approximately 135 n mi to 55 n mi, which was associated with an intensity increase of 30 kt near the end of the integration (Figure 4.25). In reality, Typhoon Nabi underwent rapid intensification from the beginning of the integration well into day three. It is suggested that a prolonged spin-up period in the ARW may have prevented the model from forecasting rapid intensification during days one and two.

Rapid intensification also occurred in Typhoon Talim for nearly the entire three days of the first integration for this storm (Figure 4.19). In this case, the ARW (and the MM5) did not forecast rapid intensification during any portion of

the integration. Whereas days one and two of the ARW integration were marred by severe spin-up adjustments (discussed in Chapter IV.C.2), by 48 h the vortex was reasonably vertically stacked and had contracted to a very small radius (Figure 4.37). In addition, a distinct warm core was predicted for the first time, and the central pressure began falling (Figure 4.38), which indicates convection near the eye was becoming organized. Despite these positive signs for intensification, the maximum winds in the vortex remained in the upper troposphere (around 0.30 sigma-p level) and well above the PBL, so increases in these winds were not accompanied by a corresponding increase in surface latent heat flux (not shown) and the predicted maximum surface winds remained fairly constant. The maximum winds slowly descended on day three, but were still above the PBL at the end of the integration.

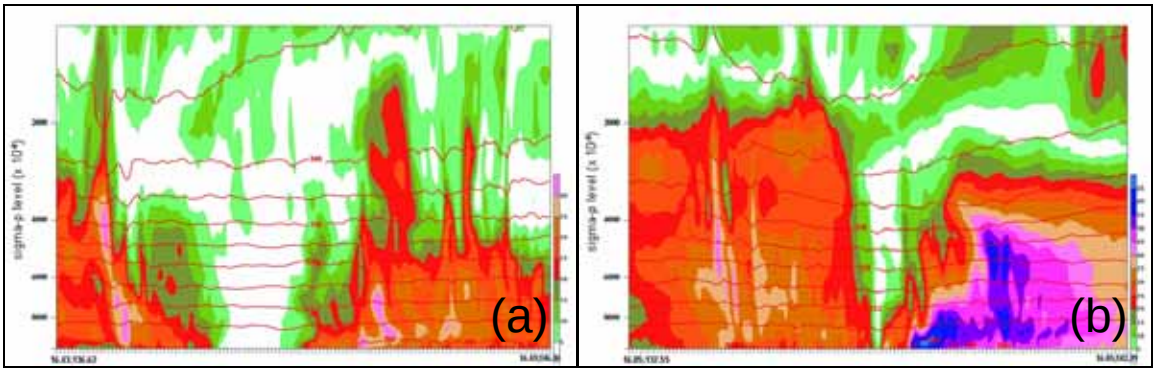

Figure 4.36 As in Figure 4.21, except for the ARW (a) 42-h forecast and (b) 60-h forecast from the first Nabi integration. After a long spin-up period, contraction of the vortex led to rapid intensification in the model from 48-72 h. Note in (b) the enhancement of the warm core once intensification was predicted.

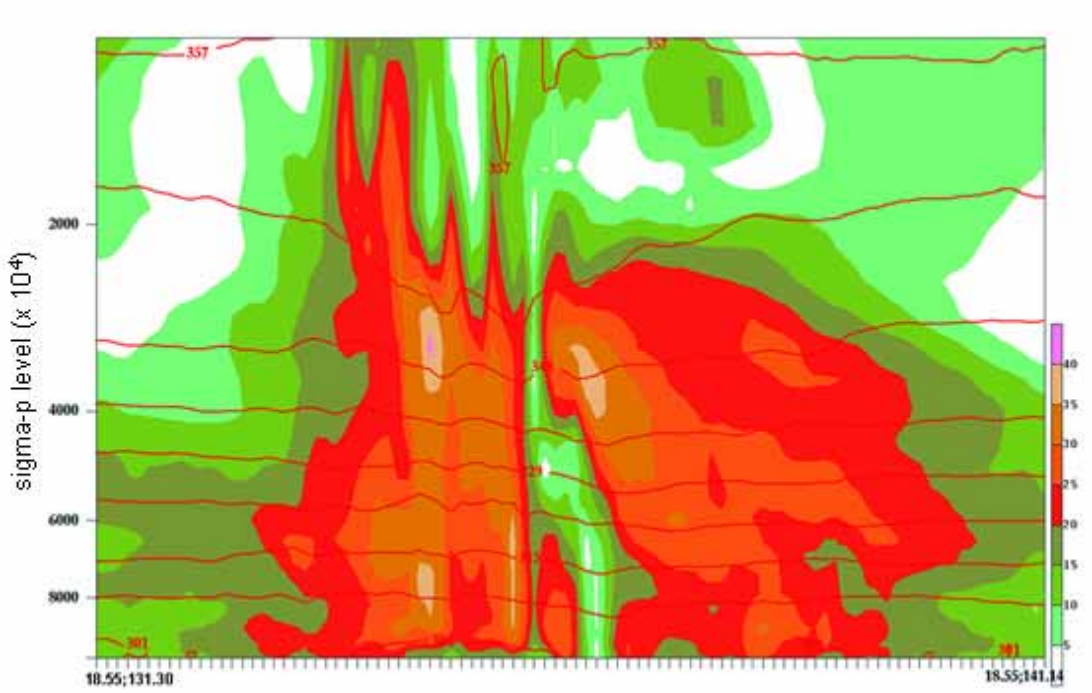

Figure 4.37 As in Figure 4.21, except for the ARW 48-h forecast from the first Talim case. Despite a fairly tight eye and small radius of maximum winds, significant intensification never occurred. Note the strongest winds in the vortex are in the mid-levels, which is not conducive to enhancing convection.

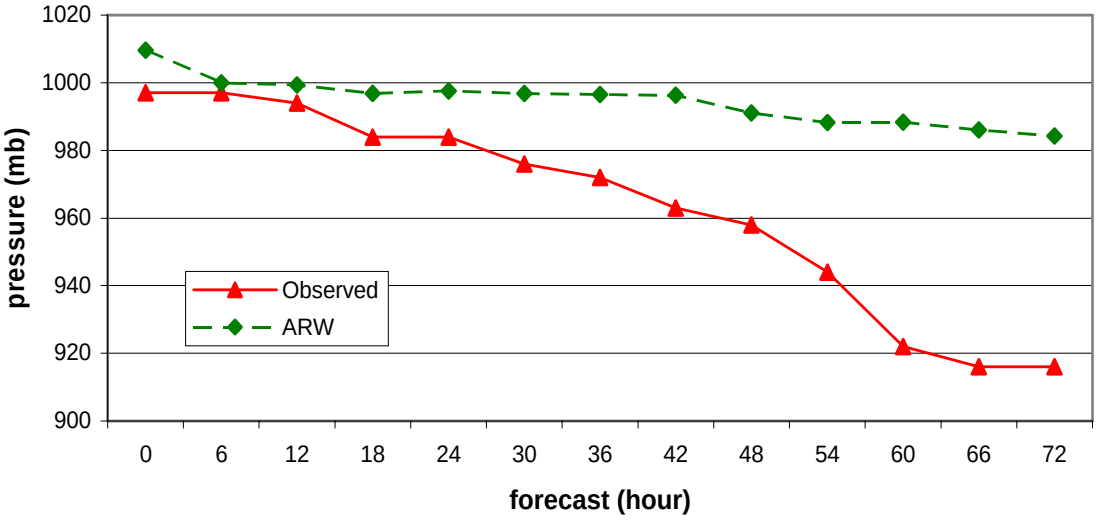

Figure 4.38 Observed (red solid line with triangular points) and ARW forecast (green dashed line with diamond points) central pressure during the first Typhoon Talim case. The pressure began decreasing in the ARW forecast after 42 h, but the intensity of the storm remained nearly constant.

This tendency of the ARW to predict the maximum winds too high in the vortex was observed during the early hours in many of the integrations. In all cases except this first Talim case, the region of maximum winds had descended to the top of the PBL by the time other spin-up effects (such as vortex contortion) had mostly disappeared. With such a small sample, it is uncertain if the unusually prolonged period of predicting maximum winds too high in the vortex in the first Talim ARW integration was simply due to residual spin-up effects, or if it is indicative of a systematic shortcoming in the model.

4. Decay and Reintensification Cycles

The second Typhoon Nabi case (Figure 4.29) was selected as an example because after Nabi reached an intensity of 140 kt it went though a decay and reintensification cycle associated with eyewall replacement (Willoughby et al. 1982). This phenomenon occurs when an outer eyewall forms and “chokes off” the low-level inflow of the existing eyewall, the inner eyewall is weakened and a decrease in storm intensity occurs. Reintensification of the storm occurs if and when the new eyewall contracts.

Two distinct eyewall bands were visible in microwave satellite imagery valid 33 h into the integration while Typhoon Nabi was decaying (Figure 4.39a). Nabi continued to decay until 42 h, at which point the outer eyewall had completely replaced the inner eyewall. Reintensification began at 54 h as the new eyewall began to contract.

In the ARW forecast for this case, oscillations and vortex contortion due to spin-up had subsided by 27 h and the overall structure of the TC appeared relatively normal thereafter aside from an eye that was very large (radius near 250 n mi), and a predicted intensity roughly 50 kt too low. The intensity forecast decreased 8 kt between 36 h and 54 h, and then reintensified by 11 kt at 66 h. The timing of this reintensification matched very closely the observed reintensification, and several concentric bands of precipitation were intermittently predicted in the 3-h precipitation fields from the ARW outer nest (Figure 4.39b-f). However, the evolution of these bands did not show strong evidence of eyewall

replacement, and the reintensification in the forecast was likely due to contraction of the existing eyewall. Since eyewall replacement is most frequently observed in TCs that are intense, the large eye and corresponding low intensity of Nabi in the ARW forecast may have precluded the model from forecasting the phenomenon.

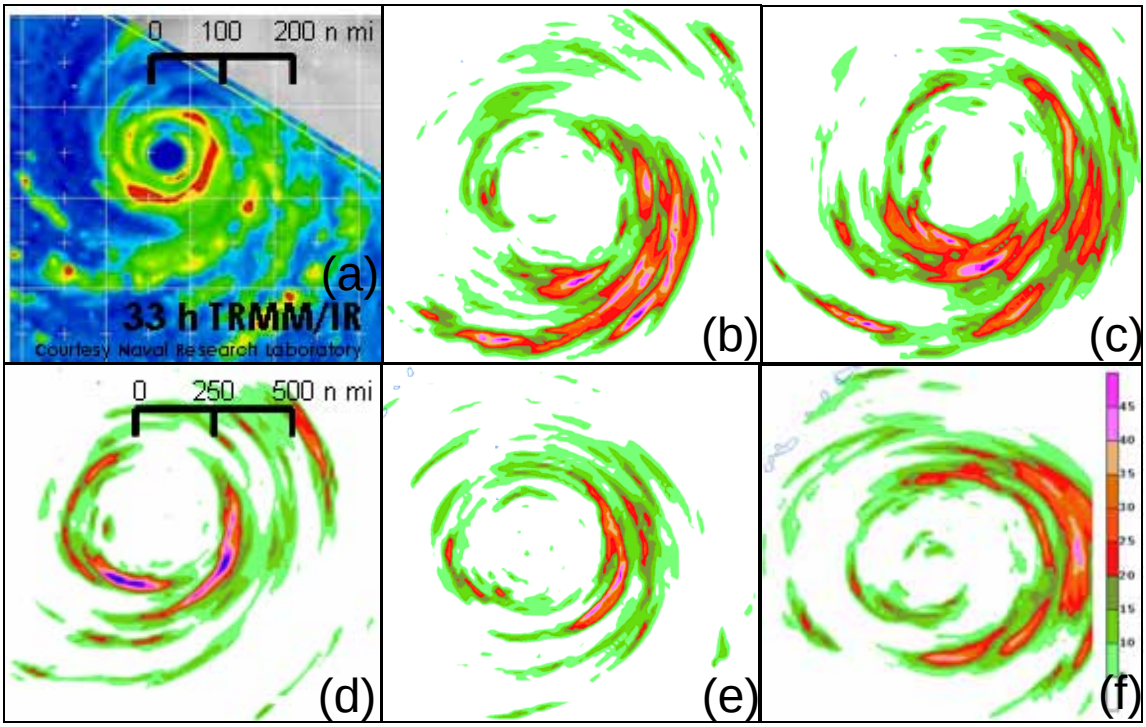

Figure 4.39 (Satellite imagery from: The Naval Research Laboratory) (a) Microwave and infrared imagery showing regions of heaviest precipitation valid around 09 UTC 3 September 2005 (33 h into the integration). (b-f) 3-h precipitation fields (mm) in the outer-nest ARW valid in 6-h intervals beginning at 36 h showed little evidence of eyewall replacement during the second Typhoon Nabi case. The radius of the eye remained relatively constant at 250 n mi. The precipitation scale is not valid for the satellite imagery. [Satellite imagery available online at http://www.nrlmry.navy.mil/tc_pages/tc_home.html (current as of 28 February 2006)].

Nabi was the only TC in this study that underwent eyewall replacement, and none of the other ARW forecasts had clear indications of the phenomenon. The Typhoon Mawar ARW forecast (Figure 4.23) had several instances of

splitting and merging of rain bands during fluctuations in intensity between 33 h and 57 h (not shown), but classifying this as eyewall replacement would be an exaggeration, particularly given the low forecast intensity by the ARW. Whereas eyewall replacement is most frequently observed in symmetric TCs, nearly all the convection in the Mawar forecast was (accurately) on the east side of the vortex during this integration.

5. Rapid Decay over Land

Typhoon Khanun (Figure 4.28) was observed to rapidly decay beginning 36 h into the integration period as the storm approached the east coast of China. The center of the storm made landfall around 43 h, and rapid decay continued until the end of the integration. Reasons for the lack of decay in the ARW forecast (related to organization of upper-level outflow) were discussed in Chapter IV.C.3. However, the effects of landfall were not completely absent from the model forecast. A drastic decrease in the winds on the west side of the TC was predicted, and the frictional effects of land and hilly terrain of the region caused intense mesoscale updrafts and downdrafts that were evident by oscillations in the potential temperatures (Figure 4.40). In addition, the vertical extent of the cyclonic circulation on the west side of the storm was reduced during this period and replaced by upper-level southerly flow from a deep trough in central China (this flow is evident in Figure 4.40c as the strong winds in the upper-left portion of the cross section). The 54-h forecast had the TC entering the rather flat North China Plain, and the mesoscale updrafts and downdrafts were not as apparent. The much flatter terrain of this region also allowed the low-level winds to slightly increase on the west side of the storm at this time.

It is impossible to determine if the ARW forecast for Khanun would have included rapid decay had the effects of spin-up not been so severe in this case. The evaluation was complicated further by track error (albeit rather small) that allowed virtually the entire eastern half of the TC to remain over the sea. Since the SST was nearly 26° C in the model, latent heat flux and convection persisted

unabated in the eastern half of the storm. The MM5 forecast, which also never intensified the storm but had a poor track forecast, did predict rapid decay after landfall.

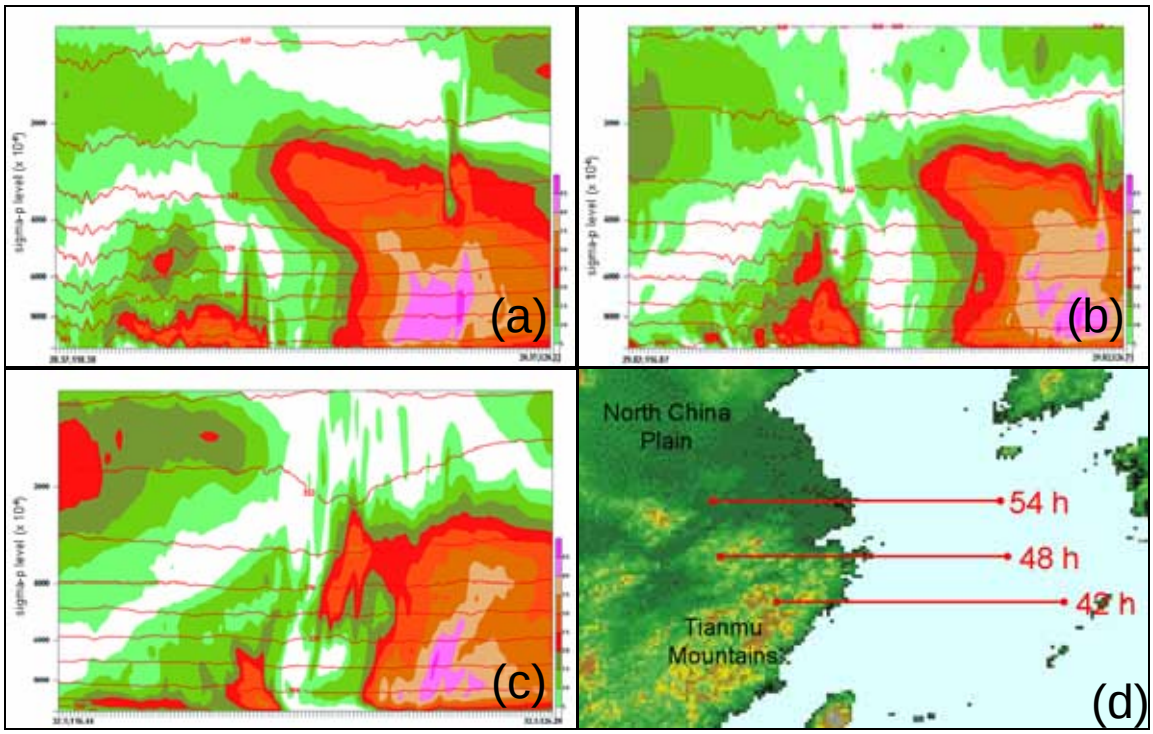

Figure 4.40 (Map after: The United States Geological Survey) As in Figure 4.21, except for the ARW (a) 42-h forecast, (b) 48-h forecast, and (c) 54-h forecast from the Khanun case. As the west side of the storm began to interact with land, high frequency rising and sinking oscillations were predicted as convection decreased, and winds on the west side of Khanun weakened. Interaction with terrain was not as destructive at 54 h when the storm was entering the North China Plain. The topography and location of each cross-section is indicated in panel (d). [Map available online at http://www.usgs.gov (current as of 28 February 2006)].

Spin-up in the ARW was not as severe in the second Typhoon Talim integration (Figure 4.26), which covered the period when Talim rapidly decayed between 36 h and 72 h as it made landfall on Taiwan and eventually mainland China (Figure 4.4d). Decay in this case was especially rapid (a decrease of 70 kt

on day three) in part due to frictional effects of the Central Mountain Range (CMR) of Taiwan, which is a nearly continuous series of north-south ridges with multiple peaks above 3000 m elevation.

The effects of the CMR were apparent in the ARW forecast as an overall weakening of the winds near the ridge, an abrupt fluctuation in the potential temperature profile, and a decrease in the vertical extent of the circulation (Figure 4.41). Between 48 h and 60 h, the ARW forecast decreased the intensity by 22 kt.

Once the center of Typhoon Talim had nearly crossed the CMR in the ARW forecast, winds on the west side of the TC began increasing again, and decay of the storm stopped. During the final 12 of the integration, the ARW actually strengthened the storm, and winds >90 kt were forecast at 72 h just above the surface on the east side of the TC between the center of circulation and the CMR (not shown).

Unlike the Khanun case, the insufficient decay in the second Talim case was predicted well after spin-up and during a period when the ARW forecast intensity closely matched the observed intensity (around 70-80 kt at the time of ridge crossing). Track error certainly played a role in the insufficient decay since the storm never reached mainland China in the ARW forecast. However, Talim was observed to rapidly decay even during the time it was in the Taiwan Strait, before reaching mainland China. Furthermore, the radius of tropical-storm force winds after crossing the ridge was significantly larger in the ARW forecast than in the JTWC analysis, which suggests the frictional effects of the landfall did not weaken the outer portions of the TC sufficiently in the ARW (Figure 4.42).

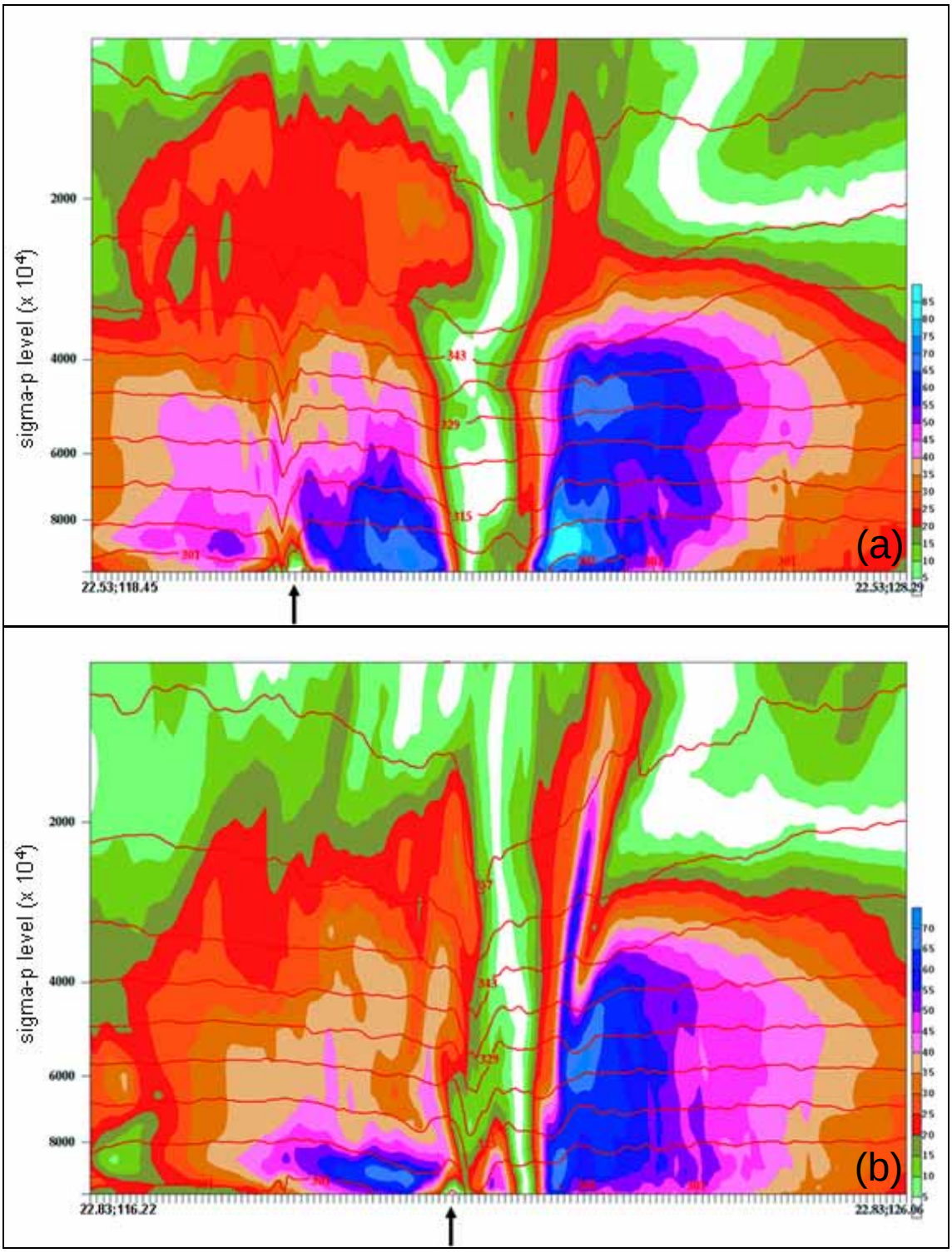

Figure 4.41 As in Figure 4.21, except for the ARW (a) 48-h forecast, and (b) 60-h forecast from the second Talim case. As Talim approached Taiwan, the frictional effects of the Central Mountain Range (black arrow) disrupted the flow. Winds are predicted to increase west of the Central Mountain Range at 60 h.

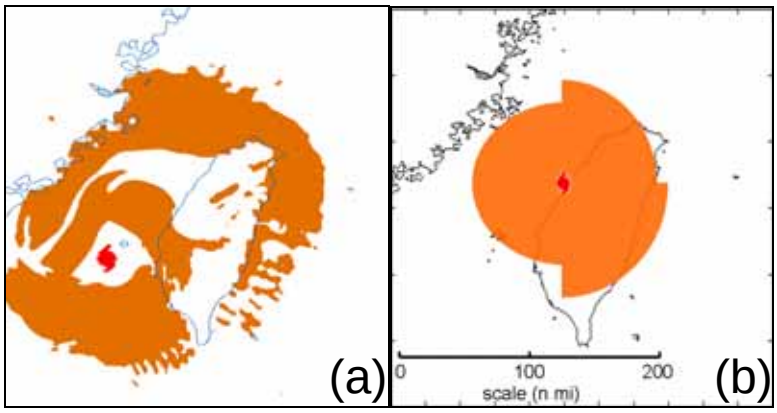

Figure 4.42 Radius of 34-kt winds from the (a) ARW inner-nest forecast valid at 60 h, and (b) JTWC analysis valid at 72 h in the second Typhoon Talim case . After crossing Taiwan, the TC was significantly too large in the ARW forecast.

6. Suppression of Convection by Mid-level Ridge

The distinctly different locations of precipitation relative to the TC in the Matsa (Figure 3.2) and Khanun (Figure 3.9) cases were associated with different strengths of the mid-level ridge to the northeast of each TC (see Chapter III.B for a full discussion). In the Matsa case, suppressed convection north of the storm seemed to be due to a strong ridge. Despite the erroneously weak STR in the ARW forecast for this case, the model accurately forecast relatively little precipitation north of the storm (Figure 4.43a).

Convection in Typhoon Khanun was observed to be relatively abundant on all sides of the storm, with the strongest convection north of the TC. In contrast to Matsa, the ARW integration for Khanun had severe spin-up effects leading to gross intensity errors. Despite this error, the placement of convection in the ARW forecast was relatively accurate (Figure 4.43b) compared to microwave imagery (not shown).

For these two cases, the ARW forecast of outer rainband convection location was evidently not largely impacted by forecast errors of STR strength, TC track, or TC intensity. Furthermore, no large errors were observed in the placement of outer rainband precipitation for any of the seven integrations in this study beyond 24 h. In contrast, convection near the eyewall and inner rainbands

was subject to large fluctuations in the ARW predictions as the size of the eye and overall intensity of the TC changed. A more exhaustive evaluation with numerous cases is needed to fully determine the sensitivity of ARW convection to various factors.

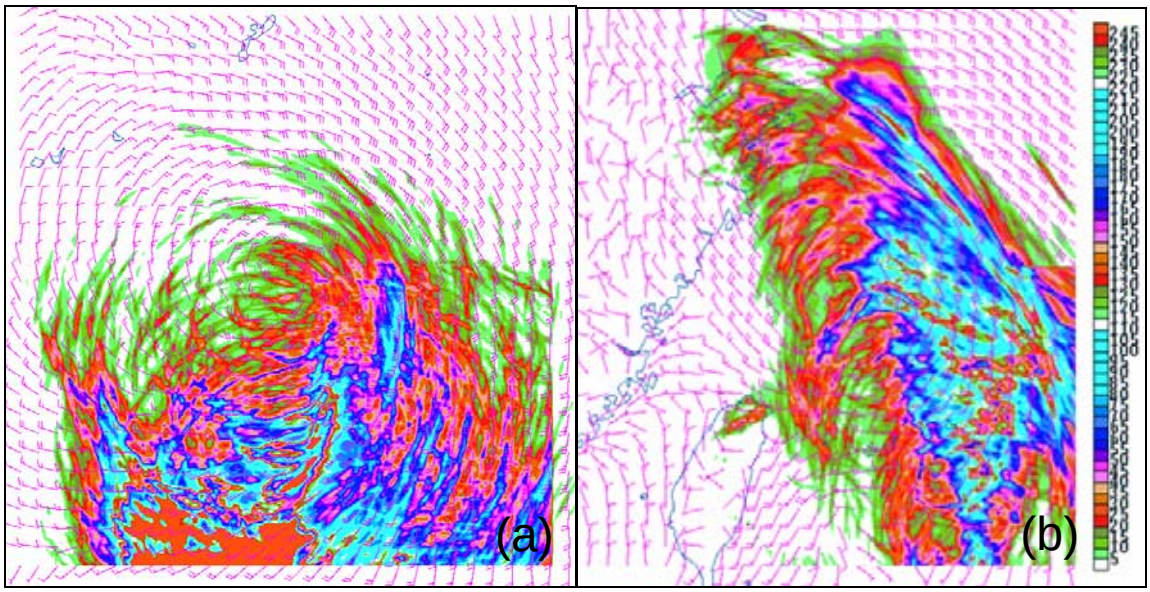

Figure 4.43 Total accumulated precipitation (mm) and 10-m winds (kt) from the ARW inner nest for the (a) Typhoon Matsa case valid at 72 h, and (b) Typhoon Khanun case valid at 39 h. A mid-level ridge suppressed convection in the northern half of the Matsa case, while convection in the Khanun case was strongest in the northern and eastern quadrants.

7. Landfall

A summary of the observations and ARW forecasts of sustained winds and precipitation during landfall is given in Table 4.4. The under-forecast of maximum winds during landfall for the first Nabi integration and the Khanun integration are consistent with the overall under-forecast of the intensity of these TCs in the ARW. The wind forecast for Andersen Air Force Base, Guam during the first Nabi integration was fairly accurate due to track error that resulted in the TC being closer to Guam than the observed storm. This track error compensated for the overall intensity of the storm being too weak in the ARW forecast.

Table 4.4 Summary of observed and ARW forecast wind and precipitation during landfall. Wind observations are 1-min averages except 10-min averages are used where noted. Otherwise, 1-min averages are used. The ARW forecast maxima were for all locations, so the values may be higher than the observations if an observing station is not nearby. The landfall in China of the second Typhoon Talim integration is not included because the ARW did not predict landfall in this case.

	Maximum Sustained Wind		Maximum Rainfall		Selected Locations				
						Maximum Wind		Total Rainfall	
	Observed	ARW	Observed	ARW	Location	Observed	ARW	Observed	ARW
MAWAR	54 kt* Miyake-tsubota Island, S of Tokyo	70 kt Eastern Tokyo	528 mm Hokane, Japan	745 mm 16 n mi NW of Hakone	Yokota Air Base	26 kt	15 kt	94 mm	102 mm
TALIM II	74 kt* Yaeyama Islands	70 kt Southeastern Taiwan	155 mm Yaeyama Islands	825 mm Northern Central Mountains					
NABI I	65 kt Saipan	40 kt Central Guam	155 mm Andersen Air Forece Base,	190 mm Central Guam	Andersen Air Force Base	29 kt	25 kt	155 mm	114 mm
KHANUN	87 kt* Dachen Dao, China	45 kt 227 n mi N of Dachen Dao	465 mm Xiaozhilingjiao, China	135mm 147 n mi S of Xiaozhilingjiao					
	* ten-minute average								

The forecast precipitation amounts were reasonable with the exception of the Khanun case, which was markedly too low (and also probably tied to intensity error). The ARW precipitation amount forecasts were generally higher than the observations, but this is most likely because the locations of the ARW maxima were highly localized and not always near an observation site. Terrain had a large affect on the precipitation amount forecasts, and the ability to resolve the mesoscale effects of terrain on localized precipitation is one of the benefits of the high resolution inner nest. This led to a forecast of 825 mm of precipitation at one location in the data-sparse CMR in the second Talim integration. The maximum precipitation in the Typhoon Mawar integration was also heavily influenced by the high terrain southwest of Tokyo. However, in this instance there were several available observations nearby, and the observed location of maximum precipitation in the all of coastal Japan was only 16 n mi away from the location of maximum precipitation in the ARW forecast.

V. CONCLUSION

A. SUMMARY

The far superior model resolution of the ARW moving nest relative to the tropical MM5 was only able to be utilized in seven of the 10 cases due to failure of the ARW vortex tracker algorithm used to move the inner nest in three of the cases. This algorithm, which tracks the minimum 500-mb geopotential height field, was also responsible for small tracking errors in the ARW for the remaining seven cases. In these seven cases, the ARW track forecast errors were smaller than both the MM5 and CLIPER errors during most forecast intervals. However, the MM5 intensity forecast errors were smaller than the ARW intensity errors at all forecast intervals, and the CLIPER intensity forecast errors were smaller than both the ARW and MM5 intensity errors at all forecast intervals.

The ARW track forecasts had erratic changes during the early hours of the integrations due mostly to imbalances in the initial conditions (but also tracker error). Some smaller erratic track changes also occurred in some of the MM5 integrations, despite a more comprehensive initialization procedure that includes a bogus vortex and a warm-start. Despite the early spin-up problems, the ARW 48-h and 72-h track forecasts were quite good because the environmental steering flow around the TCs was normally forecast accurately. The ARW usually predicted relatively accurately the strength and location of the STR, and it performed very well when the STR was eroded by a transient mid-latitude trough in the second Typhoon Nabi integration. Even the poor intensity forecasts did not significantly degrade the track forecasts except in certain cases when STR modification was observed. In these cases, insufficient STR modification was predicted by the ARW if the ARW intensity forecast was too low and could be traced to a TC size that was too small, rather than an eye that was too large.

Other sources of small track errors in the ARW included an erroneously strong anticyclone in China, and the creation of a spurious TC that interacted with the STR and altered the steering flow in the second Typhoon Matsa integration.

The poor intensity prediction performance of the ARW was largely due to the flawed initial TC structure provided by the 1/2° lat./lon. GFS model fields. The initial TC vortex structures in the ARW were thus too large and often asymmetrical, and the maximum winds were too high in altitude. Every ARW integration started with an initial intensity around 30 kt, regardless of the actual TC intensity, which led to five of the seven cases having an initial intensity that was more than 35 kt below the observed intensity.

The flawed initial TC structure in the ARW led to spin-up effects during which the vortex was contorted and disorganized. The duration of the spin-up ranged between 12 h and 54 h, and was tied to the degree of asymmetry of the initial vortex (the more symmetrical vortices had the shortest spin-up period). In all except the first Talim case, the maximum winds eventually descended to the top of the PBL.

Even though the MM5 intensity forecasts benefited from inclusion of a bogus vortex and warm-start, indications of weaker spin-up were still present. The negative intensity bias at the initial time in the MM5 was not as large as in the ARW, and the MM5 initial intensities were higher for the stronger TCs.

The large intensity errors in the ARW caused by the initial conditions are likely to have masked other intensity error mechanisms. However, evaluating the forecasts after the spin-up period still provided useful data on certain behaviors of the model. In many of the cases, the outer wind structure of the TC in the ARW forecast was correct, and the ARW was able to predict rapid intensification when the eye of the TC eventually contracted to a reasonable size. If the outer wind structure was not large enough in the ARW forecast (as in the Mawar case),

significant intensification did not occur. Cases in which the outer wind structure was too small appeared to be most vulnerable to track error due to insufficient STR modification.

The predicted location of outer rainband precipitation was usually reasonable in the ARW forecasts, including some cases in which convection was virtually absent in one or more quadrants of the storm. Inner rainband convection was not well-predicted, and fluctuated as the size of the eye and overall intensity of the TC changed.

The ARW forecasts had a tendency for insufficient decay of the TCs over land in two integrations (second Talim and Khanun) that were continued for several hours after landfall. The insufficient decay in the Khanun integration could have been due to track error, but a possible explanation was less clear in the second Talim integration, which involved the TC crossing the CMR of Taiwan.

Reintensification due to the eyewall replacement cycle was not definitively predicted in any of the ARW forecasts. The large negative intensity error may have prevented the ARW from forecasting this phenomenon, and many more cases are needed before an accurate assessment of reintensification prediction can be achieved. Since the precipitation in the ARW forecasts was often organized in well-resolved, distinct bands, there is potential for the model to predict eyewall replacement.

B. FUTURE WORK

The small sample size in this study makes it far from a complete description of biases and characteristics of the ARW moving nest. However, it does identify potential strengths of the model, as well as highlight weaknesses that deserve further attention. Future evaluation and development of the ARW version 2.1 should be along three pathways.

The first development should be to revise the vortex-tracker algorithm used to determine the movement of the inner nest. Following the 500-mb height minimum proved to be inadequate in three of the ten cases in this study, and a new tracker should focus on low-level features of the TC. This development is especially important if the high-resolution inner nest is to be utilized for early TC development because the storm may not yet have an organized mid-level low in these cases. Wei Wang (personal communication, 5 January 2006) indicates NCAR will be working toward improving the tracker in the future.

The second pathway should be to improve the initial TC structure in the ARW. It is fairly clear from this study that the non-bogused GFS fields are not sufficient to initialize the 4-km resolution ARW inner-nest. A vortex initialization of the NCAR ARW using the Geophysical Fluid Dynamics Lab (GFDL) model had positive results for both track and intensity prediction in the Atlantic (Wang et al. 2006). A similar procedure is planned to be tested in the western North Pacific using the GFDL-Navy (GFDN) version to initialize the AFWA WRF. The vortex in the GFDN on a 1/6° lat./lon grid will provide the ARW with a more representative initial TC structure. Even though the GFDN vortex is likely to reduce the severity and duration of spin-up in the ARW, imbalances will still be present when the fields are interpolated to the high-resolution grid of the ARW (especially the inner nest).

The third pathway of future development may focus on further reducing spin-up by developing a warm-start initialization procedure for the ARW in which a 6-h or 12-h forecast from a previous ARW integration is used as the first-guess field. Since the grid points are collocated, no interpolation is necessary in a warm start.

Improving the initialization and reducing spin-up in the ARW is likely to improve track and (especially) intensity prediction, but it may also unmask other model sensitivities and biases that will need to be evaluated at that time. Several interpretations from this study suggest a few of these sensitivities and biases, and are provided as an account of potential areas for further evaluation in the

middle- and long-term as these changes are implemented. The first of these potential weaknesses is the creation of spurious TCs. Two spurious (very intense) TCs were generated by the ARW in this study (one of them caused inner-nest movement failure in the first Matsa integration), which suggests a possible bias toward excessive TC development.

Second, insufficient TC decay over land was observed in both of the ARW forecasts that continued for several hours after landfall. In one of these cases (Khanun), the insufficient decay could have been attributed to track error. The insufficient decay in the second Talim case occurred as the TC was crossing the CMR of Taiwan and should have been decaying rapidly. The observations in these two cases could suggest a possible bias in the ARW to underestimate the detrimental effects of land on the TC.

In nearly all the cases, the level of maximum winds (which was a too high elevation due to the faulty initial conditions) eventually descended to the top of the PBL. However, for reasons not entirely clear, the maximum winds remained very high in the atmosphere in the first Talim ARW integration well after the other effects of spin-up had diminished. Improving the initial conditions of the ARW may eliminate this phenomenon, but the failure of the winds to descend in the first Talim case may signal an underlying bias in the model since the winds should have eventually been mixed downward via convective fluxes. If this is a bias in the model, it could lead to large intensity errors because the surface latent heat flux will be too low if the maximum winds are not near the top of the PBL.

Finally, the resolution of the SST data may contribute to spin-up effects in the form of high-frequency oscillations in the low levels of the ARW (albeit certainly of much lower amplitude than those caused by the initial atmospheric conditions). A sensitivity study using various SST resolutions in otherwise identical ARW runs could determine if higher resolution SST data is needed.

NCAR is already planning or evaluating updates in various components of the model, including the microphysics, radiation (longwave and shortwave), PBL, surface layer, land use, and cumulus schemes. These updates may eliminate many of these potential ARW shortcomings.

APPENDIX: TECHNICAL DESCRIPTION OF THE ARW MOVING-NEST VORTEX TRACKER ALGORITHM

The vortex center-finding algorithm first computes the 500-mb geopotential height from the ARW state variables on the inner nest. Next, a horizontal index range is computed for the inner nest based on the previous vortex center (lat, lon) and a specified search radius. Next, the code searches for the minimum in the 500-mb geopotential height within this index range and stores the location of this minimum. The code then loops over all (I, j) points in the search window and computes the difference d(i,j) between the geopotential height at each gridpoint and the maximum geopotential height within the search window. For each gridpoint in the window, the d(i,j)-weighted average is of the deviation of the gridpoint location from the estimated center d(i,j), which yields an averaged center that will tend to exhibit less variability with time than the initial center. The new location of the inner nest is adjusted so that the averaged vortex center is as close as possible to the center of the inner nest.

Note that this scheme may not yield good results if the search window extends beyond the bounds of the nest in which the center is being calculated. In practice this is not a problem since the search window is contained completely within the inner nest.

THIS PAGE INTENTIONALLY LEFT BLANK

LIST OF REFERENCES

Aberson, S. D. and C. R. Sampson, 2003: On the predictability of tropical cyclone tracks in the Northwest Pacific basin. *Mon. Wea. Rev.* Vol., **131**, 1491–1497.

Barker, D. M., W. Huang, Y.-R. Guo, A.J. Bourgeois, and Q.N. Xiao, 2004: A three-dimensional variational data assimilation system for MM5: Implementation and initial results. *Mon. Wea. Rev*., **132**, 897-914.

Bender, M. A., I. Ginis, T. P. Marchok, H. L. Pan, B. Thomas, and R. E. Tuleya, 2003: A summary of upgrades to the operational GFDL hurricane model for 2003. [HYPERLINK http://ams.confex.com/ams/pdfpapers/75131.pdf (Current as of 18 Mar 06)].

Blackerby, J. S., 2005: The accuracy of western North Pacific tropical cyclone intensity guidance. M.S. thesis, Dept. of Meteorology, Naval Postgraduate School, Monterey, CA 93943-5114, 127 pp.

Bower, C. A., 2004: Prediction of tropical cyclone formation in the western North Pacific using the Navy global model. M. S. thesis, Dept. of Meteorology, Naval Postgraduate School, Monterey, CA 93943-5114, 139 pp.

Carr, L. E., III and R. L. Elsberry, 2000: Dynamical tropical cyclone track forecast errors. Part I: Tropical region error sources. *Wea. and Forecasting*., **15**, 641–661.

Carr, L. E., III and R. L. Elsberry, 1990: Observational evidence for predictions of tropical cyclone propagation relative to environmental steering. *J. Atmos. Sci*., **47**, 542–546.

Carr, L. E., III and R. L. Elsberry, 1997: Models of tropical cyclone wind distribution and beta-effect propagation for application to tropical cyclone track forecasting. *Mon. Wea. Rev.,* **125**, 3190–3209.

Carr, L. E., III, M. A. Boothe, and R. L. Elsberry, 1997: Observational evidence for alternate modes of track-altering binary tropical cyclone scenarios. *Mon. Wea. Rev.,* **125**, 2094–2111.

Carr, L. E., III, R. L. Elsberry, and J. E. Peak, 2001: Beta test of the Systematic Approach Expert System Prototype as a tropical cyclone track forecasting aid. *Wea. Forecasting*, **16**, 355-368.

Dudhia, Jimy. *WRF Physics Options.* January 23-27, 2006. WRF-ARW Tutorial. [HYPERLINK http://www.mmm.ucar.edu/wrf/users/tutorial/SlideShows/ARW_Physics_Dudhia.pdf (Current as of 18 Mar 06)]

Elsberry, R. L., G. J. Holland, H. Gerrish, M. DeMaria, and C. P. Guard, 1992: Is there any hope for tropical cyclone intensity prediction?—A panel discussion. *Bull. Amer. Meteor. Soc.*, **73**, 264-275.

Elsberry, R. L., and L. E. Carr, III, 2000: Beta test of the Systematic Approach Expert System Prototype as a tropical cyclone track forecasting aid. *Wea. Forecasting*, **16**, 355-368.

Elsberry, R. L.. Class Lecture. Meteorology 3252: Tropical Meteorology. Naval Postgraduate School. Fall 2005.

Franklin, J. L., 1990: Dropwindsonde observations of the environmental flow of Hurricane Josephine (1984): Relationships to vortex motion. *Mon. Wea. Rev.,* **118**, 2732–2744.

Franklin, J. L., 2005: 2004 National Hurricane Center verification report. *Preprints for the 57th Interdepartmental Hurricane Conference*, Miami. [HYPERLINK http:www.ofcm.gov/ihc05/Presentations/01%20Session1/s1-03franklin.ppt (Current as of 20 Sep 05)]

Goerss, J., 2000: Tropical cyclone track forecasts using an ensemble of dynamical models. *Mon. Wea. Rev*., **128**, 1187-1193.

Goerss, J. S., C. R. Sampson, and J. M. Gross, 2004: A history of western North Pacific tropical cyclone track forecast skill. *Wea. Forecasting,* **19**, 633–638.

Hausman, S., 2001: Models, models everywhere…literally. *Observer,* Jul-Aug, 2001.

Hong, S-Y., J. Dudhia, and S-H. Chen, 2004: A revised approach to ice microphysical processes for the bulk parameterization of clouds and precipitation. *Mon. Wea. Rev.,* **132**, 103–120.

Kain, J. S. and J. M. Fritsch, 1998: Multiscale convective overturning in mesoscale convective systems: Reconciling observations, simulations, and theory. *Mon. Wea. Rev.,* **126**, 2254–2273.

Knaff, J. A., M. DeMaria, C. R. Sampson, and J. M Gross, 2003: Statistical five-day tropical cyclone intensity forecasts derived from climatology and persistence. *Wea. Forecasting*, **18**, 1093-1108.

Kurihara, Y., M. A. Bender, and R. J. Ross, 1993: An initialization scheme of hurricane models by vortex specification. *Mon. Wea. Rev.,* **121**, 2030–2045.

Lambert, T. D. B., 2005: Accuracy of Atlantic and eastern North Pacific tropical cyclone intensity guidance. M.S. Thesis, Dept. of Meteorology, Naval Postgraduate School, Monterey, CA 933943-5114, 119 pp.

Liou, C-S., and Y. Jin, 2004: Recent improvements to coupled ocean/atmosphere mesoscale prediction system for tropical cyclone intensity forecast. *25th Conf. Hurr. Trop. Meteor.*, Miami, FL, 258-259.

Low-Nam, S. and C. Davis, 2001: Development of a tropical cyclone bogussing scheme for the MM5 system. Preprints, *Eleventh PSU/NCAR MM5 Users' Workshop*, Boulder, Colorado, 130-134.

Leslie, L. M. and G. J. Holland, 1993: Data assimilation techniques for tropical cyclone track prediction. *Tropical Cyclone Disasters* (Ed J. Lighthill, Z. Zheng, G. J. Holland, and. K. Emanuel), Peking University Press, Beijing, ISBN 7-301-02086-4/P.31, 92-103.

Marchok, T. P., 2002: How the NCEP tropical cyclone tracker works. Preprints, *25th Conf. Hurr. Trop. Meteor.*, San Diego, CA, 21-22.

Sampson, C. R., and A. J. Schrader, 2000: The automated tropical cyclone forecasting system (Version 3.2). *Bull. Amer. Meteor. Soc.*, **81**, 1231-1240.

Serrano, E., and P. Undén, 1994: Evaluation of a tropical cyclone bogusing method in data assimilation and forecasting. *Mon. Wea. Rev.*, **122**, 1523-1547.

Vigh, J., S. R. Fulton, M. DeMaria, and W. H. Schubert, 2003: Evaluation of a multigrid barotropic tropical cyclone track model. *Mon. Wea. Rev.,* **131**, 1629–1636.

Wang, W., C. Davis, J. Klemp, G. Holland, and M. DeMaria, 2006: Evaluation of WRF-ARW high-resolution tropical storm forecasts in the 2005 season. Preprints, *27th Conf. Hurr. Trop. Meteor*., Monterey, CA 24-28 April 2006, (Paper 2A.5).

Warner, T. T., L. E. Key, and A. M. Lario, 1989: Sensitivity of mesoscale-model forecast skill to some initial-data characteristics, data density, data position, analysis procedure and measurement error. *Mon. Wea. Rev.* **117**, 281–1310.

Weatherford, C. L., and W. M. Gray, 1988: Typhoon structure as revealed by aircraft reconnaissance. Part II: Structural variability. *Mon. Wea. Rev.,* **116**, 1044–1056.

Willoughby, H. E., J. A. Clos, and M. G. Shoreibah, 1982: Concentric eyewalls, secondary wind maxima, and the evolution of the hurricane vortex. *J. Atmos. Sci*., **39**, 395-411.

INITIAL DISTRIBUTION LIST

1. Defense Technical Information Center
   Ft. Belvoir, Virginia

2. Dudley Knox Library
   Naval Postgraduate School
   Monterey, California

3. Air Force Weather Technical Library
   Asheville, North Carolina

4. Air Force Institute of Technology
   Wright-Patterson Air Force Base, Ohio

5. Professor Philip A. Durkee
   Naval Postgraduate School
   Monterey, California

6. Professor Russell L. Elsberry
   Naval Postgraduate School
   Monterey, California

7. Lieutenant Colonel Karl D. Pfeiffer
   Naval Postgraduate School
   Monterey, California

8. Joint Typhoon Warning Center
   Pearl Harbor, Hawaii

9. Maj Frederick Eckel
   Air Force Weather Agency Meteorological Models Branch
   Offutt Air Force Base, Nebraska

10. Dr. Jerry Wegiel
    Air Force Weather Agency Meteorological Models Branch
    Offutt Air Force Base, Nebraska

11. Mr. Steve Rugg
    Air Force Weather Agency Meteorological Models Branch
    Offutt Air Force Base, Nebraska

12. Maj. Robert Stenger
Naval Postgraduate School

13. Capt William Ryerson
25 Operational Weather Squadron
Davis-Monthan Air Force Base, Arizona